TRANSCRIPTIONAL REGULATION PARADIGMS IN THE DUAL HOST-AQUATIC LIFESTYLE OF *VIBRIO PARAHAEMOLYTICUS*

by

Oriana Robinson

Submitted in partial fulfillment of the requirements
for the degree of Master of Science

at

Dalhousie University
Halifax, Nova Scotia
July 2024

Dalhousie University is located in Mi'kma'ki, the
ancestral and unceded territory of the Mi'kmaq.
We are all Treaty People.

Dedicated to Dr. Gertrude J. Robinson

Table of Contents

List of Tables

List of Figures

Abstract

Increased incidence of disease by marine pathogens correlates with rising sea surface temperatures. These changing marine conditions have resulted in the geographic expansion of pathogenic *Vibrio* spp. like *Vibrio parahaemolyticus* and increases in temperature are driving large scale virulence priming, suggesting infectious *Vibrio* spp. are in higher abundance in bivalve populations. As a result, the facultative pathogen *V. parahaemolyticus* remains the causative agent of gastroenteritis from the consumption of raw or undercooked seafood. This expansion is largely driven by the dual host-aquatic lifestyle of *V. parahaemolyticus* where the bacterium employs numerous coordinated mechanisms to survive and adapt across a broad range of niches. However, the underlying genetic regulatory mechanisms that promote *V. parahaemolyticus* fitness during its dual host-aquatic lifestyle remain poorly understood. Chitin catabolism is an important contributor to the environmental survival of *V. parahaemolyticus* and previous efforts to characterize the chitin catabolic cascade in *V. parahaemolyticus* using transposon sequencing identified the transcriptional regulator VP1236 as a critical fitness determinant for growth on chitin as a sole carbon source. Using a variety of phenotypic assays, I characterized VP1236 as the central carbon metabolism regulator HexR and explored the role of coordinated metabolism across cell morphology, biofilm formation, carbon assimilation, and motility. The data revealed the significant role regulated carbon metabolism plays in *V. parahaemolyticus* fitness in the aquatic environment. In contrast, *V. parahaemolyticus* relies on many virulence factors during infection but the Type 3 Secretion Systems (T3SS) 1 and 2 remain critical virulence determinants. T3SS-1 is present in all clinical and environmental isolates and contributes to host cell killing and cytotoxicity. The expression of the T3SS-1 is coordinated by the transcriptional regulator HlyU, which relieves a DNA cruciform, a non-B-DNA superstructure, to drive the expression of the T3SS-1 master regulator *exsA.* However, HlyU also regulates numerous other virulence factors in multiple pathogenic *Vibrio* spp. This global regulation of virulence by HlyU prompted us to explore additional targets for HlyU in *V. parahaemolyticus.* Using a chromatin-immunoprecipitation sequencing approach, I investigated the global binding of HlyU in *V. parahaemolyticus* during infection. This screen identified five putative targets for HlyU regulation which included a gene encoding an extracellular endonuclease, *exeM*. Characterization of the *exeM* promoter region for cruciform-forming elements identified two putative cruciform and demonstrated HlyU-dependent regulation of activity. These results validate the developed genomic screen for identifying HlyU-regulated targets and provide evidence for a DNA cruciform in regulating gene expression in *V. parahaemolyticus.* Altogether, investigations of the genetic regulatory mechanisms that support the dual host-aquatic lifestyle of *V. parahaemolyticus* are crucial for understanding the impacts of foodborne zoonosis to both human and marine organism health as climate change persists.

List of Abbreviations and Symbols Used

CCM	central carbon metabolism
ChIP-Seq	chromatin-immunoprecipitation sequencing
CW	cell wall
CV	crystal violet
ED	Entner-Duodoroff
GlcNAc	N-acetylglucosamine
KDPG	2-keto-3-deoxy-6-phosphogluconate
LBS	Luria broth salt
MM9	marine minimal media
MurNac	N-acetylmuramic acid
PBS	phosphate buffered saline
PPP	pentose phosphate pathway
SIS	sugar isomerase
TCA	tricarboxylic acid
Tn-seq	transposon mutagenesis sequencing
TR	transcriptional regulator
T3SS-1	type III secretion system 1
T3SS-2	type III secretion system 2
wHTH	winged helix-turn-helix
WT	wild type

Acknowledgements

It is quite the privilege to be writing this section, having come to the end of my MSc through the support of innumerable individuals. However, I will do my best to acknowledge all those who had a hand in helping me along these past two years.

Firstly, a big thank you to my family who provided me with unlimited support and guidance throughout this exciting and new time of my life. From chatting science to always picking up the phone call to literally providing me a place to live, I couldn't have done this without you. Thank you to Dr. Heather Wilkinson for all the help navigating this chapter of my life, cheers! Finally, to my grandmother Dr. Gertrude Robinson who has always stood as an example for the young women in my family, thank you.

I would be remiss to not thank my supervisor Dr. Nikhil Thomas. Thank you for all the support and encouragement while working on the project. It has been a wonderfully collaborative process and you allowed me the freedom to drive the project in interesting directions. I feel like I have grown as a scientist under your mentorship and as a result, this work feels like a real contribution to the *Vibrio* field. I look forward to continuing to work alongside you!

Many others have contributed significantly to the success of my MSc. A big thank you to my supervisory committee: Dr. Francesca Di Cara and Dr. John Rohde. Both fostered discussions informally and during committee meetings and with their mentorship, I felt like my project always became stronger. Thank you to Dr. Zhenyu Cheng and Dr. Craig McCormick for all their support while I navigated my first year here at Dalhousie. Thank you to Dr. Gerard Gaspard at the CORES CMDI facility for all the troubleshooting during my microscopy and to Dr. Andre Comeau at IMR for the valuable support during the development of the ChIP-Seq workflow. As well, thank you to Rhea Nickerson for all the qPCR help! And of course, I must acknowledge that the work of this thesis builds off a significant body of research by Dr. Landon Getz.

To my friends, thank you! This would have been a completely different experience without you. To Helen, who was there through the thick and thin of my first year out East! To Maggie, Rhea, and Mel, for all the walks, hilarious conversations, fun-filled weekends, and game nights! To Taylor and Marlon for letting me into Apartment 603 and being the most excellent roommates (It is *never* a hard pass to hang out with you). Thank you to A.H. for all the laughter and thoughtful discussions and Taegan Holmes for being there! As well, a big thank you to all the other graduate students in the MICI department for the conversations, collaborations, and warm welcome.

I am sure I am forgetting plenty of folks who have supported me during the past two years but know that is not my intention! Thanks a bunch!

Chapter 1 Introduction

1.1 The Global Ocean

Prokaryotes represent 15% of earth's total biomass, putting these single-celled organisms second only to plants (~80%) and ahead of animals, fungi, and protists which altogether make up the remaining 10% (1). In the global ocean, which covers approximately 70% of Earth's total surface, it is estimated that microbes make up 90% of total marine biomass (>10^{29} cells) (2). Indeed, most bacteria on earth exist in a variety of marine environments: deep oceanic sub-surfaces, oceanic sediments, in the ocean water column, and associated with marine organisms (3). The flow of carbon and nitrogen through the global oceans is largely facilitated by these resident bacteria who connect the ocean food webs and geochemical cycles, resulting in the maintenance of the habitability of Earth (2, 4). Heterotrophic marine microorganisms sequester anthropogenic carbon into sediments and cycle marine nitrogen, allowing transformed nitrogen to be returned into the global nitrogen cycle (5).

Worryingly, climate change threatens to disrupt these critical processes. Microbial physiology and metabolism rely on the fluxes of nutrients through their environment and the maintenance of abiotic factors (e.g., pH, salinity, temperature, redox chemistry, and UV radiation) (6–8). Significant changes to any of the abiotic and biotic factors that drive microbial metabolism will have profound effects on the productivity of the global oceans. In fact, these environmental changes, including increases in sea surface temperature and decreasing salinity, have been correlated to enhanced pathogenicity of marine pathogens (9–11). As well, significant changes in climate have also been linked to the impairment of marine host immune systems, leading to a greater incidence of disease (12–14).

1.2 Climate Change and Pathogenic *Vibrio* spp.

Coinciding with increased pathogenicity is the increase in abundance of marine bacterial pathogens like *Vibrio* (15). The genus *Vibrio* are gram negative heterotrophic bacteria that can be found ubiquitously in the global ocean. While the genus contains over a 100 species, only a handful are pathogenic (16). Notable pathogenic members include *Vibrio cholerae, Vibrio vulnificus, Vibrio anguillarum, Vibrio alginolyticus,* and *Vibrio parahaemolyticus* (17). *Vibrio* spp. cause infections in humans (18–21) and in a broad host of marine organisms including shellfish (22), finfish (23), crustaceans (24), and copepods (25). Abundance of *Vibrio* spp. is seasonal, with increased detection in summer months where sea surface temperatures exceed 18°C and salinity is <2.5% (26). As a result, the geographic distribution of *Vibrio* spp. in the ocean is directly influenced by marine conditions. Indeed, severe weather events like heatwaves has resulted in *Vibrio*-related infections in subarctic regions (27). Concerningly, direct temperature regulation of virulence gene expression has been demonstrated in pathogenic *Vibrio* spp., where water temperatures exceeding 27°C caused a marked increase in the expression of virulence factors involved in motility, secretion, and antimicrobial synthesis (11). As such, the increases in pathogen abundance that are coinciding with increase in marine hosts (28) makes *Vibrio* spp. some of the most notable enteric marine pathogens.

The global burden of *Vibrio* infection is enormous, estimated at around 3.5 million cases annually but this is likely a gross underestimate due to limitations in surveillance and reporting of infection (29). While *V. cholerae* is a significant contributor to the global burden of infection and disease, other pathogenic *Vibrio* spp. contribute up to half a million cases annually (30). Due to the increase in sea surface temperature, Vibriosis outbreaks are becoming common in developed countries. One important contributor is *V. parahaemolyticus,* with the worldwide prevalence of the O3:K6 pandemic strain making the bacterium the leading cause of gastroenteritis from the consumption of raw or undercooked seafood like mollusks or shellfish (31). Notably, during low tide, strains infecting shellfish appear to benefit from exposure to climate change-associated warming of air temperature, permitting further growth of pathogenic *V. parahaemolyticus* strains in previously low Vibriosis-burdened regions (32).

Several lines of evidence support a positive correlation between environmental fitness and pathogenicity. Interactions of pathogenic *Vibrio* spp. with other marine hosts can serve as replication niches for the bacteria or priming of virulence gene expression (33). *V. parahaemolyticus* has been observed to adhere to chitinous diatoms in the marine environment using a Type IV pili (34). As a result, diatom blooms during summer months often provide a reservoir for *V. parahaemolyticus* populations. It is predicted that these reservoirs will only increase with climate change and rising sea surface temperatures.

Of the pathogenic *Vibrio* spp., only *V. cholerae* and *V. parahaemolyticus* have the ability for pandemic expansion (35). This pandemic ability is believed to be derived from the competitive advantage of the *V. cholerae* El Tor and *V. parahaemolyticus* O3:K6 serotypes in the aquatic environment. For example, recent studies have shown that pandemic *V. cholerae* utilizes a Type IV Secretion System (T6SS) to inject a conserved array of toxic effectors into neighboring microbes to outcompete and colonize the aquatic niche (36). These conserved pandemic-associated effectors are believed to have been acquired via horizontal gene transfer from the fish pathogen *V. anguillarum* and indicate that fish colonization may be an important step in the evolution of the pandemic expansion of *V. cholerae* (36). Likewise, the expansion of pandemic *V. parahaemolyticus* is proposed to be facilitated by the Type III Secretion System 2 (T3SS-2), a hallmark of pandemic strains (37, 38). Interestingly, recent evidence has demonstrated that T3SS-2 positive (T3SS-2+) *V. parahaemolyticus* strains grew better in the presence of environmental protists, suggesting an important role for the T3SS-2 in interactions with marine protists (e.g., facultative parasitism) to promote environmental persistence and invasiveness. Furthermore, *Vibrio*-protist interactions have been shown to enrich for T3SS-2+ strains in the environment (37). Overall, the environmental fitness of pathogenic *Vibrio* spp., is a critical contributor to the development of pandemic strains and ultimately bacterial pathogenesis.

1.3 General Biology of *V. parahaemolyticus*

V. parahaemolyticus is a significant opportunistic pathogen and infections can present as acute gastroenteritis, with infected individuals experiencing diarrhea, vomiting, headaches, nausea, and low-grade fevers (39, 40). *V. parahaemolyticus* infection rarely results in death unless the individual is immunocompromised, where disease presentation is typically wound infections or septicemia (41). In contrast to *V. cholerae* infections, which result in secretory diarrhea from the production of the Cholera toxin (42), *V. parahaemolyticus* infection often presents as an inflammatory diarrhea (40). The distinct disease presentations can be attributed to the encoded virulence determinants within the *V. parahaemolyticus* genome.

1.3.1 *V. parahaemolyticus* Critical Virulence Determinants

During infection, *V. parahaemolyticus* employs an arsenal of virulence factors; however, Thermostable Direct Hemolysin (Tdh) and Tdh-related (Trh) hemolysins are major contributors to pathogen virulence and a characteristic of clinical isolates. Tdh and Trh target red blood cells (RBC) and have been shown to induce cytotoxicity, enterotoxicity, hemolytic activity, and cardiotoxicity (43). The enterotoxicity of Tdh is caused by its pore-forming ability. Tdh forms a pore of ~2nm on erythrocytes (44) and expression impacts the movement of solutes, ions, and water across the membrane. Specifically, Tdh induces cellular Ca^{2+} accumulation. Elevated intracellular Ca^{2+} levels stimulate the secretion of Cl^- ions out of the cell (45). The resulting effluxes disrupts critical cellular processes including cytoskeletal rearrangement and ion secretion (46), and results in the accumulation of fluid in the intestines (47). Likewise, the rapid influx of water into the erythrocytes to maintain osmolarity causes cell swelling and lysis (43). Tdh-associated cytotoxicity is caused by the interaction of Tdh and lipid rafts (48) which promotes apoptosis and results in host cell death via remodeling of host cytoskeleton (49).

1.3.2 *V. parahaemolyticus* Type 3 Secretion Systems

T3SS-1 and -2 are crucial virulence factors during *V. parahaemolyticus* infection and play important yet unique roles during pathogenesis. Expression of the T3SS on the outer cell membrane promotes bacterial colonization upon arrival in the intestinal lumen.

The T3SS is a needle-like apparatus that bridges three separate biological membranes: the inner and outer bacterial membrane as well as the host eukaryotic membrane, to translocate an array of effector proteins and toxins to disrupt and hijack host-cellular processes, resulting in host cell death (50). Numerous bacterial pathogens including *Yersinia, Shigella,* pathogenic *Escherichia coli* spp. and *Salmonella,* use T3SSs during infection (51). *V. parahaemolyticus* T3SS-1 effectors induce cytotoxicity and cellular disruptions (e.g., lysosomal rupture (52) and actin rearrangement (53)) in cultured human cells (54) whereas T3SS-2 expression results in enterotoxicity to infected animal models and cytotoxicity to intestinal cell lines (55). The T3SS-1 is found in all clinical and environmental isolates and shares high sequence homology with T3SSs in other *Vibrio* spp., indicating that these genes were ancestrally acquired and conserved, likely playing an important role in environmental fitness and persistence (38). In contrast, the T3SS-2 is encoded on the same chromosome 2-associated pathogenicity island (Vp-PA1) as Tdh and is only present in clinical strains (38, 54).

1.3.3 *V. parahaemolyticus* Zoonotic Infections

V. parahaemolyticus is also a significant burden to the aquaculture industry. Shrimp are particularly affected as certain *V. parahaemolyticus* strains cause acute hepatopancreatic necrosis disease (AHPND) which coincides with early mortality (24).

This disease has been particularly devastating to shrimp farming in southeast Asia and China, which accounts for 89.6% of world production (57). Infection by AHPND-causing *V. parahaemolyticus* has resulted in production and economic losses totaling 60% and $1 billion dollars annually (58). Analyses of AHPND-causing strains identified the pVA1 plasmid which encodes the binary PirAB toxins, whose cytotoxicity is derived from their pore-forming ability. Interestingly, some AHPND-causing *V. parahaemolyticus* strains have had partial or total losses of the *pirAB* genes and are still capable of causing disease, indicating the contributions of other virulence factors during infection (59). Concerningly, pVA1 contains a set of conjugative transfer genes suggesting the plasmid was acquired via horizontal gene transfer and is likely transferable between bacterial cells (60, 61).

1.4 The Environmental Adaptations of *V. parahaemolyticus*

The unique dual host-aquatic lifestyle of *V. parahaemolyticus* makes the bacterium highly successful in the marine environment. *V. parahaemolyticus* is incredibly abundant in aquatic environments and can be found in cellular densities up to 100,000 cells per liter of water, by proficiently colonizing substrates or free-swimming in the water column (62). In ideal growth conditions, *V. parahaemolyticus* rapidly replicates with a generation time of <10 minutes and <1 hour in the natural environment (63). The ubiquitous distribution of *V. parahaemolyticus* is attributed to the numerous mechanisms that *V. parahaemolyticus* employs to efficiently colonize and disseminate in the aquatic environment.

1.4.1 Biofilm Formation

As previously stated, the ability of *V. parahaemolyticus* to associate with biotic and abiotic surfaces in the form of biofilms promotes persistence, dissemination, and diversification of the organism. These sessile communities of bacteria are embedded within a secreted extracellular polymeric matrix consisting of DNA, polysaccharides, and proteins (64). In clinical settings, bacterial biofilms pose a significant threat to human health and outcome of infection. A study in 2018 by the National Institute of Health (NIH) determined that 60-80% of total microbial infections were caused by biofilms (65). Biofilm-associated bacteria are more resistant to antimicrobials and detergents compared to their planktonic form and can colonize critical medical equipment in patients (66). Additionally, environmental biofilms of pathogenic bacteria represent reservoirs for further disease. For example, *V. cholerae* or *V. parahaemolyticus* biofilms on chitinous copepods play a significant role in disease transmission (67–69).

Environmental biofilms also serve to maintain cellular homeostasis when bacteria are confronted with fluctuating or non-ideal environmental conditions (70). By generating an ideal local environment, critical signaling pathways can be maintained within the cell (71) and nutrients (e.g., macromolecules) can be concentrated (72). While *V. parahaemolyticus* biofilm formation is critical for the hydrolytic degradation of complex macromolecules like chitin (69), it may also important for the formation of satellite colonies to promote survival in tidal zones that undergo cyclical desiccation and flooding events (73). One study estimated that in one tidal cycle, 8.2×10^{13} cells are flushed into tidal creeks (74), allowing for the formation of new satellite colonies and the colonization of a new niche (73). Physical environmental features like plant stalks or marine burrows, which accumulate the colonized suspended matter, serve to increase the concentration of *V. parahaemolyticus* in the local environment (74).

The ability of *V. parahaemolyticus* to form biofilms is influenced by abiotic environmental conditions. Unlike other pathogenic *Vibrio* spp., *V. parahaemolyticus* demonstrates increased halotolerance, with growth in moderate (20ppt) to very high (>40ppt) salinity (33). Higher salinity is often associated with warmer sea surface temperatures. Since *V. parahaemolyticus* prefers a narrow but warmer temperature range in comparison to other *Vibrio* spp. and has been found in higher abundance in warmer sea water (33), this adaptation to high salinity may allow for the bacterium to persist in ideal growth conditions. Coincidently, increases in biofilm formation corresponds with increases in temperature from 15°C to 25°C (75, 76), with some evidence suggesting pathogenic *V. parahaemolyticus* strains are more effective at biofilm formation in comparison to environmental strains (76).

Altogether, the colonization of substrates and the increasing abundance of *V. parahaemolyticus* in coastal waters driven by fluctuating sea surface temperatures is leading to an even greater incidence of infection and disease (77).

1.4.2 Cell Shape and Motility

V. parahaemolyticus can differentiate into alternative cell and colony morphologies. Utilizing separate flagellar systems, *V. parahaemolyticus* cell morphologies include a distinct curved rod-shaped “swimmer” cell and a filamentous (30μm in length) “swarmer” cell. The switch from swimming to swarming cell shape is mediated by inhibition of the single polar flagellum and partial starvation conditions (e.g., iron limitation) (78). Prevention of flagellar rotation and low iron induces expression of a lateral flagellar system and elongated cell shape (79). The tightly coordinated control of swarmer cell differentiation suggests that elongated cell morphology provides a fitness advantage under non-ideal growth conditions, where the formation of sessile communities is advantageous (80, 81). The ability to transiently differentiate into the different morphologies is facilitated by the repression and activation of cell division, which must be tightly controlled to allow for swarmer cell growth without complete terminal repression (81). These cell morphologies are distinct from the club-shaped, round, or rabbit-eared cell morphologies associated with entry into the viable but non-culturable (VBNC) phase *V. parahaemolyticus* undergoes when under cold and/or nutrient starvation stresses (82).

The differentiated cell types of *V. parahaemolyticus* contributes to biofilm formation and colonization. Colonies on substrates express non-homogenous cell morphologies, with rod-shaped cells dominating the center while swarmer cells are localized to the periphery (73). Additionally, the biofilms can undergo variable phase switching between opaque (OP) and translucent (TR) colonies. This transition is mediated by the master regulator OpaR, a LuxR homologue quorum sensing output regulator (83, 84). OP colonies form significantly more extracellular polysaccharide (10-fold increase) in comparison to TR colonies however both phases form robust biofilms (85). The scrABC operon links phase transition with swarmer cell differentiation in *V. parahaemolyticus* (86). The products of the *scrABC* operon are predicted to form a sensory signaling cascade, where cytoplasmic ScrA and periplasmic ScrB are connected by the membrane associated ScrC, which contains both a cytoplasmic domain and a periplasmic receptor. ScrB has solute-binding properties, suggesting it may respond to stimuli within the periplasm and can act on ScrA via ScrC, resulting in signal transduction (86). Furthermore, ScrC appears to be involved in the biogenesis and degradation of the secondary signaling molecule cyclic-di-GMP. Overexpression of *scrABC* induces swarmer cell formation, even in liquid cultures, while inhibition of *scrABC* increased the production of capsular polysaccharide (CPS) (86). The *scrABC* operon mediates the switch between lateral flagellar gene expression and CPS, reflecting the importance of coordinating when surfaces are initially colonized (swarmer cell differentiation) versus the formation of biofilm for bacterial persistence (CPS production) in the aquatic environment.

Numerous surface-responsive genes are upregulated upon induction of the swarming phenotype, indicating that the alternative cell morphologies have a role beyond structural in biofilm formation. The Type VI Secretion System 1 (T6SS-1), a mechanism used by *V. parahaemolyticus* for interbacterial competition, is expressed upon swarmer cell differentiation (87). T6SS-1 has been found to be upregulated in warm temperatures and high salinity conditions, mimicking the conditions of marine coastal waters in summer, when *V. parahaemolyticus* is most abundant (87). However, the T6SS-1 was not active at temperatures simulating the mammalian host (≥37°C), suggesting the T6SS-1 does not play a role in mammalian virulence (87). Linking the expression of the T6SS-1 to swarmer cell differentiation may aid *V. parahaemolyticus* during the colonization of a new niche by outcompeting other resident bacteria in the aquatic environment. Other surface-responsive genes found to be upregulated upon swarmer cell differentiation is the protein VPA1598, which encodes an important colonization factor involved in N-acetylglucosamine (GlcNac) and chitin-binding (80). VPA1598 shares high sequence similarity to the *V. cholerae* GbpA (GlcNac Binding Protein A) which is involved in adherence and absorption onto zooplankton (88).

Some evidence indicates that the distinct cell differentiation states of *V. parahaemolyticus* promote dissemination and survival in the aquatic environment (73, 80, 89). Cell shape and motility are intrinsically linked in *V. parahaemolyticus.* The rod-shaped swimming cell employs a single sheathed polar flagellum to move in liquid environments while the filamentous swarming cell utilizes a completely distinct unsheathed lateral flagellar (laf) system comprising of hundreds of flagella for movement over surfaces (89). These cell morphologies have distinct protein profiles, with swarmer cells having an increase in *laf* gene expression, genes associated with chemotaxis, and a decrease in cell division-associated genes (90).

Freitas et al. (2019) observed that swarmer cells and swimming cells are both present during colonization of substrates and the motile ability of each cell type reflects their function. Their model proposes that swimming cells are initiators of surface colonization (73). The association with the substrate (e.g., chitin) impedes flagellar rotation, triggering the differentiation into the less motile swarmer state (80, 89). The swarmer cell colonies are a continuous source of cells to be released into the environment. However, swarmer cells are not released upon transition into liquid environment and instead another differentiated state, which Freitas et al. (2019) calls an adventurer cell, is released. Adventurer cells have a distinct protein profile from swimming and swarming cells (73). However, these cells, like swimming cells, are mobile and are optimized for swimming to find and colonize new substrates in the environment. Taken together, these different cell types may allow *V. parahaemolyticus* to maintain biofilm while also successfully exploring new niches.

1.4.3 Metabolic Flexibility and Diversity

Another notable feature of *V. parahaemolyticus* aquatic fitness is the organism's ability to use a diverse array of nutrient sources. Having a versatile carbon assimilation program allows for *V. parahaemolyticus* to persist across diverse environments (e.g., estuaries, open ocean, biofilm-associations with marine organisms) (74, 91). This metabolic program is especially useful in the context of the *V. parahaemolyticus*-marine organism associations. *V. parahaemolyticus* can metabolize derivatives from various marine organisms including shrimp, crab, and oysters, to acquire the necessary amino acids, vitamins, and minerals required for growth (63). However, *V. parahaemolyticus* must compete with other endogenous microbiota during the colonization of a niche. For this reason, having a flexible carbon assimilation program is advantageous.

A well-established hypothesis regarding microbial colonization is the Nutrient-Niche Hypothesis (92, 93). For successful colonization, a species must be able to use a carbon source better than any endogenous microbiota and that the abundance of this specific carbon source is the limiting-factor with regards to population growth (92). Chitin is a significantly enriched macromolecule in the marine environment, where it is found in the exoskeletons of crustaceans and phytoplankton and is a complex and often inaccessible carbon source for most marine heterotrophs, with only 0.4% - 19% of culturable marine bacteria capable of degrading chitin (94, 95). However, *Vibrio* spp. can efficiently hydrolyze chitin using secreted chitinases to acquire carbon, nitrogen, and energy required for growth (96). Indeed, the number of chitinase genes in *Vibrio* spp. is significantly higher than other marine bacteria, ranging from 9 genes in the smallest genome to 16 in the largest genome sequenced (97), demonstrating the importance of chitin catabolism to *Vibrio* spp. lifestyle. Ultimately, the chitinolytic ability of *Vibrio* spp. drives species distribution and supports a generalist behavior to allow for both free-swimming or host-associated lifestyles (e.g., biofilm formation or intestinal infection) (95, 98).

Metabolic flexibility is a characteristic of *Vibrio* spp. and assessments of the metabolic ability of *V. parahaemolyticus* found that *V. parahaemolyticus* can use 71 out of 190 different carbon sources that were tested (84). Any perturbations to metabolism significantly affect *V. parahaemolyticus* fitness (84), highlighting the importance of being able to utilize a carbon source when it is abundant and the significant contributions of metabolism to *V. parahaemolyticus* fitness in the aquatic environment.

Genomic islands harbor numerous carbohydrate metabolic systems in *V. parahaemolyticus* (99). Acquiring of gene clusters and single gene transporters by horizontal gene transfer have significant impacts on bacterial fitness in the dual host-aquatic lifestyle. For example, the acquisition of citrate metabolism is a hallmark of emerging pathogenic *V. parahaemolyticus* strains but is not found in environmental strains, suggesting an adaptation to host intestine conditions (99). In contrast, L-arabinose metabolism is conserved across *V. parahaemolyticus,* representing a key physiological feature of the species. The acquisition of metabolic diversity has enabled *V. parahaemolyticus* to target more complex metabolites and exploit patchy or non-ideal nutrient sources, opening new niches to colonize (97).

1.5 Rationale and Hypotheses

The dual host-aquatic lifestyle of *V. parahaemolyticus* allows for the bacterium to infect a broad range of hosts and disseminate proficiently throughout the aquatic environment. Specific strains with increased pathogenic potential and drug resistance (including a pandemic O3:K6 clone) have spread globally. Critically, the rapid increase in sea surface temperature due to climate change is furthering *Vibrio* spp. abundance and migration into coastal waters, leading to an even greater number of bivalve populations with infectious doses of *Vibrio* spp. Therefore, identifying the contributions of genetic regulatory mechanisms to bacterial fitness is critical for understanding the impacts of foodborne zoonosis in the context of impending climate change.

In this thesis, I set out to explore two transcriptional regulation paradigms present in the host-aquatic lifestyle of *V. parahaemolyticus* and their contributions to bacterial fitness. Firstly, I investigated the role of coordinated central carbon metabolism in the aquatic fitness of *V. parahaemolyticus* using a variety of phenotypic characterization assays and genetic tools. Next, I utilized a next-generation sequencing technology to investigate protein-DNA interactions during *V. parahaemolyticus* infection to identify targets of a global virulence regulator in *Vibrio* spp.

Aquatic fitness and pathogenesis are tightly linked in *V. parahaemolyticus*. Therefore, the mechanisms that underly bacterial fitness in the aquatic environment is well worth study. The ability to catabolize chitin is an important yet under-investigated facet in the aquatic lifestyle of *V. parahaemolyticus*. Building off previous work that utilized transposon mutagenesis (Tn-seq) to characterize the chitin utilization paradigm in *V. parahaemolyticus* (100), I set out in chapter 3 to explore VP1236, a gene that demonstrated a significant role in bacterial fitness on chitin as a sole carbon source. While uncharacterized, VP1236 is annotated as a MurR/RpiR/HexR family transcriptional regulator in the *V. parahaemolyticus* RIMD 2210633 genome. MurR and HexR are transcriptional regulators of cell wall recycling and central carbon metabolism, respectively. I hypothesized that VP1236 is a critical regulator for *V. parahaemolyticus* chitin catabolism and that *vp1236* mutants have dysregulated cellular processes, resulting in the observed fitness defect. Prior to characterization, I validated the Tn-seq results by generating a *vp1236* mutant and a plasmid with a cloned *vp1236* was used for trans-complementation. Using a variety of phenotypic assays, I investigated the role of VP1236 in bacterial fitness. In this study, I identified VP1236 as the *V. parahaemolyticus* HexR homologue and implicated coordinated regulation of central carbon metabolism and chitin utilization as a critical fitness determinant for *V. parahaemolyticus* in the aquatic environment.

As marine pathogen abundance increases and the resulting burden of disease grows, understanding how genes are mechanistically repressed and coordinately activated during infection is of great importance. Our lab previously identified how T3SS-1 is regulated in *V. parahaemolyticus* during infection. During infection, the transcriptional regulator HlyU relieves an H-NS-associated DNA cruciform at the promoter of the T3SS-1 master regulator *exsA,* which goes on to activate T3SS-1 expression (101). In other pathogenic *Vibrio* spp., HlyU acts as a global virulence regulator by coordinating the expression of numerous virulence factors (102). Therefore, I hypothesized that HlyU regulates multiple genetic loci in *V. parahaemolyticus* during infection. In chapter 4, I developed a Chromatin-Immunoprecipitation Sequencing (ChIP-seq) approach to identify global HlyU binding in the *V. parahaemolyticus* genome and sought to characterize additional HlyU targets. In this study, I identified 5 putative HlyU targets during *V. parahaemolyticus* infection. I validated the ChIP-seq assay by characterizing one of the targets that corresponded to the ExeM Extracellular Endonuclease using a previously developed *in vivo* quantitative assay to assess promoter activity (54). Since HlyU relieves a cruciform at *exsA* promoter, I investigated using both *in silico* and *in vitro* assays whether there are any DNA cruciform associated with the *exeM* promoter. I provide evidence for a DNA cruciform at the *exeM* promoter and identify a regulatory role for HlyU in *exeM* expression. These results establish HlyU as a global virulence regulator in *V. parahaemolyticus* and implicate HlyU regulated DNA cruciform as a mechanism for regulation of virulence gene expression in *Vibrio* spp.

Chapter 2 Materials and Methods

2.1 Bacterial Strains and Growth conditions

Vibrio parahaemolyticus RIMD2210633 was grown in Luria Miller Broth (LB; Bioshop; LBL417.1), Luria Broth Salt (LBS; 10g tryptone, 5g yeast extract, 20g NaCl, 20mM Tris-HCl pH 8.0), or M9 Minimal Media (MM9; 420mM Na_2HPO_4, 220mM KH_2PO_4, 86mM NaCl, 187mM NH_4Cl, $MgSO_4$, $CaCl_2$, 0.4% w/v glycerol). Cultures were grown at 37°C and 200rpm unless otherwise stated. Antibiotics were used in the growth medium as required: chloramphenicol (Sigma) at 2.5μg/ml or 30μg/ml (for *V. parahaemolyticus* and *Escherichia coli* respectively), ampicillin at 100μg/ml (for *E. coli),* erythromycin at 10 μg/ml (for *V. parahaemolyticus*) and neomycin at 25μg/ml (for *E. coli*). For growth on colloidal chitin, 0.4% colloidal chitin was substituted for glycerol and cultures were grown at 30°C and 250 rpm. For biofilm assays, 0.2% casamino acids (Fluka, 70171) was added to MM9. Agar (Bioshop; AGR003.1) was added to a final concentration of 1.5% (w/v) for solid media preparations unless otherwise stated. Spent Media was prepared by growing WT *V. parahaemolyticus* in LB, subculturing into LB at a starting OD_{600nm} of 0.025 for 16 hours at 37°C and 200rpm. Cells were pelleted at 5000rpm and 4°C until supernatant was clear (30 minutes) and then liquid media was filter sterilized using Nalgene Rapid-Flow 0.22μm filter (Thermofisher; 564-0020). See Table 2.1 for strains and plasmids used in this study.

Table 2.1 Strains and Plasmids used in this study

Strain or Plasmid	Description	Reference or Source
WT *V. parahaemolyticus*	Wild-type (WT) *V. parahaemolyticus* RIMD 2210633	(38)
Δ*hexR*	*V. parahaemolyticus hexR* null mutant with truncated *hexR* integrated into chromosome generated with pRE112-Δ*hexR*	This study
Δ*hexR/*VSV105	*V. parahaemolyticus hexR* null mutant with empty pVSV105 vector	This study
Δ*hexR/*VSV105-*hexR*	*V. parahaemolyticus hexR* null mutant carrying *hexR*-pVSV105 by conjugation, complementation construct	This study
WT/VSV105-*hexR*	WT *V. parahaemolyticus* expressing pVSV105-*hexR*. Used in spent media assay	This study
WT/Tn5::GFP (+)	WT *V. parahaemolyticus* containing transposon from pEVS168	This study
Δ*hexR* /Tn5::GFP (-)	*V. parahaemolyticus hexR* null mutant containing transposon from pEVS168	This study
WT/VSVlux-*murQP (CI)*	WT *V. parahaemolyticus* with pVSVlux-*murQP*	This study
Δ*hexR/*VSVlux-*murQP (C1)*	Δ*hexR* with pVSVlux-*murQP*	This study
WT/VSVlux-*nagZ*	WT *V. parahaemolyticus* with pVSVlux-*nagZ*	This study
Δ*hexR*/VSVlux-*nagZ*	Δ*hexR* with pVSVlux-*nagZ*	This study
WT/VSVlux-*exeM*	WT *V. parahaemolyticus* with pVSVlux-*exeM*	This study
Δ*hlyU*/VSVlux-*exeM*	Δ*hexR* with pVSVlux-*exeM*	This study
WT/VSVlux-*glgX*	WT *V. parahaemolyticus* with pVSVlux-*glgX*	This study
Δ*hexR*/VSVlux-*glgX*	Δ*hexR* with pVSVlux-*glgX*	This study
WT/VSVlux-*zwf*	WT *V. parahaemolyticus* with pVSVlux-*zwf*	This study
Δ*hexR*/VSVlux-*zwf*	Δ*hexR* with pVSVlux-*zwf*	This study
WT/VSVlux-*murQP (CII)*	WT *V. parahaemolyticus* with pVSVlux-*murQP (C2)*	This study
Δ*hexR*/VSVlux-*murQP (CII)*	Δ*hexR* with pVSVlux-*murQP (C2)*	This study
WT/VSVlux-*pgi*	WT *V. parahaemolyticus* with pVSVlux-*pgi*	This study
Δ*hexR*/VSVlux-*pgi*	Δ*hexR* with pVSVlux-*pgi*	This study
Δ*hlyU/*VSV105-*hlyU*-FLAG	FLAG-tagged *hlyU* construct in the *V. parahaemolyticus hlyU* null background	(100)

Strain or Plasmid	Description	Reference or Source
Δ*hlyU*/VSV105-*hlyU*(Q55A)-FLAG	*V. parahaemolyticus hlyU* null mutant expressing FLAG-tagged *hlyU* with a mutation Q55A in DNA binding domain. Cannot bind DNA.	(100)
DH5$\alpha\lambda$pir	*E. coli* host for oriR6K-dependent plasmid replication	
pVSV105	*Vibrio* shuttle vector with *lac* promoter and multiple cloning site, replication competent in *V. parahaemolyticus* and DH5$\alpha\lambda$pir.	(103)
pVSVlux	*LuxCDABE* cassette cloned into SmaI site of pVSV105	(100)
pEVS104	Conjugation helper plasmid with mobilization machinery, used in triparental mating	(104)
pEVS168	Mini-Tn5 transposon plasmid, containing a promotor-less *gfp,* erythromycin selection, R6K origin of replication	(105)
pRE112	Suicide plasmid, R6K origin of replication, for allelic exchange	(106)
pRE112-Δ*hexR*	Δ*hexR* allele in pRE112, for allelic exchange	This study
pBS	General cloning vector	Stratagene
pBS-*exeM*	pBS containing blunt cloned *exeM* intergenic region. Used in T7 mapping assay	This study
pUC(A/T)	Vector containing known stable cruciform, positive control for cruciform mapping assay	NEB
pVSVlux-*murQP (CI)*	*murQP* promoter cloned upstream of *LuxCDABE* cassette in pVSVlux	This study
pVSVlux-*nagZ*	*nagZ* promoter cloned upstream of *LuxCDABE* cassette in pVSVlux	This study
pVSVlux-*exeM*	*exeM* promoter cloned upstream of *LuxCDABE* cassette in pVSVlux	This study
pVSVlux-*glgX*	*glgX* promoter cloned upstream of *LuxCDABE* cassette in pVSVlux	This study
pVSVlux-*zwf*	*zwf* promoter cloned upstream of *LuxCDABE* cassette in pVSVlux	This study
pVSVlux-*pgi*	*pgi* promoter cloned upstream of *LuxCDABE* cassette in pVSVlux	This study
pVSVlux-*murQP (CII)*	*murQP (C2)* promoter cloned upstream of *LuxCDABE* cassette in pVSVlux	This study

2.2 Generation of Δ*hexR* and Δ*hexR* chromosomal mutant strains

Primers NT495 and NT496 (synthesized by Integrated DNA Technologies (IDT)) were used in a PCR to amplify the upstream flanking DNA and encompassed the start codon of *vp1236* with *V. parahaemolyticus* RIMD 2210633 as template. Similarly, primers NT497 and NT498 were used to amplify a distal and downstream coding sequence of *vp1236.* The resulting amplicons were digested with SacI/EcoRI and EcoR1/KpnI respectively. pRE112 was likewise digested with SacI and KpnI and a triple ligation was performed between the two digested amplicons and pRE112 prior to heatshock into *E. coli* DH5$\alpha\lambda$pir. Screening for successful ligation was performed on LB agar containing chloramphenicol. Successful transformants contained the plasmid pRE112 with a truncated *vp1236.* pRE112-truncated *vp1236* served as a chromosomal integration suicide construct for homologous recombination and was conjugated into *V. parahaemolyticus* through tri-parental mating. Briefly, equal volumes of donor DH5αλpir carrying pRE112-truncated *vp1236,* recipient WT *V. parahaemolyticus* and helper strain *E. coli* pEVS104 were spotted on LBS agar at 28°C overnight. Chromosomal integrants were selected on LBS containing chloramphenicol at 22°C and underwent *sacB*-mediated sucrose selection on 5% sucrose LB agar to promote the loss of the integrated pRE112 construct carrying WT *vp1236*. This was followed by a chloramphenicol sensitivity screen to identify colonies that had lost the integrated pRE112 plasmid. Stable integrants were screened by PCR for truncated *vp1236* using primers NT495 and NT498.

2.3 Genetic Complementation

To generate a genetic complement, primers NT495 and NT499 (synthesized by IDT) were used in a PCR with genomic DNA derived from WT *V. parahaemolyticus* RIMD 2210633 to amplify *hexR*. The resulting amplicon of 1,266bp size was phosphorylated with T4 Polynucleotide Kinase (NEB; M0201L) and blunt end cloned into dephosphorylated pBlueScript (pBS) digested with EcoRV. pBS containing WT *hexR* was transformed into *E. coli* DH5$\alpha\lambda$pir for propagation on MacConkey Agar (Biohsop; MAC001.500) to screen for recombinant DNA positive colonies. Provisional positive clones indicated by the formation of white colonies were selected and plasmids containing the *hexR* coding sequence were digested with SacI and SphI before being cloned directionally into pVSV105. pVSV105 containing WT *hexR* was transformed using heatshock into *E. coli* DH5$\alpha\lambda$pir for propagation and were delivered via tri-parental conjugation using the helper strain *E. coli* pEVS104 into the Δ*vp1236* mutant strains. Transconjugants were selected on LBS supplemented with chloramphenicol and were streak purified for stable plasmid expression.

2.4 Growth Assays

Strains were grown overnight in LBS supplemented with chloramphenicol. Aliquots of cultures were collected, and cells were washed twice with 1x MM9 salts. The strains were normalized to a starting $\mathrm{OD}_{600\mathrm{nm}}$ of 0.025 in either LB or MM9 (0.4% Glycerol) and inoculated in triplicate into a 96 well plate. $\mathrm{OD}_{600\mathrm{nm}}$ measurements were taken at 37°C every 20 minutes for 18 hours in a VictorX5 Multi Label Plate Reader. Each experiment was performed with three technical replicates. For colloidal chitin growth assays, strains were grown overnight in LBS supplemented with chloramphenicol and inoculated at a starting CFU/mL of approximately 10^5 cells into MM9 (0.4% colloidal chitin). Sampling was done every 6-12 hours post-inoculation and serial dilutions were plated in duplicate on MM9 Agar to determine the number of cells present.

2.5 Biofilm Formation Assay

Biofilm assays were performed as previously described (107, 108), with minor adjustments. Biofilms were grown in glass tubes by inoculating cells in LBS containing chloramphenicol overnight followed by an overnight subculture in MM9 at a starting OD_{600nm} of 0.025. Liquid media was removed, and cells were washed twice in sterile phosphate buffered saline (PBS; 137 mM NaCl, 2.7 mM KCl, 8.1 mM Na_2HPO_4, 1.46mM KH_2PO_4) before staining in 0.5% crystal violet for 30 minutes. Biofilms were washed twice with PBS to remove excess crystal violet from the tubes. The biofilms were de-stained with 3mL of 95% ethanol. Aliquots were collected and measurements were taken at an absorbance of 565nm in a 1 cm cuvette on a Biophotometer plus.

2.6 Microscopy

Microscopy was performed as previously described (109, 110), with minor adjustments. Overnight cultures were inocuslated into LB and MM9 at a starting OD_{600nm} of 0.025 for 16 hours at 37°C, 200rpm. Strains were fixed in 2µL volumes on 1% agarose pads containing 0.5% PBS. A cover slip was added, and slides were immediately imaged using a Zeiss Axio Imager Z1 microscope at 100x via Differential Interference Contrast (DIC) settings. Images were analyzed using ImageJ Fiji.

2.7 Motility Assays

Swimming motility assays were performed as previously described (111). Strains were cultured overnight in LBS, normalized to OD_{600nm} of 0.05 in 1x MM9 salt and stab inoculated into 0.2% (w/v) agar LBS plates. Measurements were recorded after 5 hours of incubation at 37°C. A swimming pattern of radial growth (outward from the inoculation site) was documented for each strain via photograph.

2.8 Mini-Tn5 Library Preparation

Briefly, a conjugal tri-parental mating occurred on LBS agar at 28°C and allowed for the delivery of the plasposon pEVS168 into either Δ*hexR* or WT *V. parahaemolyticus* RIMD 2210633. The mating mixture was serially diluted and plated on LBS containing 10 μg/mL erythromycin and incubated at 22°C for 36 hours to select for successful transposition. Colonies were further streak purified for stable integration. Strains expressing GFP were streak purified and represent transposon insertions near an active transcriptional promoter on the bacterial chromosome. Non-GFP expressing strains harbour a transposon but not near an active promoter that can support GFP expression. GFP and non-GFP producing strains for both genetic backgrounds were selected for further characterization.

2.9 Competition Assay

Overnight cultures of both GFP and non-GFP producing strains were grown in LBS supplemented with chloramphenicol at 37°C, 200rpm. The following day, 1 mL of culture was washed twice in 1x MM9 Salts and inoculated into 50 mL MM9 (0.4% Colloidal Chitin) at a starting OD_{600nm} of 0.025. Cultures grew at 30°C, 250rpm. Aliquots of 250uL were collected at 0 hpi, 6 hpi, 24 hpi, and 48hpi, serially diluted, and plated onto LB. Single colonies were counted (both the total and glowing sub-population) to determine the proportion of Glowing and Non-Glowing strains using Quantity One software (Bio Rad). Competition index was calculated using the equation (112):

$$CI = (\Delta hexR_f/WT_f)/ (\Delta hexR_i/WT_i)$$

Where subscript (f) denotes colony counts (CFU/mL) at final time point (t=48) and subscript (i) denotes colony counts of starting inoculum (t=0). Statistical significance was calculated using un-paired t-test against baseline of CI=1, where a value of 1 indicates no fitness defect.

2.10 Spent Media Assay

WT *V. parahaemolyticus* strains containing pVSV105-*hexR* were generated via tri-parental mating using helper strain pEVS104 and then subjected to growth in Spent Media along with WT, *hexR* mutant, and complement strains. Growth assays were performed as previously described with minor adjustments. Flasks of 10mL of each strain were grown for 24 hours at 37°C and 200rpm in Spent Media. OD_{600nm} measurements were taken at 6 hours, 12 hours, and 24 hours, in duplicate.

2.11 Reporter Constructs for HexR Lux Assay

Intergenic regions upstream of *pgi, glgX*, *zwf,* and *murQP* (specifically the alleles from chromosome 2 (CII)), were PCR amplified using primers NT511-NT518 (synthesized by IDT) (Table 2.2). Subsequent amplicons were digested with Sac1 and Kpn1 and directionally cloned into digested pVSVlux. Ligations were transformed into DH5$\alpha\lambda$pir via heatshock and clones were screened with restriction enzyme digestion for recombinant plasmid constructs. The constructs were then delivered via conjugation using the helper strain *E. coli* pEVS104 into WT and Δ*hexR V. parahaemolyticus* strains.

2.12 Lux Reporter Assays to assess HexR activity.

WT and Δ*hexR V. parahaemolyticus* strains containing pVSVlux bearing an upstream intergenic region of regulon members (namely *glgX, zwf, pgi*) as well as *murQP* (CII) were grown overnight in LBS with chloramphenicol. Cells were inoculated into LB at a starting OD_{600nm} of 0.05 at 30°C, 250rpm. Luminescence (counts per second (CPS)) and OD_{600nm} measurements were taken in triplicate in a VictorX5 Multi Label Plate Reader at 2 hours, 2.5 hours, 3 hours, and 3.5 hours post-inoculation.

2.13 Chemical Crosslinking of Protein-DNA complexes

A crosslinking protocol was adapted from Grainger et al. (2004) (113) with the following changes. Strains Δ*hlyu*/VSV105-*hlyu*-FLAG and Δ*hlyu/*VSV105-*hlyu* (Q55A)-FLAG were cultured overnight in LB supplemented with chloramphenicol. Strains were inoculated into 20mL of Inducing Media (LB, 15mM Mg^{2+}, 5mM EGTA) at a starting

OD_{600nm} of 0.025 for 4 hours at 30℃, 250rpmm. Cultures were cross-linked with 1% formaldehyde for 20 minutes at 30℃, 250rpm. Following crosslinking, cultures were quenched with Glycine (final concentration 0.5M) for 20 minutes at 30℃, 250rpm. Cells were harvested in volumes of 20ml and pelleted at 4℃, 5000rpm for 10 minutes. Cell pellets were washed twice with PBS (pH: 7.4) before resuspension with 20mL of Osmotic Shock Buffer (10mM Tris pH:8, 10mM EDTA pH: 8, 20% (w/v) sucrose, 50mM NaCl, 100 µg/ml lysozyme) and incubated at 37℃, for 30min. After incubation, cultures were pelleted at 4℃ and 5000rpm for 20 minutes. Pellets were resuspended in 5mL Lysis Buffer (16.7mM Tris pH:8, 1.67M. NaCl, 1.2mM EDTA pH: 8, 1.1% Triton-X100, 100ug/ml Proteinase K Inhibitor). Cellular DNA was then sheared via sonication to an average size of 500bp to 1000bp. Cellular debris were removed by centrifugation for 20min at 4℃, 5000rpm.

2.14 Anti-FLAG Immunoprecipitation

The immunoprecipitation workflow was adapted from Gu et al. (110, 111) with the following changes. Cleared lysates (5mL) were incubated with M2 anti-FLAG affinity matrix rotating overnight at 4℃. Following immunoprecipitation, the matrix was washed twice with 1mL Buffer A (150mM NaCl, 1mM EDTA pH: 8, 10mM Tris-HCl pH:8, 1% Triton-X100), twice with 1mL Buffer B (500mM NaCl, 1 mM EDTA pH:8, 10mM. Tris-HCl pH:8, 1% Triton-X100), twice with 1mL LiCl Buffer (250mM LiCl, 1mM EDTA pH:8, 10mM Tris-HCl pH:8, 0.5% Triton-X100, 0.5% sodium deoxycholate) and twice with TE Buffer (pH: 8). Each wash was followed by a 1-minute centrifugation at 4℃, 5000rpm. The affinity matrix was resuspended in 200uL elution buffer (50mM Tris-HCl pH:8, 10mM EDTA pH:8, 1% SDS) at 65℃, for 2 hours. The supernatant was collected after pelleting at 5000rpm for 1 minute. Proteins within the supernatant were digested with Proteinase K (final concentration of 200ug/ml) at 45℃, for 2 hours. The reaction products were processed with a PCR Purification Kit (Qiagen) to produce purified DNA that was eluted in ultrapure water.

2.15 Library Preparations for Sequencing

DNA fragments purified from the anti-FLAG immunoprecipitation were used for library preparation using the NEBnext Ultra II DNA Library Prep Kit for Illumina (NEB; E7645S). DNA fragment libraries were indexed using Multiplex Oligos for Illumina (NEB; E7335S) based on whether samples were generated from Δ*hlyu/*VSV105-*hlyu*-FLAG or Δ*hlyu/*VSV105-*hlyu* (Q55A)-FLAG. Libraries were size selected using NucleoMag NGS Clean up and Size Select beads (Macherey-Nagel; 744970.5). The DNA quality of the prepared libraries was assessed using NEBNext Library Quant Kit for Illumina (NEB; E7630S). Adaptor dimers were removed with another round of size selection on NucleoMag beads if necessary. Sequencing of the libraries was performed on an Illumina MiSeq Platform using a Nano Kit (read length 2x150bp).

2.16 Quantitative analysis of DNA reads

The generated fastq files obtained from sequencing were uploaded to the Galaxy web platform and processed using usegalaxy.org. For both samples, forward (R1) and reverse (R2) reads were generated with an average size of 480bp. Reads were individually mapped to *Vibrio parahaemolyticus* RIMD 2210633 genome (GCF_000196095.1) using

BWA-MEM2 (Galaxy Version 2.2.1+galaxy1) which maps medium to long reads to the reference genomes (116). Resulting BAM files were filtered with SAMtools (Galaxy Version 1.8+galaxy1) to remove any non-uniquely mapped reads. This restricts the data to reads with mapping quality above 20. A read count matrix was generated with DeepTools (Galaxy Version 3.4.5+galaxy0) to assess correlation among input samples (Δ*hlyu/*VSV105-*hlyu*-FLAG) and controls (Δ*hlyu/*VSV105-*hlyu* (Q55A)-FLAG) (117). The correlation was plotted as a heat map. Signal strength was assessed using DeepTools (plotFingerprint, Galaxy Version 3.4.5+galaxy0) and generated Signal Extraction Scaling (SES) plots (117). BigWig files were created for each BAM file dataset to visualize peaks. Coverage was displayed using Integrated Genome Browser (Version 10.0.0) (118).

2.17 Generation of *exeM* intergenic region lux reporter construct

Primers NT519 and NT520 (synthesized by IDT) were used in PCR with WT *V. parahaemolyticus* RIMD2210633 to amplify the intergenic region upstream of *exeM* start codon. The resulting amplicon was 583bp and was phosphorylated with T4 Polynucleotide Kinase (NEB; M0201L) and blunt clones into dephosphorylated pBlueScript digested with EcoRV. Following ligation, pBS-*exeM* was transformed via heatshock into DH5$\alpha\lambda$pir for propagation on MacConkey Agar (Biohsop; MAC001.500). Clones were screened with Sac1 and Kpn1 digestions and double digested *exeM* was cloned into the Sac1 and Kpn1 cut sites of pVSV-lux. pVSV-lux-*exeM* was delivered via conjugation using the helper strain *E. coli* pEVS104 into WT, Δ*hlyu*, and Δ*hns,* Δ*hns*Δ*hlyu V. parahaemolyticus* strains.

2.18 Lux Reporter Assay to assess *exeM* promoter activity

WT, Δ*hlyu*, and Δ*hns,* Δ*hns*Δ*hlyu V. parahaemolyticus* strains containing pVSVlux with an upstream intergenic region of *exeM* were grown overnight in LB with chloramphenicol. Cells were inoculated into Inducing Media at a starting OD_{600nm} of 0.025 at 30°C, 250rpm. After 4 hours and 4.5 hours, aliquots were harvested and luminescence (counts per second (CPS)) and OD_{600nm} measurements were taken in triplicate in a VictorX5 Multi Label Plate Reader.

2.19 *in silico* cruciform analysis of *exeM* intergenic region

The DNA sequence for the intergenic region upstream of *exeM* (Genbank ID BA000031.2; 2966549bp to 2967089bp) was used as input into Palindrome Analyzer, an online bioinformatics tool which identifies inverted repeats and energy required for the formation of a cruciform. The following criteria was used: a minimum of 6 base pairs for the cruciform stem, a spacer/loop region of at least 15 base pairs. A single mismatch was allowed.

2.20 T7 endonuclease and restriction enzyme mapping assays

The *exeM* intergenic region was evaluated for cruciform forming elements using the pBS-*exeM* construct generated previously. Briefly, fresh supercoiled pBS-*exeM* was prepared from cells using a Monach Plasmid Miniprep Kit (NEB; T1010L) Approximately 800-1000ng of DNA was subjected to digestion with HindIII alone, T7 Endonuclease alone, PvuII alone, and a sequential digest using T7 endonuclease initially, followed by PvuII as previously described (119). Digests were run on 1.75% agarose electrophoresis gels to resolve DNA fragments. pUC(A/T), which contains an engineered cruciform (119) was digested with the same strategy and served as the positive control.

2.21 Statistical Analyses

Statistical significance was calculated using a Student's t-test with a two-tailed distribution parameter. Statistical analyses were calculated with Prism 10 (10.2.3). Means are plotted with standard deviation.

Table 2.2 PCR Primers used in this study

Designation	Sequence (5' → 3')	Description or Purpose
NT495	TTGAGCTCAGTACTGGACGAACAACGC	*ΔhexR* construction
NT496	TTGAATTCGCGCTCTGACTTACTGAAATTCTCC	*ΔhexR* construction
NT497	AAGAATTCCGTTATGACAAGCTAAGTCAG	*ΔhexR* construction
NT498	AAGGTACCATGGCGATCACTAACGCTAAGTTGG	*ΔhexR* construction
NT499	AAGCATGCTTAGTACTGACTTAGCTTGTCATAACG	*ΔhexR* construction
NT511	AAGGTACCGTGTGCTGGCATGTCGTCAT	pVSVlux-*pgi* construction
NT512	AAGGTACCATGTTACAGTAGGTTCCATTCC	pVSVlux-*pgi* construction
NT513	AAGAGCTCCAAAGCGCGAACCCAGATCGTA	pVSVlux-zwf construction
NT514	AAGGTACCAACGAGGTACTTATTGTGTGCC	pVSVlux-*zwf* construction
NT515	AAGAGCTCTTGACCACCGTCAGCGTTCACG	pVSVlux-*glgX* construction
NT516	AAGGTACCGTCGTGTCATCGGAGATAACTT	pVSVlux-*glgX* construction
NT517	AAGGTAACCTGTACTGGCTGGATTACGGC	pVSVlux-*murQP (CI)* construction
NT518	AAGAGCTCGCTGAGTACGCCTCGCGACTATCT	pVSVlux-*murQP (CI)* construction
NT519	AAGAGCTCAGAGAGCTAGCCCAATACG	*ΔexeM* construction
NT520	AAGGTACCGATTAACGTGTCCATTGTCG	*ΔexeM* construction

Chapter 3 The HexR Regulator is a Critical Fitness Determinant for Chitin Utilization by *Vibrio parahaemolyticus*

3.1 Introduction

The ocean biosphere plays an important role in the maintenance of the marine carbon cycle. This dynamic interaction between plants and animals allows for the long-term sequestration of organic carbon in sediments. At the core, heterotrophic marine microbes can transform organic matter into simple inorganic forms (e.g., carbon dioxide) (120). Secreted extracellular enzymes allow for microbes to convert high molecular weight macromolecules into smaller transportable substrates like the chitin monomer N-acetylglucosamine (GlcNac) or other simple 6-carbon sugars that can be further processed in the cell or used by other microbes in the water column, thus promoting the growth of secondary microbial 'users' (121). Chitin is among the most abundant organic macromolecule in the aquatic environment, derived primarily from planktonic organisms but also from the chitinous exoskeleton of crustaceans and copepods (122). More than 10^{11} metric tons of chitin is generated every year which must be degraded to maintain marine carbon and nitrogen cycles. However, analyses of marine sediment reveal only trace amounts of chitin, indicating the presence of chitin utilizers in the marine water column and their considerable contribution to marine carbon cycling (123). The degradation of insoluble chitin, a complex polymer of GlcNac, requires a flexible and specialized carbon assimilation program (124). *Vibrio* spp. are capable of degrading chitin into the necessary metabolic precursors for amino acid and nucleotide biogenesis via the pentose phosphate pathway (125).

Chitin utilization involves a four main steps: sensing, chemotaxis and attachment, induction of gene expression, and finally catabolism (126). The first step of catabolism involves the breakdown of the macromolecule into its GlcNac oligosaccharides by extracellular chitinases followed by transport into the periplasmic space via outer membrane porins (127). Chitin oligosaccharides are degraded in the periplasm by chitinodextrinase and β-N-acetylglucosaminidase. The resulting chitin derivatives can be transported into the cytoplasm by either an ABC transporter or by a PTS transporter (124, 128–130). Eventually, the chitin monomers are converted into fructose-6-phosphate, acetate, and ammonium for further utilization in central carbon metabolism (126).

Not only is chitin an important carbon source, but Vibrio *spp*. associations with chitin also influences cellular growth and physiology. Associations of *V. cholerae* and *V. parahaemolyticus* with chitin has been shown to induce natural competence and allow the bacterium to take up free DNA from the environment (115, 131, 132). Several reports of mobilized virulence factors between *V. cholera* strains have attributed this phenomenon to chitin-induce competence, including the O1 to O139 serogroup conversion and movement of a previously un-mobilizable cholera toxin prophage between strains (133–135). Likewise, the colonization of chitinous crustaceans is critical for the persistence and dispersal of *Vibrio* spp. in the aquatic environment. Preferential biofilm formation on chitin over other abiotic surfaces has been documented to increase *V. cholerae* resistance to predation (136). The presence of GlcNac in the local environment induces the expression of Type IV pilins and Mannose-Sensitive hemagglutinin (MSHA) which are required for the formation of a Type IV Pilus and contribute to the adherence of *V. parahaemolyticus* on biotic surfaces (137, 138). In the open ocean, *V. parahaemolyticus*-

zooplankton associations comprise up to 80% of sampled zooplankton, with pathogenic strains present in environmental samples, indicating a reservoir for pathogenic *V. parahaemolyticus* (139). Therefore, chitin-associated biofilms overall contribute to the fitness of both environmental and pathogenic *V. parahaemolyticus* strains.

The comprehensive chitin utilization program was first characterized in *V. cholerae* using microarray and genetic studies to identify the genes and regulatory elements that underpin the adherence mechanisms and the catabolism of chitin (138). While chitin catabolism in *V. cholerae* is very complex, involving numerous enzymes and structural proteins, considerable effort has been put into elucidating the pathway (122, 124, 138). However, the genes involved in chitin utilization remain modestly understood in *V. parahaemolyticus.* Understanding the chitinolytic-associated genes is increasingly importance considering the chitin-induced changes in cell physiology and subsequent effects on virulence, biofilm formation, or competence.

To characterize the homologous chitin utilization program in *V. parahaemolyticus,* Getz (2022) (100) employed transposon mutagenesis coupled with next-generation sequencing (Tn-seq) to identify chitinolytic associated genes. Briefly, a saturated transposon library of *V. parahaemolyticus* chromosomal mutants was subjected to selective fitness pressure with chitin as the sole carbon source for growth. The same library was subjected to growth on glucose as a sole carbon source to identify non-chitin specific essential genes. Total DNA was sequenced for both conditions and mutants underrepresented in the sequencing pool after growth on chitin were considered less fit. Among the statistical findings, VP1236, a member of the MurR/HexR/RpiR family transcriptional regulators, was identified as a fitness determinant for growth on chitin (p-value = 0.000016). This gene was of particular interest because its *V. cholerae* homologue VC1148 (locus tag: FY484_RS05840) was not functionally implicated in *Vibrio* spp. chitin catabolism by microarray (138).

The MurR/HexR/RpiR family transcriptional regulators are all characterized as DNA-binding proteins, with an N-terminal winged helix turn helix (wHTH) motif, and a C-terminal sugar isomerase (SIS) domain which binds phosphosugars (140). DNA binding is mediated through the wHTH domain while the SIS domain of the transcriptional regulator is typically bound by the product of one of the downstream regulated enzymes to modify the regulator's activity based on environmental or cellular signals.

Key members of the transcriptional regulator family include MurR, a transcriptional repressor for cell wall recycling and biosynthesis, and HexR a transcriptional regulator of central carbon metabolism (141, 142). Cell wall (CW) recycling and synthesis is critical for maintenance of cell growth and homeostasis, as cells recycle upwards of 40% of their cell wall per generation. Strict regulation of CW recycling is required as new peptidoglycan (murein) is synthesized *de novo* and old murein is turned over to be reused (143). In *E. coli,* MurR is transcribed divergently from its target operon *murQP.* MurP and MurQ encode a N-acetylmuramic acid (MurNac) phosphotransferase, which imports peptidoglycan-derived MurNac-6-P from the periplasm into the cytosol, and a MurNac-6-phosphate etherase, responsible for converting MurNac-6-P into GlcNac-6-P which is further recycled back to the peptidoglycan layer (144) (Figure 3.1). MurR binds the intergenic region upstream of MurQP, repressing the transcription of both itself and the *murQP* locus (141). During cell wall recycling, MurNac-6-P binds the SIS domain, relieving MurR-mediated repression and allowing for the expression of *murQP* (141).

HexR is a broader transcriptional regulator, targeting a regulon of upwards of 87 genes in Proteobacteria (e.g. *Pseudomonales*, *Burkholderiales,* and Enterobacteriales) (145). Genomic reconstruction of the HexR regulon in all sequenced Proteobacteria highlighted the pleiotropic effect of HexR on central carbon metabolism, wherein HexR can be a transcriptional activator or repressor. This is a hallmark of the RpiR family, with other members like GlvR (146) in *Bacillus subtilis* functioning as a transcriptional activator or like *E. coli* RpiR as a transcriptional repressor (147). In *Pseudomonas putitida,* the SIS domain of HexR is recognized by the effector 2-keto-3-deoxy-6-phosphogluconate (KDPG), an Entner-Duodoroff (ED) pathway intermediate. Like the regulation of cell wall recycling by MurR and the effector MurNac-6-P, control of CCM by HexR is modulated by the pathway intermediate KDPG rather than an initial substrate for the pathway (141, 142). Using RegPrecise, which curates a collection of inferred prokaryotic regulons, HexR is predicted to regulate 22 genes in 16 different operons in *V. parahaemolyticus* and is regulated in turn by the effector KDPG (148). Unlike in other Proteobacteria (E.g. *Enterobacteriales* and *Pseudomonades*), the *Vibrionales* HexR regulon is expansive and is implicated in the control of 15-20 operons (145). The consensus sequence for HexR is an imperfect palindrome of TGTAATTAAATTACA. In particular, the *V. parahaemolyticus* HexR regulon includes key enzymes involved in glycolysis, the pentose phosphate pathway, the tricarboxylic acid cycle (TCA), ED pathway, alternative metabolism pathways (Glycogen or Mannitol metabolism) and shorter carbon flux pathways like gluconeogenesis and the glyoxylate shunt (148).

Notable members include glucose-6-phosphate isomerase (*pgi*), glycogen debranching enzyme (*glgX*), glucose-6-phosphate dehydrogenase (*zwf*), isocitrate lyase (*aceA*), malate synthase (*aceB*), and phosphoenolpyruvate carboxylase (*ppc*).

Dysregulation in either of these pathways that contribute to cell homeostasis and growth could result in the identification of VP1236 as a fitness determinant for growth on chitin. For example, a convergence of chitin catabolism and cell wall recycling at GlcNac during murein turnover could result in dysregulated cell wall synthesis and overall fitness defects (Figure 3.1). Alternatively, if VP1236 acts as HexR, any Fructose-6-P generated during chitin catabolism may be sent through glycolysis and other carbon flux rather than the pentose phosphate pathway where the required amino acids and nucleotides can be generated, making the cell deficient in the macromolecules required for growth on chitin as a sole carbon source (Figure 3.1).

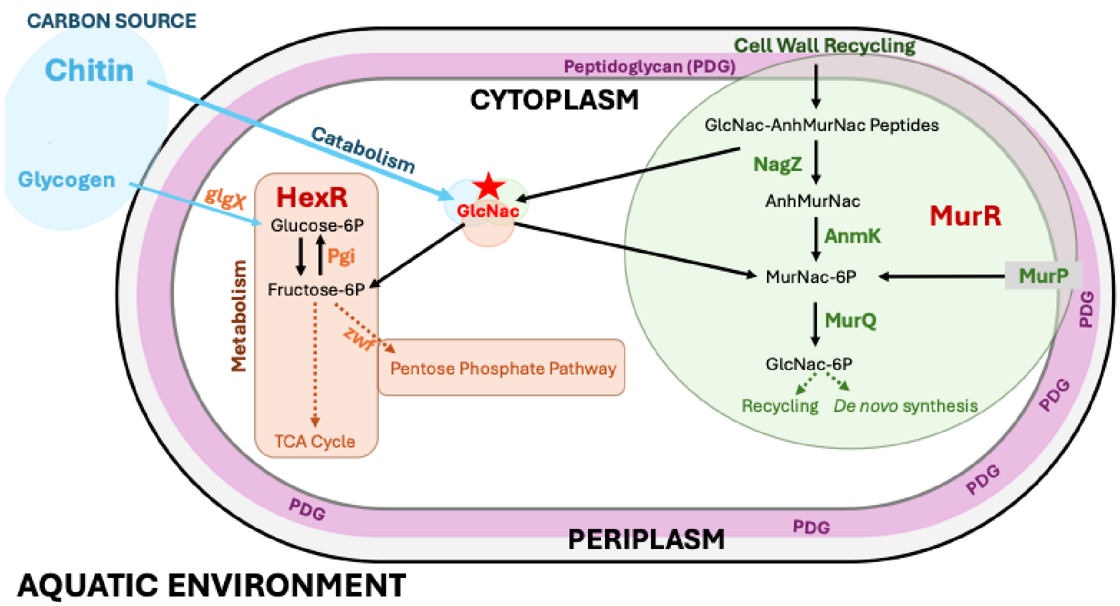

Figure 3.1 Schematic of major CCM and Cell Wall Recycling-associated pathways contributing to *vp1236* mutant phenotype. Key transcriptional regulators of CCM and CW recycling are in dark red. Light red star indicates site of potential convergence of chitin catabolism and cellular pathways at GlcNac. Representative enzymes investigated in this chapter are represented in respective pathway colours along arrows. Key enzymes involved in the conversion of intermediates in CW recycling and CCM are depicted along the arrows. Diagram adapted from (149). Abbreviations: GlcNac = N-acetylglucosamine, MurNac = N-acetylmuramic acid, AnhMurNac = 1,6-anhydro-N-acetylmuramic acid, TCA Cycle = Tricarboxylic Acid Cycle

3.2 Results

3.2.1 *in silico* analyses of VP1236 to identify *V. parahaemolyticus* HexR homologue

Prior to phenotypic characterization, the *V. cholerae* N16961 and *V. parahaemolyticus* RIMD 2210633 genomes were probed using a variety of computational and database analyses to begin to elucidate the protein identity of VP1236. Three MurR/RpiR transcriptional family regulators are present in *V. cholerae:* a MurR homologue (VC-MurR; locus tag: FY484_RS0108), a HexR homologue (VC-HexR; locus tag: FY484_RS05840), and the uncharacterized FY484_RS08895. Using EMBOSS-Needle (Needleman-Wunsch alignment) for global protein sequence alignment, the protein sequences of VP1236 with VC-HexR were aligned and revealed the highest protein sequence similarity (alignment score = 95.053%) (Figure 3.2A). Additionally, protein domains were annotated with InterProScan and confirmed that VP1236 contains the classical wHTH and SIS domains of the superfamily. Of note, VC-HexR and VP1236 share similar genetic neighborhoods on chromosome 1, encoded among pyridoxal-dependent aspartate 1-decarboxylase (PanP), lysine exporter LysO family protein, and GrxA family gluteradoxin. This preliminary search suggests VP1236 may act functionally like HexR rather than MurR. However, I was still interested whether the *V. parahaemolyticus* genome encoded a MurR homologue, and if so, where in the bacterial genome. Using NCBI BLAST, I searched the annotated genome of *V. parahaemolyticus* RIMD 2210633 with the protein sequence for VC-MurR. The top hit was VP_RS23475 (E value: $4\text{x}10^{-149}$), which was annotated as a SIS domain-containing protein on chromosome 2. Given that VP_RS23475 is located divergently from *murQP* (locus tags: VP_RS23480 and VP_RS23485 respectively) on chromosome 2 and contains an SIS domain, I further investigated whether this protein was the MurR homologue. Alignment of the protein sequences for VC-MurR and VP_RS23475 revealed 70% identities and 87% positives (Figure 3.2B). Furthermore, alignment of VP_RS23475 and VP1236 only scored 25%, suggesting that VP1236 and VP_RS23475 encode proteins that are less similar to each other and likely serve different functions (Figure 3.2C). Taken together, I predict VP1236 to be the *V. parahaemolyticus* HexR homologue while VP_RS23475 may act more like MurR. For the subsequent phenotypic characterizations, I refer to VP1236 as HexR.

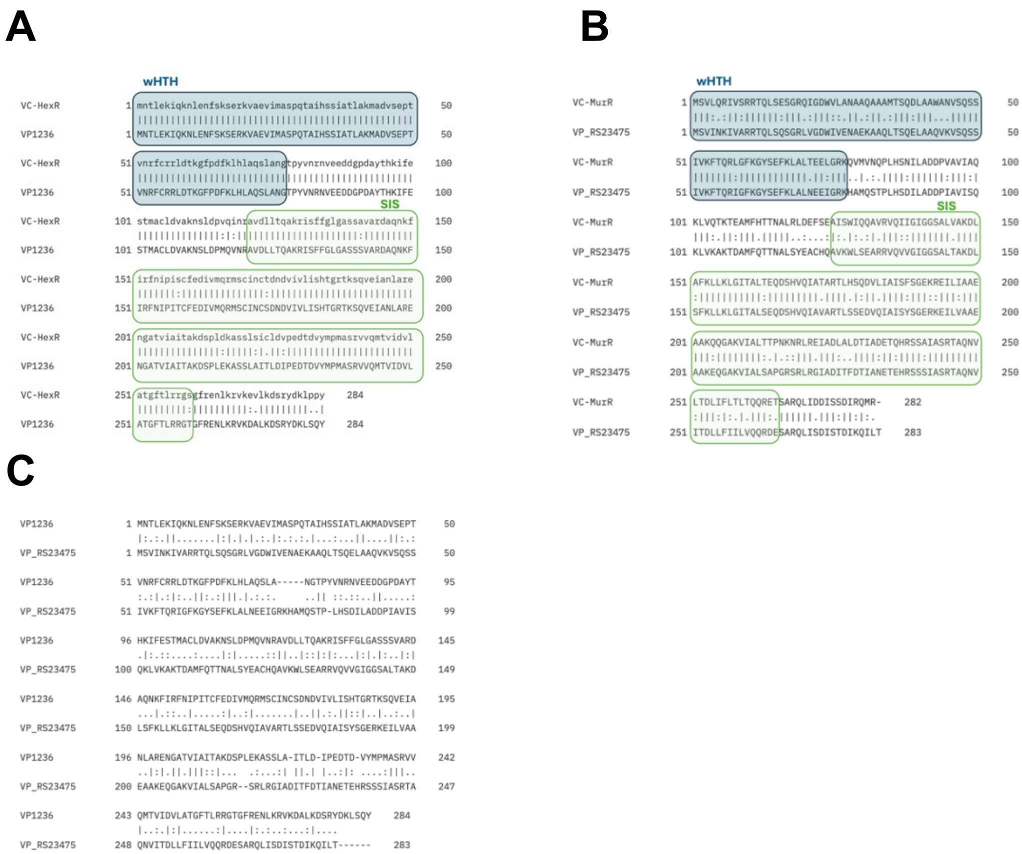

Figure 3.2 Alignment of MurR/RpiR Family Transcriptional Regulators protein sequences in *Vibrio* spp.

| = conserved identical residue, : = conserved mutation, . = semi-conserved mutation. (A) Alignment of *V. cholerae* O1 biovar El Tor str. N16961 HexR (VC-HexR) protein sequence aligned to *V. parahaemolyticus* RIMD 2210633 VP1236 protein sequence using EMBOSS Needle (EMBL-EBI). N-terminal winged helix-turn-helix (wHTH) (1-77aa) domain and C-terminal sugar isomerase (SIS) domain (120-260aa). Domains annotated using InterProScan (Interpro). Identity: 95.1%, Similarity: 98.6%, Gaps: 0%. (B) Alignment *V. cholerae* O1 biovar El Tor str. N16961 MurR (VC-MurR) protein sequence and *V. parahaemolyticus* VP_RS23475 generated using EMBOSS Needle (EMBL-EBI). VP_RS23475 is a SIS-Domain containing protein and was identified as potential MurR homologue by using NCBI BLAST and searching VC-MurR protein sequence against *V. parahaemolyticus* RIMD 2210633 genome. N-terminal winged helix-turn-helix (wHTH) (1-77aa) domain and C-terminal sugar isomerase (SIS) domain (125-265aa). Domains annotated using InterProScan (Interpro). Identity: 70.0%, Similarity: 86.6%, Gaps: 0.4% (C) Pairwise sequence alignment of VP_RS23475 to VP1236 protein sequence using EMBOSS Needle (EMBL-EBI). Identity: 25.0%, Similarity: 45.5%, Gaps: 5.8%.

3.2.2 HexR is an important regulator for growth on diverse nutrient sources

To assess the role of HexR in *V. parahaemolyticus* fitness, a chromosomal *hexR* deletion (*ΔhexR*) and a *hexR* genetic complement were generated. Complementation of *hexR* allows for *hexR*-specific conclusions to be made based on the results. Given that the *vp1236* transposon mutant had decreased fitness on the defined carbon source of chitin and that *vp1236* may be functionally alike to HexR, I first assessed the growth of WT *V. parahaemolyticus, hexR* mutant, and complement strain in both rich and minimal nutrient sources. In rich LB media, WT growth followed a classical sigmoidal curve and reached stationary phase at around 800 minutes with a maximum OD_{600nm} of 0.196. The mutant *vp1236* strain followed a similar growth trend (slope of growth curve) but entered stationary phase much earlier, at around 400 minutes. Notably, in late stationary phase (around 550 minutes) it began to have a statistically significant decrease in growth with a maximum OD_{600nm} of 0.157. In support, genetic complementation with WT *hexR* in trans restored growth trend to WT levels, emphasizing the growth defect is due to the deletion of *hexR* (Figure 3.3A).

The *hexR* mutant growth defect was exacerbated in the metabolically demanding Marine M9 (MM9) media containing glycerol as the sole carbon source. Glycerol is metabolized into dihydroxyacetone-phosphate (DHAP) which can enter either the glycolytic or gluconeogenic pathways (150). In *P. putida,* growth on glycerol as a sole carbon source is characterized by a prolonged lag phase (151). Glycerol utilization genes (*glpFK*) are repressed upon entry into a glycerol-rich environment and expression is dependent on stochastic gene expression overcoming the de-repression. Previous studies have demonstrated the switch between non-growing and a growing state to be dependent on metabolic pathway activity. As such the transition from lag phase into log phase only occurs once there is sufficient metabolic activity. While the WT *V. parahaemolyticus* strain did have an extended lag phase compared to rich (LB) conditions, the sigmoidal growth trend remained the same with a maximum OD_{600nm} of 0.054. In contrast, the *hexR* mutants had an extended lag phase in the first 750 minutes followed by statistically significant decrease in growth through log and stationary phase where cultures reached a maximum OD_{600nm} of 0.025 (Figure 3.3B). Consistently, complementation restored the growth phenotype back to WT.

Entrance into stationary phase prompts significant metabolic changes and the flux of carbon (152). Likewise, adaptations of bacteria into stationary phase include significant changes to cell morphology and physiology to allow the cell to persist during environmental stressors (e.g., changes in pH or nutrient depletion) (153, 154). Changes in CCM in a *hexR* deficient cell could result in significant impacts on bacterial fitness during this growth stage, as seen in the LB growth assay (Figure 3.3A). Therefore, I investigated the growth of the *hexR* mutant in spent media assays. Spent media was collected from stationary phase cultures, filter sterilized, and re-inoculated. The *hexR* mutant had an exacerbated growth defect in spent media, with a nearly flat growth curve, suggesting that the growth defect in late stationary phase in LB is likely due to the cells using up the accessible nutrients and being unable to metabolize what remains (Figure 3.3C-D). Strikingly, the *hexR* trans-complemented strain outgrew both WT and *hexR* mutants in a statistically significant manner (Figure 3.3C). This suggests that *hexR* overexpression provides an advantage in nutrient limited environments. I was then interested in whether WT *V. parahaemolyticus* growth could be increased by the overexpression of *hexR* in trans in nutrient-limited conditions. Indeed, WT *V. parahaemolyticus* expressing *hexR* had increased growth compared to WT strain (Figure 3.3D). Growth trends of the overexpression HexR strain and the complement were similar. Both strains entered stationary phase at 12 hours with an OD_{600nm} of approximately 0.7. While the WT strain had a growth defect (comparable to Δ*hexR*) in the first 12 hours of growth, it surpassed both overexpression and complement strains and did not enter stationary phase over the course of 24 hours.

Taken together, this suggest that while the overexpression of HexR provides a growth advantage in nutrient-limited environments, ultimately strains with coordinated CCM (WT) have the greatest fitness advantage over CCM-active but deregulated (overexpression and complement strains) cells (see discussion).

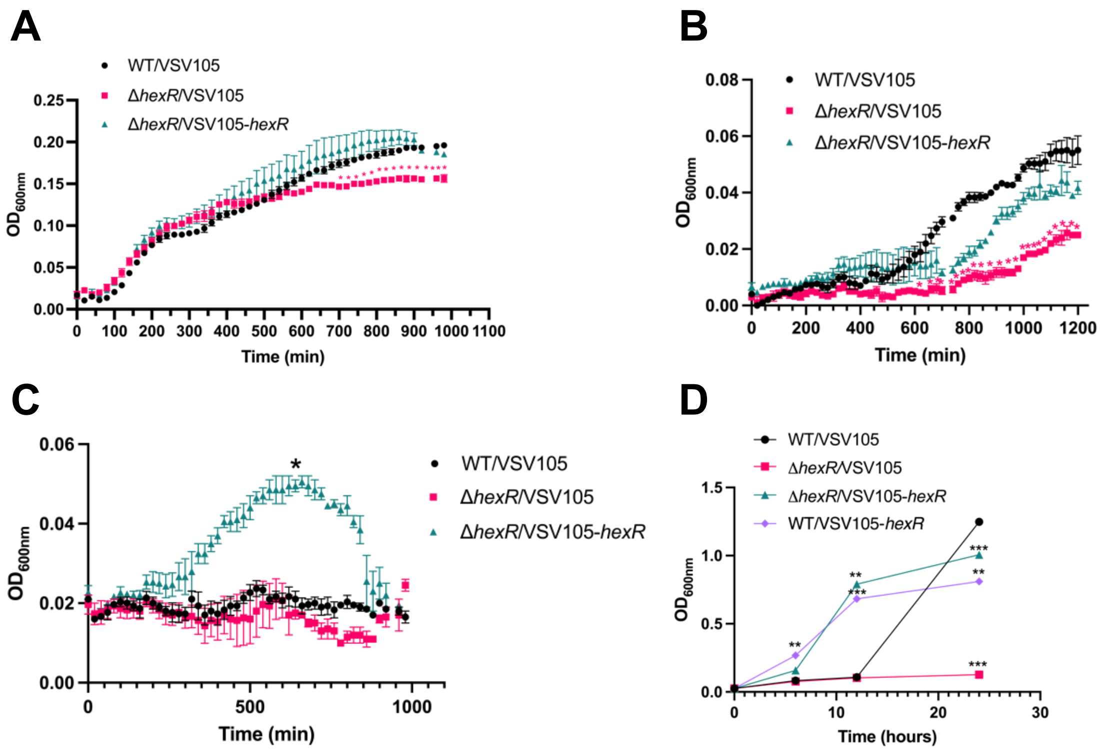

Figure 3.3 *hexR* mutants have a growth defect in rich and minimal media.
A) Mutant has a statistically significant growth defect in stationary phase in LB. Experiment was repeated three times. Strains were cultured overnight in LBS and normalized to starting OD_{600nm} of 0.025. OD_{600nm} were taken every 20 minutes for 14 hours at 37°C in a VictorX5 Multi Label plate reader. Statistical significance was measured with unpaired t-test (n=3, *:p < 0.05). (B) Mutant has an extended lag phase followed by a statistically significant growth defect in log and stationary phase in MM9. Strains were cultured overnight in LBS and normalized to starting OD_{600nm} of 0.025. OD_{600nm} were taken every 20 minutes for 14 hours at 37°C in a VictorX5 Multi Label plate reader. Statistical significance was measured with unpaired t-test (n=3, *:p < 0.05). (C) Overnight LBS cultures were inoculated into Spent Media at a starting of OD_{600nm} of 0.025. OD_{600nm} were taken every 20 minutes for 14 hours at 37°C in a VictorX5 Multi Label plate reader. Statistical significance was measured with unpaired t-test (n=3, *:p < 0.05). (D) *hexR* overexpression strains grown in Spent Media. Overnight LBS cultures were inoculated into Spent Media at a starting of OD_{600nm} of 0.025. OD_{600nm} was taken every 6-12 hours for 24 hours in duplicate on a spectrophotometer. Statistical significance was measured with unpaired t-test (n=3, **:p < 0.01, ***:p<0.001).

3.2.3 HexR is an important regulator for growth on chitin as a sole carbon source

Chitin is one of the critical carbon sources utilized by *V. parahaemolyticus* during its aquatic lifestyle. To validate the TN-seq observations, I performed growth assay with WT, Δ*hexR*, and *hexR* complement strains using MM9 supplemented with 0.4% colloidal chitin as a sole carbon source. Due to the insoluble properties of chitin, chitin can be chemically modified to generate colloidal chitin. Colloidal chitin has a smaller particle size which facilitates homogenous distributed in solution. Basic preparation of colloidal chitin involves manual pulverizing followed by acid hydrolysis. Large chitin chunks are filtered out and the remaining chitin is precipitated. The colloidal chitin puck is then extensively washed and neutralized (pH ~7) and can be used for further applications (155, 156).

Since colloidal chitin contains solid flakes, I was not able to measure cell growth using OD_{600nm} measurements in the plate reader. Instead, I developed an assay where colony counts (CFU/ml) were measured over time and where at every time point, aliquots were serially diluted, plated, and colonies were counted. Since WT *V. parahaemolyticus* can use chitin as a sole carbon source in the marine environment (132, 157), I expected to observe the WT strain to follow classical sigmoidal growth over the course of 54 hours (Figure 3.4A). Unexpectedly, while the *hexR* mutant had a statistically significant growth defect in the first 16 hours, the mutant strain consistently outgrew the WT strain by 20 hours and continued this growth trend until reaching stationary phase at a CFU/ml similar to WT by 54 hours (Figure 3.4A). When *hexR* was complemented, the mutant strain returned to WT levels of growth. Therefore, while *hexR* mutants do display reduced growth, in isolation the strain can use chitin as a sole carbon source.

Since this observation of de-regulated growth was contradictory to previous growth assays and the Tn-seq data, I next investigated the competitive fitness of WT and *hexR* mutants. I hypothesized that the short growth defect early on in the chitin growth curves may have contributed to the *hexR* mutant disappearing from the sequenced population in the TN-seq experiment while in isolation the bacteria is able to overcome this defect and once primed for growth on chitin, can rapidly use the metabolites for required biogenesis (Figure 3.4A). WT and *hexR* mutants containing Tn5-GFP transposons were generated for a head-to-head competition assay. If the transposon inserts directly adjacent to an active promoter, cells will transcribe the GFP allele, allowing for GFP expression and strain identification by green fluorescence. The non-fluorescent *hexR* mutant strain contained the transposon (same strain genetic background, but the transposon insertion was not adjacent to an appropriate promoter) and did not produce GFP. Both WT::Tn5-GFP (+) and Δ*hexR*::Tn5-GFP (-) strains used in the experiment were screened for any transposon-associated growth defect by performing growth assays in LB. The selected strains had no significant changes in growth compared to parental WT or *hexR* mutant strains (data not shown). Following inoculation at the same starting OD_{600nm} into MM9 (0.4% colloidal chitin), serial dilutions of the cultures were plated over the course of 48 hours. There was no significant change in growth of either WT or *hexR* mutant strains during the first 24 hours post-inoculation (Figure 3.4B). In contrast, the WT strain significantly outgrown the *hexR* mutant at 48 hours. The average competition index (CI) of the *hexR* mutant at 48 hours was approximately 0.4 (Figure 3.4C). Given that a CI < 1 indicates a fitness defect, these results support that in mixed culture, cells lacking functional *hexR* are at a disadvantage and have a statistically significant growth defect in chitin (see discussion). Taken together, the competition assay data supports the results of the TN-seq experiment, validating that *hexR* is a critical fitness determinant in chitin as a sole carbon source.

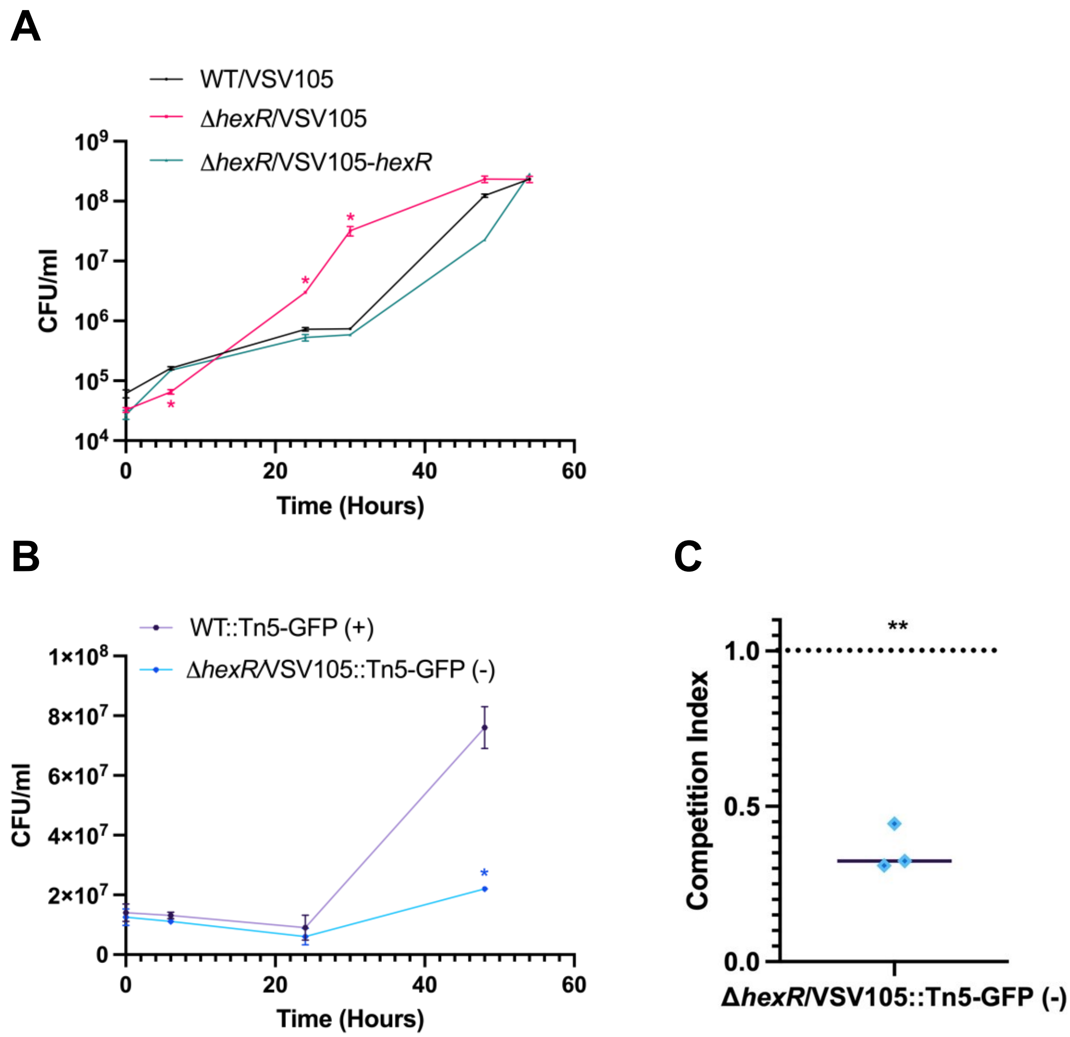

Figure 3.4 HexR is a fitness determinant for *V. parahaemolyticus* on chitin as a sole carbon source. (A) Overnight LBS cultures of strains were inoculated into M9 Minimal Media containing colloidal chitin as a sole carbon source. Samples were collected every 6-12 hours for 54 hours. Serial dilutions were plated to determine the number of cells present. Statistical significance was measured with unpaired t-test (n=3, *:$p < 0.05$). (B) Competition assay to assess fitness defect of *hexR* mutants compared to WT *V. parahaemolyticus*. Overnight LBS cultures of WT GFP (+) transposant and Δ*hexR* GFP (-) transposant were inoculated together into MM9 (0.4% colloidal chitin) at a starting OD_{600nm} of 0.025. Samples were collected every 6-12 hours for 48 hours. Serial dilutions were plated to determine the number of fluorescent cells and total cells present. Statistical significance was measured with an unpaired t-test (n=3, *: $p<0.05$) (C) Competition index (CI) calculated for Δ*hexR* GFP (-) transposants at final timepoint t=48h. Dotted line is at CI=1 and CI < 1 indicates a fitness defect. Statistical significance was measured with unpaired t-test (n=3, ** $p<0.01$).

3.2.4 HexR is a regulator for biofilm formation, cell differentiation, and motility

V. parahaemolyticus employs a numerous of mechanisms to adapt and survive in the marine water column. Notably, biofilms contribute significantly to the aquatic survival of *V. parahaemolyticus* and require considerable investment in the synthesis and export of polysaccharides (108). Robust biofilm formation is additionally critical for chitin catabolism as initiation occurs post-cellular attachment to chitin. Since the *hexR* mutants displayed growth defects on various nutrient sources, this led me to investigate biofilm formation. Initial assays were performed in MM9 with 0.4% Glycerol which resulted in successful biofilm formation in WT and complement backgrounds but *hexR* mutant biofilms were unable to adhere to glass tubes for crystal violet staining and quantification. This led me to supplement the MM9 media with 0.2% casamino acids. Casamino acids are a mixture of amino acids, relieving the cell from synthesizing all required molecules *de novo.* As expected, WT *V. parahaemolyticus* displays robust biofilm formation. However, the *hexR* mutant has a statistically significant reduction in biofilm formation even when cell number is normalized (Figure 3.5A). Complementation restored biofilm formation to WT indicating biofilm formation is at least somewhat regulated by HexR. To note, all strains could form robust biofilms in rich media indicating biofilm biosynthesis machinery was still intact.

Previous studies have investigated the role of transcriptional regulators in central carbon metabolism (CCM) of gram-negative bacteria (158, 159). Mutations in these central regulators often lead to defects in cell morphology (109, 110). As well, in minimal media and chitin sources, *V. parahaemolyticus* exhibits elongated cell morphologies as a response to environmental cues (73). This prompted me to investigate whether *hexR* plays a role in *V. parahaemolyticus* cell morphology. Observations of cells in LB media revealed no apparent differences in cell shape (Figure 3.6A). In liquid environments, *V. parahaemolyticus* cells are rod shaped swimmer cells. In contrast, WT cells cultured in nutrient limiting MM9 developed a filamentous subpopulation of cells. These cells are likely the differentiated cell state known as swarmer cells (73). Strikingly, *hexR* mutant cells remained rod-shaped and lacked any filamentous cells (Figure 3.6A). Genetic trans complementation restored the filamentous cell subpopulation. This phenotype was extremely robust across multiple microscopy observations. Given how consistent these observations were, I quantified the filamentous subpopulation. Across 50 fields of view (FOV) with a minimum of 30 cells, the filamentous swarmer cells made up 20-30% of the total cells observed in both WT and complement backgrounds but were completely lacking in the mutant background (Figure 3.6B). Based on this striking phenotype, I concluded that HexR is a significant contributor to the swarmer cell morphology (see discussion).

V. parahaemolyticus morphology and motility are linked, therefore I quantified the swimming motility of these strains (89). *V. parahaemolyticus* cells are highly motile in the aquatic environment where the different cell morphologies (swimming and swarming cells) utilize different flagellar systems to promote dissemination and colonization (80). By stab inoculating each strain in soft agar LBS medium (0.2% w/v agar), swimming motility could be quantified via measurements of dense outward radial growth. As expected, measurements of radial growth confirmed WT *V. parahaemolyticus* motility. In contrast, *hexR* mutants had a statistically significant increase in radial growth indicative of increased cell motility (Figure 3.5B). This increase in swimming motility was lost following genetic complementation with *hexR*. This data reveals that HexR contributes to regulated motility, and more specifically that its absence leads to increased motility (see discussion).

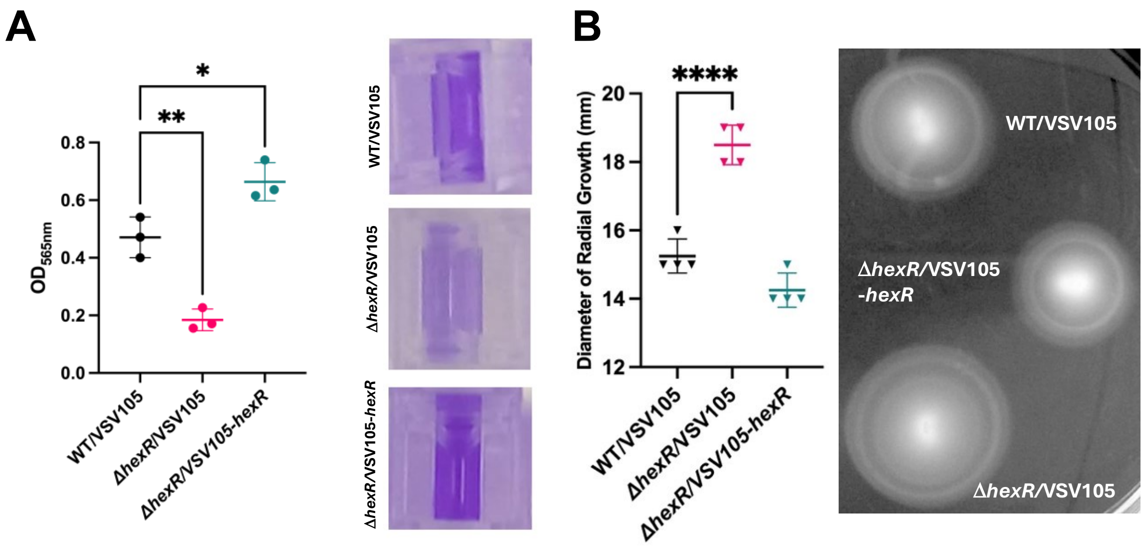

Figure 3.5 HexR is a regulator of *V. parahaemolyticus* biofilm and motility.
(A) Biofilm formation of strains grown in MM9 (0.4% Glycerol, 0.2% Casamino Acids) for 18 hours at 37°C. Each dot represents an individual sample. Statistical significance was measured using a t-test (n=3, *:$p < 0.05$, **: $p < 0.01$). After de-staining of biofilms, retained 0.5% crystal violet (CV) stain is collected for OD_{565nm} measurement. Representative image shown (right) of cuvettes containing CV aliquot post-staining. Intensity of stain is indicative of amount of biofilm formed. (B) Quantification of swimming via measurement of diameter of radial growth. Strains were cultured overnight in LBS, normalized to OD_{600nm} of 0.05 in 1x MM9 salt and stab inoculated into 0.2% (w/v) agar LBS plates. Measurements were recorded after 5 hour incubation at 37°C. Statistical significance was measured using a t-test (n=4, ****:$p < 0.0001$). Each dot represents a biological replicate. Representative image shown (right) of radial growth patterns on agar swimming plate.

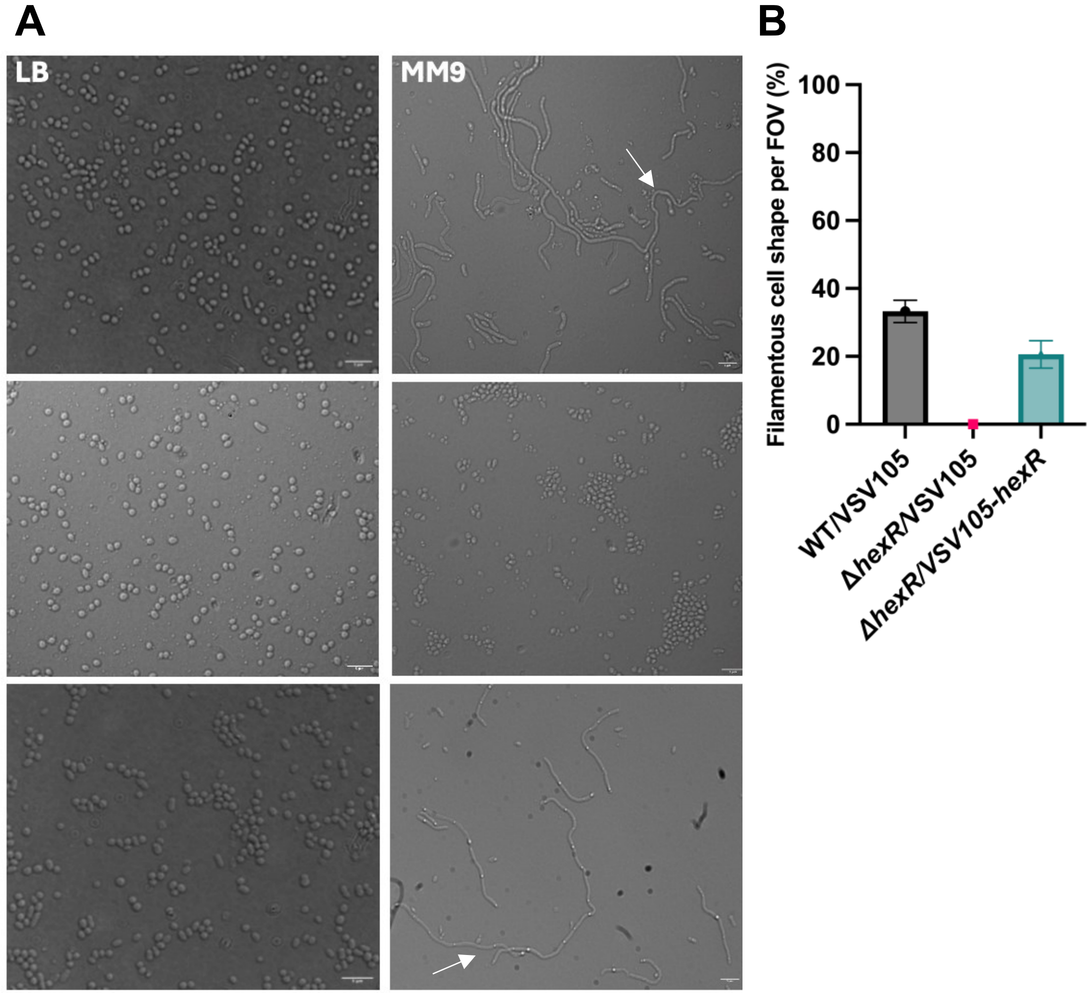

Figure 3.6 HexR is a regulator of *V. parahaemolyticus* cell differentiation.
(A) Observations of WT, *hexR* mutant, and complement strains (Top to Bottom) using DIC microscopy at 100x. Strains were imaged after 16 hours of growth in MM9 (0.4% Glycerol) or LB. White arrow indicates filamentous cells. Scale bar = 5µm.
(B) Quantification of filamentous subpopulation. All cells were counted and elongated cells further enumerated to determine the percentage (%) of filamentous cells per field of view (FOV).

3.2.5 HexR regulates carbon metabolism-associated genes

Unlike other proteobacteria, the HexR regulon of *Vibrio* spp. is broad, allowing the bacterium to adapt cellular metabolism to best suit available nutrients and abiotic extracellular conditions. The ability to adjust the flux of metabolites to support the equilibrium of anabolic and catabolic pathways maintains bacterial fitness throughout the diverse array of environments (e.g., free-swimming in the water column, chitin-associated biofilms, and in the human intestine) *V. parahaemolyticus* encounters during its lifecycle. Therefore, disruptions to CCM via the chromosomal deletion of *hexR* is likely contributing to the fitness defects as observed in biofilm formation, growth, and cellular morphology.

To further confirm VP1236 functional identity as HexR and to provide evidence that the *hexR* mutant phenotype is due to a deregulation of underlying CCM pathways, I assessed the promoter activity of three predicted *V. parahaemolyticus* HexR regulon members: Glycogen Debranching Enzyme (*glgX;* Locus Tag: VPA1645), Glucose-6-P dehydrogenase (*zwf;* Locus Tag: VP1710) and Glucose-6-P isomerase (*pgi;* Locus Tag: VP2731) in both the WT and Δ*hexR* strains. These regulon members were selected based on the HexR consensus sequence (TGTAATTAAATTAACA) scores identified on RegPrecise (ranging from 4.5 to 7.8) but have not been experimentally validated as genes regulated by HexR in *V. parahaemolyticus*. The consensus sequence score represents the likelihood of each base occurring at each location of the motif. Lux assays were performed in LB which *hexR* mutants were shown to have a statistically significant growth defect in late stationary phase and multiple timepoints (2 hours to 3.5 hours post-subculture) were recorded to best capture when the promoters were active during growth.

While I was interested in the activity of these promoters in more metabolically demanding media (e.g. MM9), my previous microscopy has shown that the morphology of the cell populations is non-homogenous across WT and *hexR* mutant strains. Therefore, any OD_{600nm} measurement taken could be artificially inflated/non-representative of the actual cell density at the time of measurement (160). I assessed promoter activity using the vector pVSV105 containing the luxCDABE cassette. Cloning the promoter upstream of this cassette drives the production of light, recorded as Counts Per Second (CPS). A difference in light production from the *hexR* mutant to the WT strain would indicate a regulatory role for *hexR* at this specific locus.

Zwf catalyzes the first step of the oxidative pentose phosphate pathway (PPP) and the Entner-duodoroff (ED) pathway, where glucose-6P is converted into gluconate-6P. Gluconate-6P can either enter the PPP via 6-phosphogluconate dehydrogenase or the ED pathway via phosphogluconate dehydratase (161). The primary role of the oxidative PPP is the generation of cofactors like NADP and NADP(H) which provide reducing power. In contrast, the non-oxidative PPP produces vitamins, nucleotides, and amino acids necessary for growth (162). Therefore, I expected that any dysregulation of the PPP would contribute to the fitness defects of the *hexR* mutant across the diverse carbon sources. Interestingly, *zwf* promoter activity in the *hexR* mutant was significantly higher than WT at each time point (Figure 3.7A). While comparative genomic approaches did not identify *zwf* as a member of the reconstructed *V. parahaemolyticus* HexR regulon, *zwf* is a member of the *P. putida* HexR regulon and is transcriptionally repressed by HexR (142). In line with those observations, HexR appears to also act repressively at the *zwf* locus in *V. parahaemolyticus,* implicating *zwf* as an additional member of the HexR regulon and emphasizing the importance of strict regulation of the PPP.

As well, promoter activity of *glgX* was significantly different in the *hexR* mutant compared to WT. Unlike *zwf*, *glgX* promoter activity in the *hexR* mutant steadily increased at 3 hours but then fell at 3.5 hours (Figure 3.7B). In comparison, the WT strain alternated high and low expression levels over the course of the time points. GlgX is a key enzyme in glycogen metabolism, responsible for cleaving the α1-6 linkages, and in *E. coli,* the enzymes responsible for glycogen biosynthesis and degradation appear to be expressed concomitantly. As well, synthesis of glycogen is known to occur when carbon sources are abundant, but another essential nutrient is limiting (163). The more variable expression over the time course could be the bacterium responding to changes in nutrient concentrations of the rich media (see discussion).

Pgi is an enzyme that catalyzes the conversion of glucose-6-phosphate to fructose-6-phosphate. As such, it plays an important role in glycolysis, gluconeogenesis, the PPP, and the production of reducing power for the synthesis of biomass. Disruptions of *pgi* in *E. coli* have demonstrated significant rerouting of CCM towards the PPP rather than glycolysis (164) and *V. cholera* lacking functional *pgi* have significant cell morphology defects by the formation of spherical cells and the accumulation of toxic glycolysis intermediates (109). Given HexR is predicted to be the transcriptional regulator of *pgi,* I expected *hexR* mutants to have deregulated *pgi* expression resulting in considerable effects on glycolysis, gluconeogenesis, and the PPP. Indeed, the promoter activity of *pgi* in the hexR mutants was significantly increased in comparison to WT over each timepoint (Figure 3.7C), indicating the central role of this enzyme in carbon metabolism pathways.

These preliminary *in vivo* assays provide evidence of deregulated CCM in the *hexR* mutants and confirms *zwf, glgX,* and *pgi* as members of the HexR regulon. Furthermore, this data supports the *in silico* analyses of VP1236 as the functional homologue of HexR in *V. parahaemolyticus.*

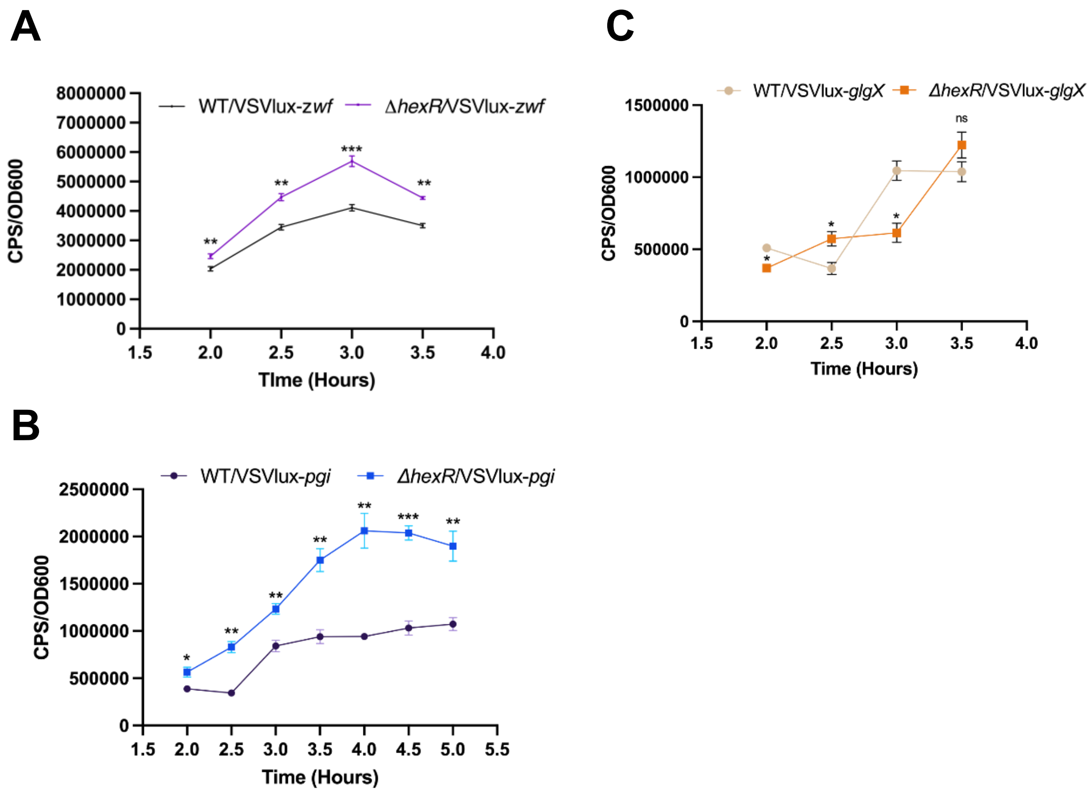

Figure 3.7 CCM-associated regulons are deregulated in *hexR* mutants.
(A) Lux Reporter assay of *zwf* promoter region in WT and hexR mutants. Strains were grown overnight in LBS and inoculated at a starting OD_{600nm} of 0.05 into LB. CPS and OD_{600nm} readings were taken 2 hours post-subculture every 30 min. Statistical significance was calculated using a t-test (n=3, **: p<0.01, ***: p<0.001). (B) Lux Reporter assay of *glgX* promoter region in WT and *hexR* mutants. Strains were grown overnight in LBS and inoculated at a starting OD_{600nm} of 0.05 into LB. CPS and OD_{600nm} readings were taken 2 hours post-subculture every 30 min. Statistical significance was calculated using a t-test (n=3, *: p<0.05). (C) Lux reporter assay of *pgi* promoter region. Strains were grown overnight in LBS and inoculated at a starting OD_{600nm} of 0.05 into LB. CPS and OD_{600nm} readings were taken 2 hours post-subculture every 30 min. Statistical significance was calculated using a t-test (n=3, **: p<0.01, ***: p<0.001).

3.2.6 *V. parahaemolyticus* HexR is a regulator at the *nagZ – murQP* locus

Vibrio spp. commonly have multiple copies of the *murQP* locus, a characteristic that differs from other Proteobacteria (e.g., *E. coli* or *Pseudomonas aeruginosa*). One is frequently associated in the same genomic region as *murR,* perhaps acting as the MurQP homologue and implicated in CW recycling. Indeed, NCBI blastp using *E. coli* MurR in the *V. cholerae* O1 biovar El Tor str. N16961 identified VC-MurR (40.88% identity, E-value: $3x10^{-65}$). However, the role of the other *murQP* copy is not clear. In *V. parahaemolyticus,* a *murQP* locus is located divergently from a β-hexosaminidase (NagZ) on chromosome 1. NagZ catalyzes the conversion of imported periplasmic AnhMurNac-GlcNac into AnhMurNac and GlcNac derivatives by cleaving at the β-1,4 linkage between GlcNac and β-anhydro-N-acetylmuramic acid peptides in the cytoplasm (165). Another target of interest was the intergenic region of *murQP* on chromosome 2 which is located divergently from the putative VP-MurR (locus tag: VP_RS23475). While all evidence supports a HexR-like functional identity of VP1236, I wanted to thoroughly assess the potential of MurR-like activity by quantifying any promoter activity at the *murQP* loci. Using a lux reporter assay, I assessed *hexR* regulatory activity at the loci of *murR-murQP* and *nagZ-murQP.*

The *murQP* locus located on chromosome 2 (CII) shows little *hexR*-dependent activity. Differences in expression between WT and the *hexR* mutant were non-significant (Figure 3.8A). This data supports the *in silico* analysis, indicating that *murQP* (CII) is likely the *V. parahaemolyticus* cell wall recycling *murR-murQP* homologue.

While expression of *murQP* (CI) showed no significant changes in the *hexR* mutant (Figure 3.8B), expression of *nagZ* was significantly increased following 3.5 hours of subculture in LB (Figure 3.8A). This suggests a potential regulatory role for HexR at the *nagZ* locus. In *E. coli,* NagZ is implicated in CW recycling and *nagZ* null mutants have been found to accumulate cytoplasmic amino sugars during growth in LB thus supporting a potential role for NagZ in CCM as well in *V. parahaemolyticus* (see discussion) (165).

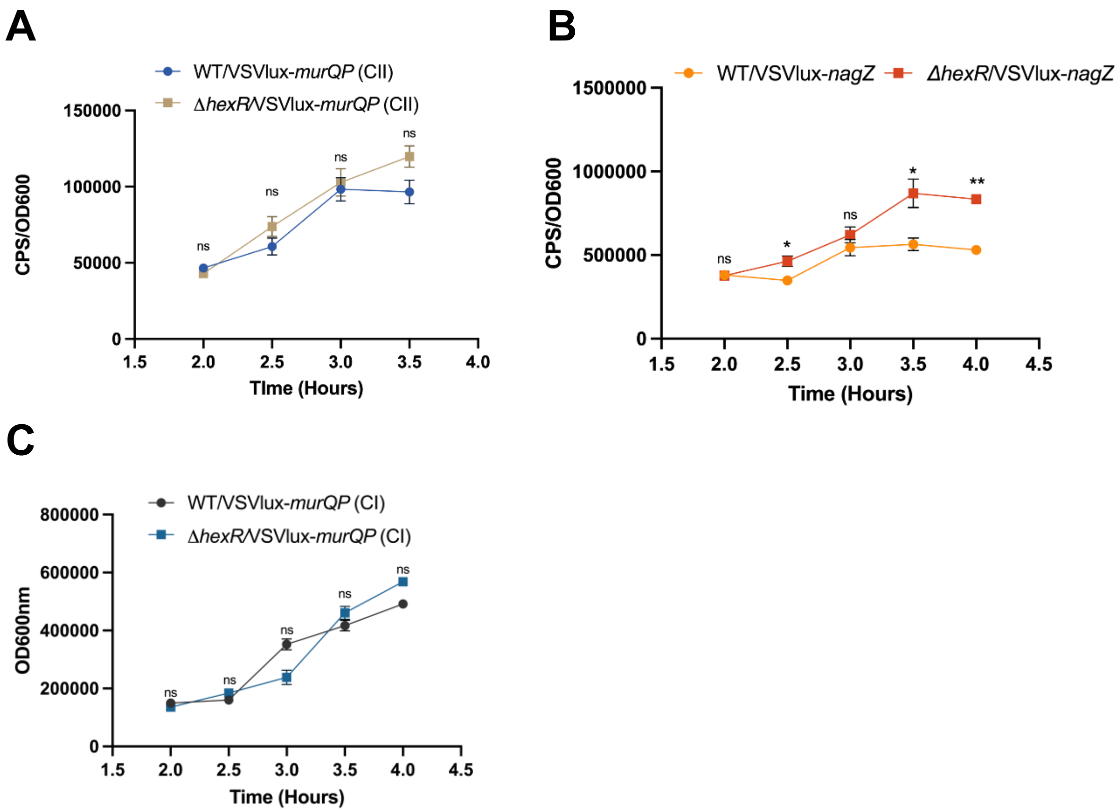

Figure 3.8 HexR is a regulator of *nagZ* expression but not *murQP* on chromosome 1. (A) Lux reporter assay of *murQP (CII*) promoter region. Strains were grown overnight in LBS and inoculated at a starting OD_{600nm} of 0.05 into LB. CPS and OD_{600nm} readings were taken 2 hours post-subculture every 30 min. Results are non-significant (n=3). (B) Lux Reporter assay of *nagZ* promoter region in WT and *hexR* mutant in V. parahaemolyticus. Strains were grown overnight in LBS and inoculated at a starting OD_{600nm} of 0.05 into LB. CPS and OD_{600nm} readings were taken 2 hours post-subculture every 30 min. Statistical significance was calculated with a t-test (n=3, *:p<0.05, **:p< 0.01). (C) Lux Reporter assay of *murQP (CI)* promoter region in WT and hexR mutants in V. parahaemolyticus. Strains were grown overnight in LBS and inoculated at a starting OD_{600nm} of 0.05 into LB. CPS and OD_{600nm} readings were taken 2 hours post-subculture every 30 min. Differences are non-significant (n=3)

Chapter 4 Investigation of HlyU-regulated genetic loci in *Vibrio parahaemolyticus*

4.1 Introduction

Vibrio spp. are facultative pathogens and do not require constant expression of virulence-associated genes. Overexpression of non-essential genes is costly to the cell. It is only once the bacteria have entered a host (e.g., marine organism or human) that the expression of virulence factors is necessary (166). Pathogenic *Vibrio* spp. utilize numerous virulence factors to colonize within a host, evade host immunity, disseminate, and ultimately cause infection (167). Therefore, understanding the contributions of genetic regulatory mechanisms of virulence-associated genes is important for understanding bacterial pathogenesis.

A proposed mechanism for gene regulation is via the architecture of the DNA. The Watson and Crick model postulates that DNA resides in a static B-form state characterized by negative supercoiling (168). Maintenance of this helical state determines the collection of bound proteins and acts as a repository of genetic information (169). However, biological information is encoded in both the sequence of nucleotides and the topology of the DNA (169). Intrinsic features of DNA, including inverted repeats, nucleotide enrichment, supercoiling, and DNA-binding proteins, can cause local conformational changes resulting in the formation of complex DNA superstructures (170, 171). Notable DNA superstructures that deviate from the canonical B-helical form include cruciform, Z-DNA (172), triplexes, G-quadruplexes (173), hairpins, and Holliday junctions (174, 175).

Notably, DNA cruciform, unusual 4-way DNA junctions formed by intra-strand stem loops, have been proposed as a novel regulatory mechanism of gene expression (176). Certain A/T rich DNA sequences are more prone to cruciform formation due to the presence of more than one of the intrinsic features highlighted above. Critically, inverted repeats, stretches of nucleotides followed by their reverse complement which flank a spacer element, can make up the key stem structure of the cruciform by forming hydrogen bonds with bases on the same strand (177). Inverted repeats are ubiquitous across prokaryotic genomes but are enriched at promoters and origins of replication, suggesting a functional role in gene expression or DNA replication (171, 178). The structure of a cruciform is energetically unfavorable due to the unbound bases in the spacer element of the hairpin loop and the disruption of the B-helical state. Therefore, energy in the form of negative supercoiling is required to facilitate cruciform formation (179).

Negative supercoiling can be induced and maintained in multiple ways. Firstly, by the start of transcription: as RNA polymerase and DNA topoisomerase unwind the DNA to promote transcription, the coding strand is displaced and forced to coil as the polymerase reads the DNA. This translocation of the DNA generates negative supercoiling behind the transcription complex (180) which can arrest gene expression in neighboring genes. Alternatively, DNA-binding proteins can induce conformational changes in the DNA to either promote or inhibit transcription via changes in DNA structure. Histone-like Nucleotide Structuring protein (H-NS) is an incredibly abundant protein that binds chromatin and constrains negative supercoiling (181), thus maintaining DNA topology. H-NS has a high affinity for A/T rich regions of DNA, a characteristic of transcriptionally active gene promoters (182, 183), making it a prolific global gene regulator with the ability to alter DNA accessibility by inducing DNA loop formation (DNA-protein-DNA bridges) or long H-NS polymers which prevent the RNA polymerase and transcriptional activators from binding the promoter (184, 185). *hns* mutants typically have decreased growth rate compared to WT cells which is worsened under low temperatures and have increased sensitivity to changes in osmolarity (186). Specifically, it has been observed that the binding of H-NS to A/T rich intergenic regions and the constraining of negative supercoiling, inhibits gene expression (187–189). Since inverted repeats are enriched in promoter regions, the negative supercoiling facilitated by H-NS provides the energy to form a H-NS-associated cruciform (175) which may block promoter activity by overlapping with the -10 and -35 sequences of the promoter (190), preventing RNA polymerase binding and transcription complex formation (191). It is in this manner, that bacteria can use alternative DNA structures like cruciform to repress gene expression.

However, upon environmental stimuli the cell would seemingly require a mechanism to relieve the transcriptionally repressive DNA cruciform to allow for gene expression. One possible mechanism to de-repress DNA cruciform is by protein-binding, especially in cases where proteins have high affinity for bent rather than relaxed DNA (192). While protein binding can promote cruciform formation, like in the case of H-NS or the eukaryotic protein PARP-1 (193), some proteins can also relieve cruciform elements. Notably, *V. parahaemolyticus* employs the DNA-binding transcriptional regulator HlyU during infection to relieve a cruciform that regulates the expression of the T3SS-1 (54, 101).

V. parahaemolyticus relies on many virulence factors during infection but the T3SS-1 and 2 remain critical virulence determinants. The T3SS-1 is a molecular syringe that secretes effector proteins into host cells during early infection, contributing to host cell killing and cytotoxicity, and is present in all clinical and environmental isolates (194, 195). The T3SS-1 is regulated by the ExsACDE cascade, where ExsA acts as a master transcriptional regulator of 40+ genes that contribute to T3SS-1 expression (196, 197). ExsA expression is regulated by the transcriptionally repressive H-NS along with HlyU. During host colonization, HlyU binds the A/T rich palindrome within the DNA cruciform at the cryptic promoter in the *exsB-exsA* intergenic region and relieves the H-NS-associated superstructure. This kickstarts promoter activity of *exsA,* and transcribed *exsA* results in ExsA protein expression that autoregulates the *exsA* promoter, further upregulating *exsA* transcription. Increased *exsA* expression results in the downstream expression of the ExsA-dependent T3SS-1 operons to produce a functional T3SS-1 apparatus for effector translocation during infection (101).

HlyU is a small homodimeric protein with a wHTH DNA binding motif. The protein belongs to the Metalloregulator ArsR/SmtB family transcriptional regulators but lacks the key metal binding residues characteristic to the rest of the family (198). The core helix of the motif interacts with the major groove of the DNA whereas the winged regions bind the minor grooves (199). Binding of HlyU to its DNA targets introduces a bend to the DNA to bring the wHTH motif in contact with the major and minor grooves (198), promoting HlyU-specific gene regulation.

HlyU is a critical virulence determinant for *in vivo V. vulnificus* infection (200), with *V. cholerae hlyU* mutants having 100-fold increase in LD_{50} compared to wild-type

(201), and has been implicated in overcoming other H-NS-mediated silencing of virulence-associated genetic loci in *Vibrio* spp. (202, 203). Liu et al. (2009) propose that to overcome the H-NS repressive effect, HlyU relieves DNA supercoiling upon binding to a distal site and bending DNA (203). The initial transcription of the cryptic promoter would then drive conformational changes that destabilizes the H-NS nucleoprotein complex, allowing for RNA polymerase activity and ultimately promoter expression (198).

HlyU activity is conserved across *Vibrio* spp., as it regulates multiple virulence factors across multiple species, namely the hemolysin HlyA and Type VI Secretion System-associated hemolysin-coregulated protein (Hcp) in *V. cholerae* (201, 204, 205), the repeat-in-toxin (rtx) RtxA1 in *V. vulnificus* (206), and the hemolysin Vah1 in *V. anguillarum* (207), along with 4 classes of exotoxins: cytolysins, secreted phospholipases, vibriolysins, and the multi-functional autoprocessing repeats-in-toxin (MARTX) (102, 208). As such, the protein is often considered a global virulence regulator. HlyU binding sites are characterized by A/T rich imperfect ~17bp palindromic sequences (207, 209) but no clear consensus sequence has been derived between *Vibrio* spp.

Given HlyU's role as a global virulence regulator in other pathogenic *Vibrio* spp., I hypothesized that along with the T3SS-1, HlyU regulates other virulence genetic loci in *V. parahaemolyticus.* Using an approach known as Chromatin-Immunoprecipitation coupled with next-generation sequencing (ChIP-seq), which allows for the global assessment of DNA-protein binding and is commonly used to investigate and map transcriptional regulators (210), I can broadly investigate how genes are coordinately regulated by HlyU during *V. parahaemolyticus* infection.

4.2 Results

4.2.1 Genome-wide screen of HlyU-binding regions in *V. parahaemolyticus*

Given that HlyU is known as a global virulence regulator in *Vibrio* spp. (102), I investigated HlyU binding at genetic loci on chromosome 1 and 2 of *V. parahaemolyticus* using ChIP-seq. It is critical to carry forward the appropriate control strains to determine the amount of background non-specific protein-DNA binding. For this experiment, I used a FLAG-tagged *hlyU* complement strain (Δ*hlyU*/VSV105-*hlyU*-FLAG) to identify HlyU-specific binding to the genome and as my control, the strain Q55A which is the *hlyU* complement strain with a glutamine to alanine mutation in the DNA-binding domain (Δ*hlyU*/VSV105-*hlyU*(Q55A)-FLAG). The Q55A strain should not be able to bind DNA and has been shown experimentally to have reduced cytotoxicity in HeLa cells in comparison to WT or HlyU complement strains (data not shown). Unlike other conventional ChIP-seq controls: DNA input (sheared crosslinked DNA-protein complexes that are not selectively enriched) and IgG mock immunoprecipitation (211), Q55A allows for the identification of non-HlyU specific DNA-protein interactions. Indeed, DNA was immunoprecipitated from the Q55A input and peaks were identified in the Q55A control input that were also present in the complement strain, speaking to the importance of having appropriate controls for background (Figure 4.1C). Therefore, peaks present in the complement strain input but not in the Q55A input represent potential and higher confidence HlyU interacting sites in the genome.

Optimization of the ChIP-seq protocol allowed for the selection of ideal experimental conditions. All strains were grown in LB containing EGTA and $MgSO_4$, a calcium-deplete and magnesium-supplemented rich environment, which has previously demonstrated the ability to induce the expression of the T3SS-1 in *V. parahaemolyticus* (54, 197). Given that I am interested in identifying other virulence-associated loci, this media was a reasonable starting point. At 4 hours of induction, sufficient recombinant HlyU-FLAG was expressed in both strains and was separated into soluble and insoluble fractions as assessed by western blot (Figure 4.1A). Alternative induction timepoints of 2.5, 3, and 3.5 hours resulted in insufficient HlyU-FLAG recovery post fractionation. HlyU binding is transient, therefore protein-DNA complexes must be crosslinked. Formaldehyde was used as a chemical crosslinker due to its cell permeability, short spacer length (0.2nm) for the entrapment of closely associated proteins and DNA, and rapid reactivity to crosslink the complexes together (212). Since HlyU binds as a dimer to the DNA targets, alternative chemical crosslinkers (e.g. EGS/DGS) which can target large protein complexes were unnecessary. HlyU has a molecular weight of 11kDa and so the presence of higher molecular weight anti-FLAG specific species at 22kDa and 33kDa in the crosslinked samples but absent in non-crosslinked samples provides evidence of successful crosslinking (Figure 4.1A)

Immunoprecipitation allows for the selective enrichment of the HlyU-DNA complexes (213). Minimal optimization of immunoprecipitation was required. Overnight incubation with M2 anti-FLAG affinity matrix reduced amount of HlyU-FLAG in soluble fraction. Elution of HlyU-FLAG from the matrix using SDS-containing elution buffer subsequently increased HlyU-FLAG amounts in the aliquots (Figure 4.1B). SDS denatures the anti-FLAG antibody, causing an increase in higher molecular weight species. Additionally, *V. cholerae* encodes a protein ChiP (Locus Tag: FY484_RS04980) which has been experimentally shown to interact and bind anti-FLAG M2 antibodies (214). A homologue is present in *V. parahaemolyticus* which may also contribute to these higher molecular weight species. HlyU and contaminating proteins were digested with proteinase K and DNA was purified using a Qiagen PCR purification kit. To confirm pool of enriched DNA and estimate DNA concentration prior to library preparation, aliquots were run on 1X TAE agarose gel. Approximate DNA concentrations were determined to be 10-20ng/μL and sheared to ~800bp fragments (Figure 4.1C).

Library preparation was performed following the protocols of the NEB kits and size selection of DNA fragments excluded any fragments <200 bp in size. Shorter DNA fragments are biased during sequencing, resulting in overamplification and false positive peaks of enrichment. Likewise, qPCR was used to assess for adaptor dimers (120-170bp), which cluster on flow cells during sequencing and generate data. Adaptor dimers outcompete other DNA during next generation sequencing (NGS): 5% contamination results in 50% of reads being adaptor dimer sequences (215). Therefore, I performed repeated steps of size selection to remove adaptor dimers from the library pool prior to sequencing.

Consistent quality control checks during crosslinking and library preparation resulted in both *hlyU* complement and Q55A strain having adequate DNA for sequencing and generated robust genome coverage (Figure 4.2).

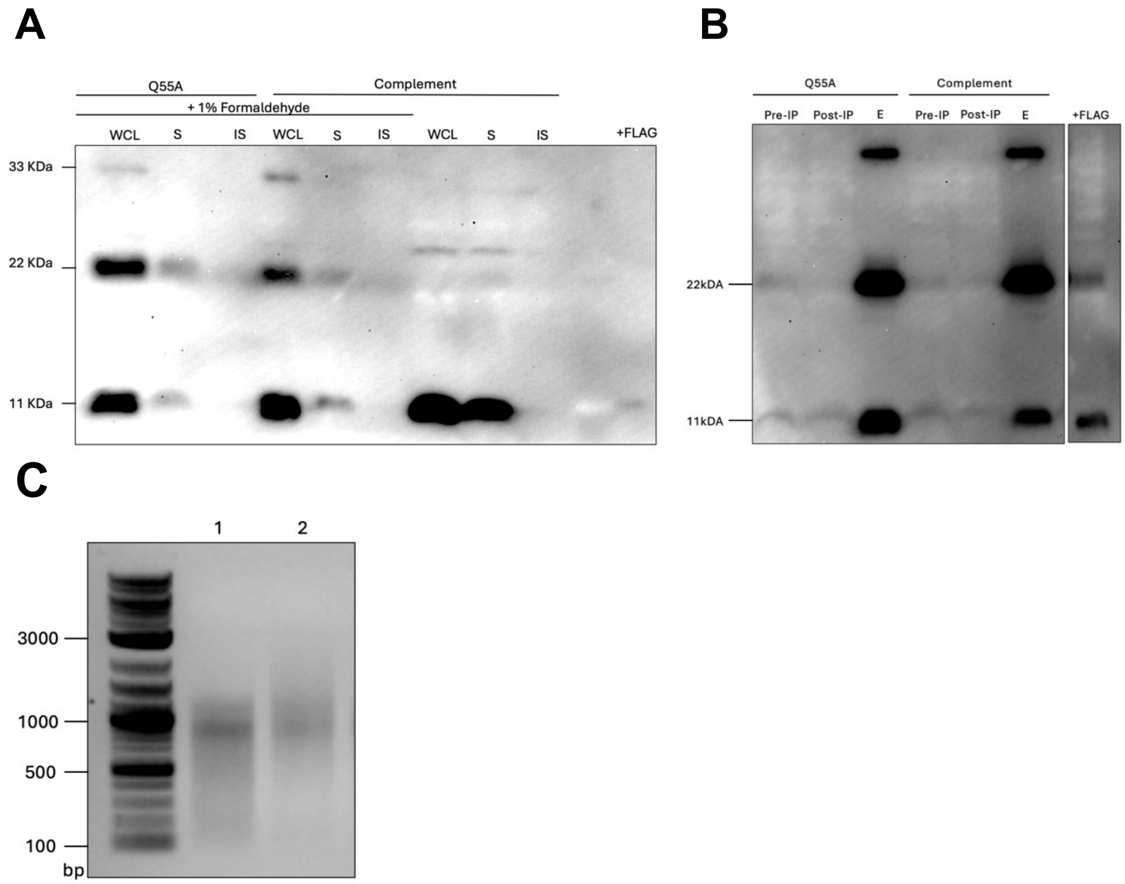

Figure 4.1 Quality Control of Chemical Crosslinking and Chromatin-Immunoprecipitation. (A). Western Blot of post-crosslinking and fractionation of Q55A (Δ*hlyU*/VSV105-*hlyU*(Q55A)-FLAG) and *hlyU* complement (Δ*hlyU*/VSV105-*hlyU*-FLAG) strains. Evidence of higher molecular weight complexes at 22 & 33KDa indicative of successful HlyU crosslinking. PVDF membrane was blotted with a mouse anti-FLAG antibody. WCL = Whole cell lysate, S = Soluble Fraction, IS = Insoluble Fraction. (B) Western Blot to confirm successful immunoprecipitation of HlyU-FLAG. Higher molecular weight bands in lanes E are representative of FLAG antibody denaturation. Pre-IP = Pre-immunoprecipitation, Post-IP= Post-immunoprecipitation, E = Elution. (C) Post-Immunoprecipitation DNA yields assessed by gel electrophoresis. Approximately 10-20ng/μL of DNA in sample. DNA smearing is indicative of successful sonication with an average fragment length of 500-800bp. 1 = Q55A, 2 = *hlyU* complement.

4.2.2 ChIP-seq identifies five putative targets of HlyU during infection

The output of ChIP-seq quantitative DNA analysis are peaks of enrichment. Enriched specific reads that align to the *V. parahaemolyticus* RIMD 2210633 reference genome represent a genetic locus that encompasses putative HlyU binding sites. The peaks that are generated are the measurements of the density of reads where the summit of the peak likely represents a more localized locus for a HlyU binding site on the chromosome. However, prior to peak calling which allows for the identification of enriched binding sites in a ChIP-seq experiment, certain quality control steps must be performed. Notably, assessing the correlation between treatments (*hlyU* complement and Q55A control). This correlation can be represented as a heatmap (Figure 4.2A), where the R1 and R2 data sets for both treatments strongly correlate to themselves but are less correlated to the respective R1 or R2 control. This indicates that there is a signal in the HlyU complement samples that is unique to those treatments. However, it is important to note that the two strains used in the experiment are very genetically and technically very similar, save for the Q55A mutation in the *hlyU* binding domain, making the correlation matrix quite similar.

Peak calling identified three putative HlyU-binding targets at 4 hours of infection across both chromosomes 1 and 2 in *V. parahaemolyticus* (Table 4.1). A peak located on chromosome 1 with a summit at the chromosomal location of 2966876-2966877th base pair, corresponds to the intergenic region between ExeM/NucH Extracellular Endonuclease (Locus tag: VP_RS13735) and a 124 amino acid Hypothetical Protein (Locus tag: VP_RS13740) (Figure 4.2B). To further characterize VP_RS13740, I used a combination of NCBI blastp+ to search *V. cholerae* genomes for homologous proteins and InterProScan to identify protein domains. VP_RS13740 did not have any significant matches in the *V. cholerae* genomes but InterProScan identified a N-terminal lipoprotein signal peptide with a cleavage site between residues G19 and C20 followed by a large non-cytoplasmic domain. Secondary analyses with TMHMM 2.0 software support the extracellular localization of this protein.

Another peak of enrichment corresponded to the intergenic region between a 102 amino acid metalloregulator ArsR/SmtB family transcriptional regulator (Locus tag: VP_RS19710) and a 61 amino acid DUF2892-domain containing protein (Locus tag: VP_RS19715) on chromosome 2 (Table 4.1). The peak was located at the chromosomal position of 981772-981773th base pair and was the most highly enriched across replicate experiments (n=2) (Figure 4.2C). Analyses by InterProScan identified a large wHTH domain containing DNA binding interfaces in VP_RS19710, a common feature in the metalloregulator superfamily. In contrast, bioinformatic analyses of the DUF2892-domain containing protein identified a YgaP domain. The *E. coli* YgaP protein is a membrane bound rhodanese, a thiosulfate-cyanide sulfurtransferase (216). TMHMM 2.0 predicts 2 transmembrane domains with cytoplasmic-oriented N- and C-terminus. NCBI blastp+ of the amino acid sequence genomes identifies a rhodanese-related sulfurtransferase homologue in *V. cholerae* strains. Rhodanese are ubiquitous in both eukaryotes and prokaryotes and functionally may be involved in both detoxification of cyanide (217) or the production of iron-sulfur clusters in ferredoxin (218). The single rhodanese-domain containing protein Q9KN65 (Locus tag: VC_A0100) involved in stress response has been described in *V. cholerae* (219, 220). Expression of a stress response protein may be beneficial to *V. parahaemolyticus* during infection, hence HlyU regulation (see discussion).

Finally, the second peak on chromosome 2 corresponds to the intergenic region upstream of a small 88 amino acid Hypothetical Protein (Locus Tag: VP_RS21200) (Table 4.1) (Figure 4.2D). NCBI blastp+ of the protein sequence identifies a potential *V. cholerae* homologue of a AbrB/MazE/SpoVT family DNA-binding domain-containing protein (Percent Identity: 58.62%). This superfamily includes numerous proteins involved in toxin sequestering and toxin-antitoxin (TA) systems and transcriptional regulators of cell state and division (221). For example, MazE-like proteins are the antitoxin protein of a toxin-antitoxin (TA) system (222) while AbrB-like proteins have been implicated in the repression of biofilm formation in *B. subtilis* (223). *V. parahaemolyticus* encodes multiple TA systems that remain modestly understood but are typically clustered in the superintegron on chromosome 1 (224, 225). However, the E-value score of the blastp+ alignment is 0.002, indicating a low probability of shared function. Additionally, TMHMM 2.0 and SignalP 5.0 predict an extracellular localization of VP_RS21200.

To validate the ChIP-seq peaks of enrichment, I characterized one of the putative HlyU-regulated loci. The upstream intergenic region of the extracellular endonuclease ExeM was selected based on annotation in the *V. parahaemolyticus* RIMD 2210633 genome. To further characterize *exeM* as a specific endonuclease, I performed preliminary *in silico* analysis. The protein coding sequence of *exeM* was used to search available *V. cholerae* genomes on NCBI blastp+. Top hits all resolved Xds, a Gly-Gly anchored extracellular endonuclease, as the potential functional identity of *exeM* (E-value: 0.0). Xds and another endonuclease Dns have been implicated during *V. cholerae* infection, with primary roles in biofilm formation, dispersal, and resistance to innate immune factors in the small intestine (226–229).

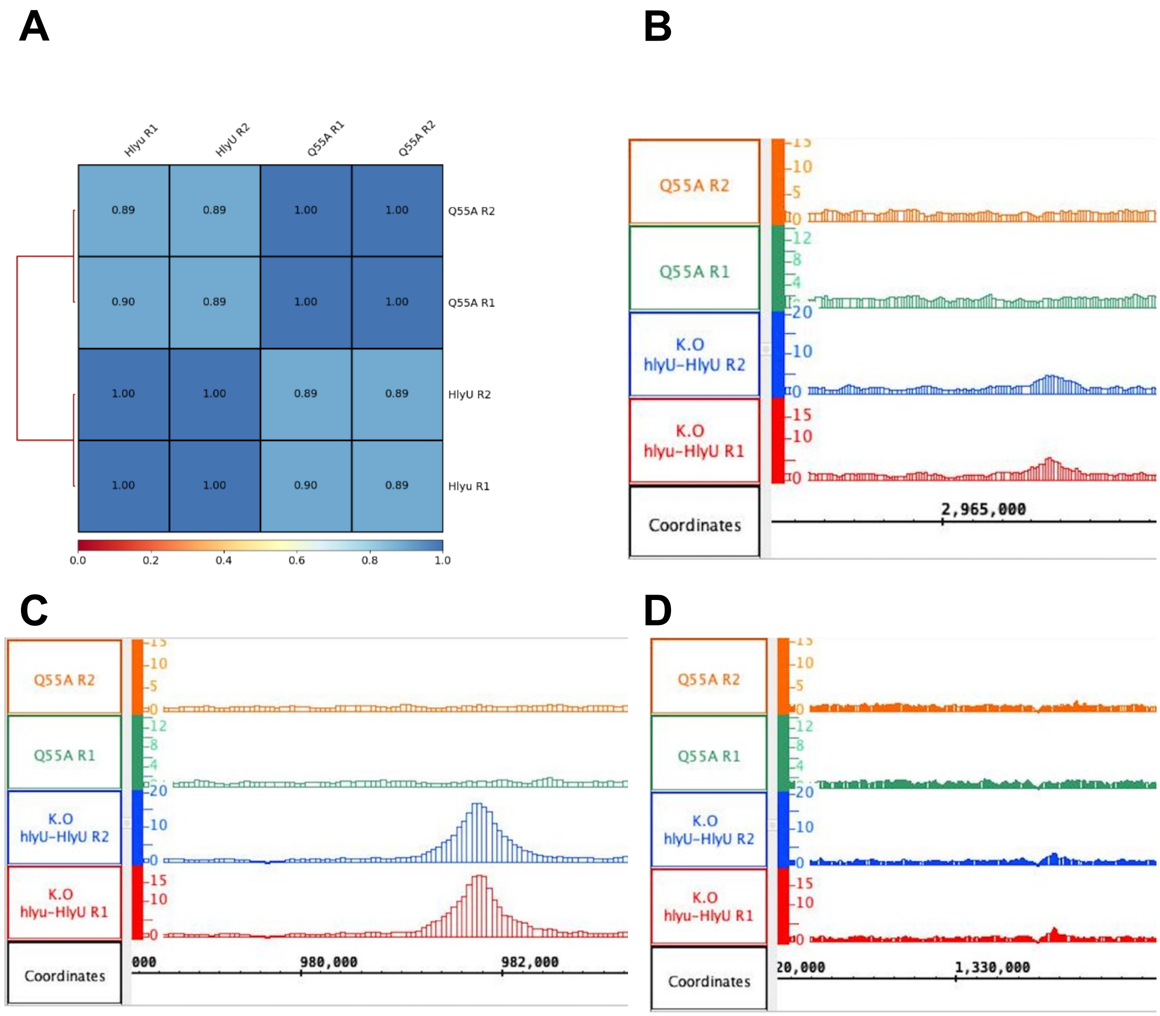

Figure 4.2 Sample correlation and peak calling of high confidence MACS2 results. R1 and R2 denote forward (R1) and reverse (R2) sequencing reads. Treatment reads were mapped unpaired with corresponding control read files. (A) Correlation between replicates of treatment (Δ*hlyU*/VSV105-*hlyU*-FLAG) and control (Δ*hlyU*/VSV105-*hlyU*(Q55A)-FLAG) samples. Correlation was plotted as a heatmap using DeepTools plotCorrelation (Galaxy Version 3.5.4+galaxy0). (B) Peak identified on chromosome 1. Peaks were viewed on Integrated Genome Browser. (C-D) Peaks located on chromosome 2. Peaks were viewed on Integrated Genome Browser.

Table 4.1 Summary of high confidence peak set identified by MACS2.

Chromosomal Location	Peak Position	Peak Summit	Locus Tag	Function
Chromosome 1	2966520-2967051	2966876-2966877	VP_RS13735	ExeM/NucH Family Extracellular Endonuclease
			VP_RS13740	Hypothetical Protein
Chromosome 2	981209-982319	981772-981773	VP_RS19710	Metalloregulator ArsR/SmtB Family transcriptional factor
			VP_RS19715	DUF2892-domain containing protein
Chromosome 2	1334396-1334941	1334762-1334763	VP_RS21200	Hypothetical Protein

4.2.3 Bioinformatic analyses of ExeM

Since *V. cholerae* expresses the nucleases Xds and Dns as virulence factors, I wanted to confirm whether ExeM may function similarly in *V. parahaemolyticus.* Alignment of the protein sequences of ExeM and Xds using a compositional matrix adjustment returned 51% identity, 65% positives, and 3% gaps, suggesting shared but not identical amino acid composition. The predicted molecular weight of ExeM is approximately 105.83 KDa in comparison to the molecular weight of Xds at 94 KDa.

Next, I analyzed the domains in ExeM and compared them to those found in Xds. SignalP-5.0, a software that can predict the presence of extracellular trafficking signal peptides, identified a signal peptide (likelihood: 0.994) with a cleavage site between residues A24 and E25 (cleavage probability = 0.7592). This is supported by the analysis of functional domains in ExeM using InterProScan (Interpro) (230) which identified an N-terminal signal peptide between residues M1-A24 (Figure 4.3). Additionally, InterProScan identified a Lamin-Tail Domain (LTD) between residues S16-G135. LTDs are typically C-terminal in eukaryotic nuclear Lamins and contain an immunoglobulin fold that has been thought to provide stability to the nuclear membrane. However, LTDs have been identified in bacterial proteins and are thought to tether the LTD-containing protein to the membrane or membrane-associated structures (228, 231). An Oligonucleotide/oligosaccharide-binding (OB) fold was identified between resides V223 and S289 and facilitates protein -RNA, -DNA, or -protein interactions (232, 233). Finally, a catalytic Endo/Exonuclease/Phosphatase (EEP) domain which cleaves nucleotide phosphodiester bonds between residues Q512-D836 was identified at the C-terminus (Figure 4.3). In *V. cholerae* Xds, the OB-fold and the EEP domain are indispensable for catalytic activity while truncations of the LTD resulted in no impact of enzyme activity suggesting that membrane anchoring is dispensable (228).

Despite low sequence similarity, Xds and ExeM share key functional domains, suggesting a similar role for ExeM in *V. parahaemolyticus* virulence. Given that the goal of the ChIP-seq was to identify additional HlyU-regulated virulence factors in *V. parahaemolyticus,* I pursued the target *exeM* for further characterization.

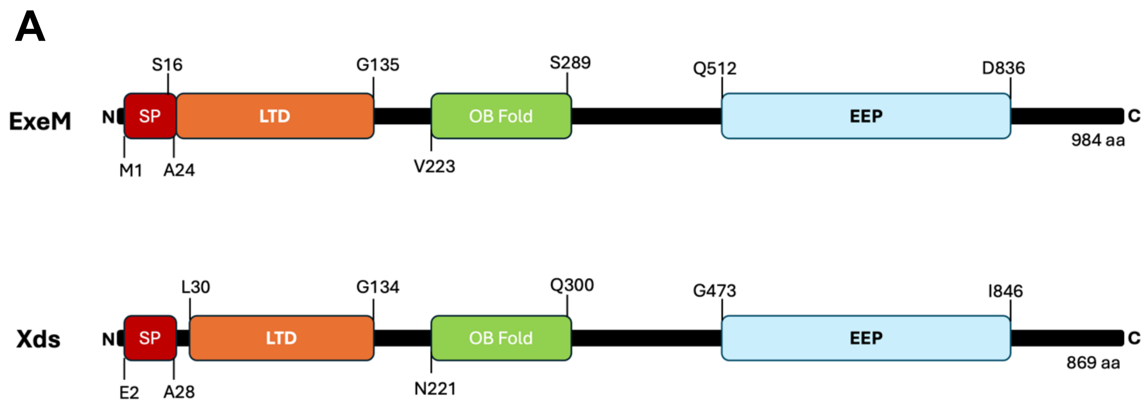

Figure 4.3 Analysis of ExeM and Xds Extracellular endonucleases protein domains. Domains were annotated with InterProScan and SignalP-5.0. Xds annotated domains adapted from (228). Abbreviations: SP – Signal Peptide, LTD – Lamin Tail Domain, OB Fold – Oligonucleotide/Oligosaccharide Binding Fold, EEP – Endo/Exonuclease/Phosphatase

4.2.4 *in silico* cruciform identification in *exeM* intergenic region

Previous work by our lab has shown that HlyU relieves a DNA cruciform at the cryptic promoter located in the intergenic region of *exsB-exsA*, thus promoting T3SS-1 expression (101). Therefore, I considered whether *V. parahaemolyticus* uses DNA cruciform structures at other HlyU-regulated loci to coordinate virulence gene expression.

Using an *in silico* approach, the 584bp intergenic region directly upstream of *exeM* was searched using Palindrome Analyzer to identify DNA sequences capable of forming a cruciform (234). I allowed for a maximum of 1 mismatch and excluded cruciform with less than 6 bp stem loops and 10 bp spacer elements. Since HlyU consensus sequences are not defined across *Vibrio* spp. I looked for cruciform forming sequences that contained features required for HlyU binding. An A/T rich palindromic core that is approximately 17 bp in length is flanked by inverted repeats. The palindromic core forms the major grooves that support HlyU-DNA binding while the flanking inverted repeats (which form the critical stem loops of the cruciform) appear to be implicated in the binding of the ‘wings’ of the wHTH HlyU structure. Palindrome Analyzer identified 29 sequences capable of forming a cruciform. Importantly, all potential cruciform had a positive ΔG value (ranging from 2.72-24.13) meaning an input of energy from DNA supercoiling is required for the formation of the cruciform.

Of the twenty-nine sequences identified, two cruciform were investigated further (Table 4.2). The putative cruciform at position 298 was selected due to its proximity to the proposed center of the ChIP-seq enrichment peak (at position 245) and the size of its spacer. Likewise, the putative cruciform at position 473 was selected due to its A/T rich palindromic sequence and size of spacer element (see discussion).

Table 4. 2 Putative cruciform in *exeM* promoter.

Sequence	Length - Spacer - Mismatch	ΔG	Position
AAGGAA GTATTGATGTA TTCCAT	6-11-1	16.91	298
TTTCTT ATTTATTTCATA AATAAA	6-12-1	15.57	473

Inverted repeats are identified in red and blue. Analyses performed using Palindrome Analyzer.

4.2.5 T7 Mapping of cruciform-forming elements in *exeM* intergenic region

To validate the predicted cruciform in the intergenic region of *exeM* identified by Palindrome Analyzer, restriction enzyme mapping was performed as demonstrated previously (101, 119). Utilizing T7 Endonuclease, which cuts DNA at cruciform elements in a two-step nicking process, and PvuII which has flanking cut sites around the cruciform forming region, I could assess the promoter region of *exeM* for the presence of cruciform and approximately identify where the cruciform was formed. The plasmid pUC(A/T) contains a known stable cruciform and served as the positive control for the mapping experiment (119). Indeed, pUC(A/T) digested with T7 resulted in linearization of the plasmid and an altered migration pattern on the DNA gel (Figure 4.4A). Since the T7 digestion is a two-step process, a subset of pUC(A/T) is incompletely digested, resulting in the highest migratory band that represents a nicked sub-population. Treatment of pUC(A/T) with PvuII results in the formation of a second 350bp band as well as linearization of the plasmid backbone. The cruciform is known to be located within the 350bp PvuII DNA segment (in uncut, supercoiled DNA). A sequential digest of pUC(A/T) initially with T7 and followed by PvuII results in 4 DNA bands on the gel: the linearized backbone (highest band), the band at 350bp indicative of PvuII cutting, and two fragments of approximately 100bp and 250bp. These latter two fragments add up to 350bp, with the cleaved cruciform located at the position where the two DNA species conjoin (Figure 4.4A).

To functionally assess for the presence of cruciform in the *exeM* intergenic region identified by the ChIP-seq, the *exeM* promoter was cloned into the EcoRV site located between the two PvuII sites in pBS. pBS alone does not contain any cruciform (101) thus any cruciform identified in the pBS-*exeM* construct are located within the cloned DNA. Digestions of pBS-*exeM* followed a similar pattern to pUC(A/T). Firstly, treatment of pBS-*exeM* with T7 resulted in linearization indicating the presence of a cruciform in the promoter region (Figure 4.4A). To note, there is a large population of pBS-*exeM* that was only nicked by T7. Secondly, cutting with PvuII forms a band that runs at approximately 1000bp. However, in contrast to pUC(A/T), the sequential digestion of pBS-*exeM* with T7 and PvuII resulted in four fragments (approximately 250bp, 425bp, 610bp, 750bp) that are all smaller than the 1000bp PvuII master fragment. To map the cruciform, fragments should be paired to make up a total length of ~1000bp.

Two putative cruciform are identified in the promoter region of *exeM.* Alignment of fragments 425bp and 610bp between the two PvuII cut sites map a cruciform at the 327th base pair of the *exeM* promoter. Likewise, the alignment of fragments 250bp and 750bp map a cruciform at the 446th base pair of the *exeM* promoter (Figure 4.4B). Notably, these two putative cruciform map within approximately 30 base pairs to the cruciform predicted by Palindrome Analyzer (298th base pair and 473rd base pair) (Table 4.2), supporting the *in silico* results. While both cruciform are predicted to form in the promoter region of *exeM* in pBS, whether they truly form on the chromosomal DNA remains to be seen. As well, this assay does not identify which cruciform is relieved by HlyU binding.

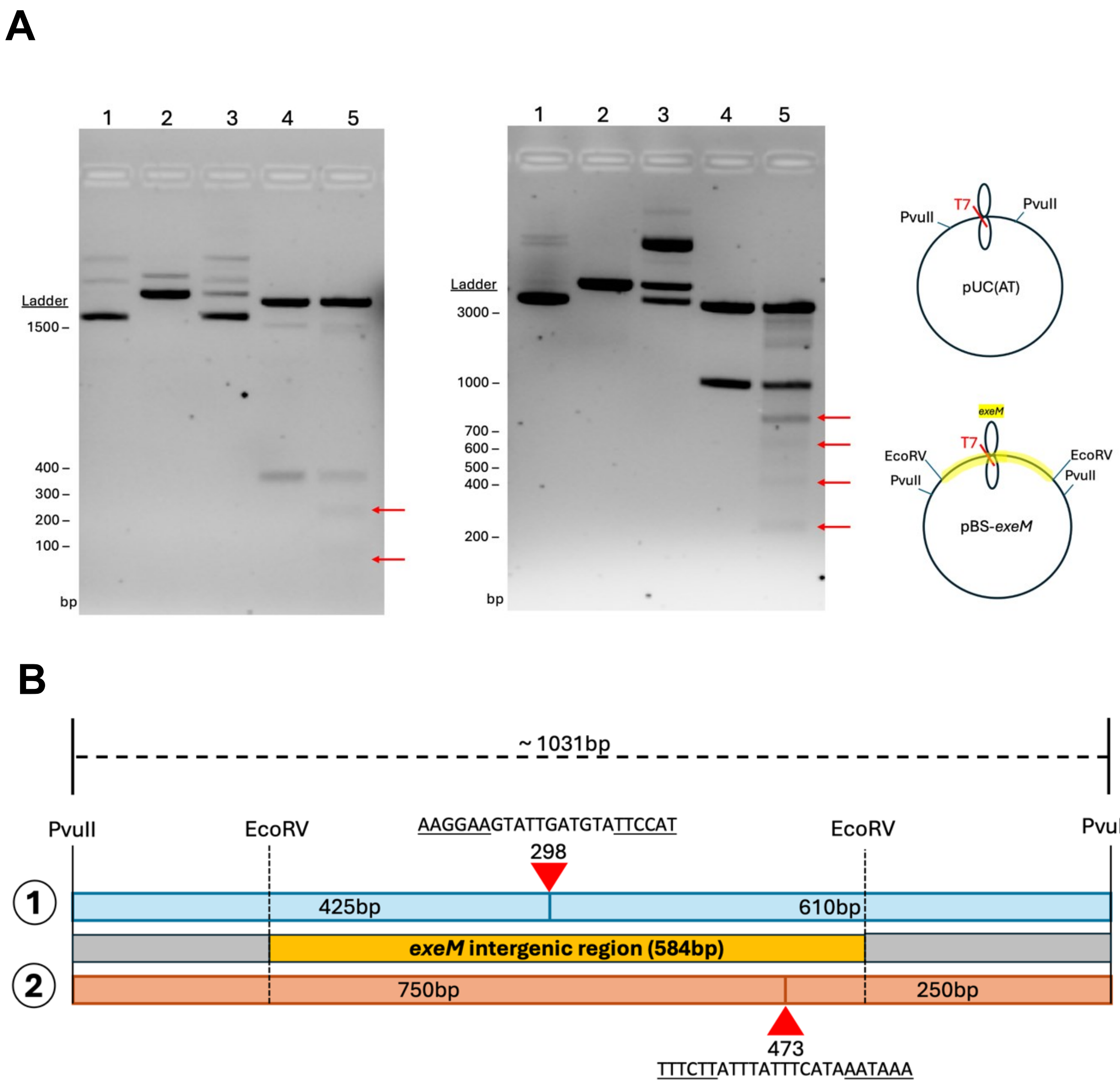

Figure 4.4 Identification of potential cruciform sites in *exeM* intergenic region. (A) DNA electrophoresis of potential cruciform-containing DNA (right) digested with 1- no enzymes, 2- HindIII, 3- T7 Endonuclease, 4- pvuII, 5- T7 followed by pvuII. HindIII was used as a control for DNA linearization. T7 endonuclease targets cruciform-forming DNA elements in a two-step process which linearizes DNA while pvuII has two cut sites that flank the MCS and could be used for cruciform mapping. Notably, complete cleavage by T7 is rare as the first cut releases the DNA supercoiling, reducing the efficiency for the secondary cut required for linearization, and resulting in the enrichment of nicked DNA (lane 3). Arrows indicate the fragments used for cruciform mapping (lane 5). pUC(AT) served as a positive control (left). Experiment was repeated three times with representative data shown. (B) Mapping of T7-pvuII digestion fragments of pBS-*exeM* onto palindrome analyzer to identify location of potential cruciform (red arrow). Sequences identified by Palindrome Analyzer at those locations are added (inverted repeats are underlined).

4.2.6 HlyU is a regulator of *exeM* expression

To assess *hlyU*-dependent regulation at a putative HlyU-regulated locus, I cloned the *exeM* intergenic region into the VSVlux vector backbone. VSVlux contains a promoter-less *luxCDABE* cassette, wherein the addition of a functional DNA promoter upstream of the cassette would drive the production of *luxCDABE* mRNA and result in light emission due to luciferase activity, recorded as CPS. A difference in light production from the *hlyU* mutant compared to the WT strain would indicate a regulatory role for HlyU at the promoter region of *exeM.* Strains were cultured and monitored for *exeM* promoter activity, and a time course was performed to identify when the promoter was active. CPS and OD_{600nm} measurements were taken three hours post-subculture and followed by measurements every 30 minutes for an additional 2 hours, for a total of a 5-hour subculture. Since *exeM* was captured in the ChIP-seq at 4 hours via HlyU binding, I expected to see promoter activity between 4 and 4.5 hours.

Based on the lux reporter assays, HlyU contributes to *exeM* promoter activity. While there was a decrease in *exeM* promoter activity at 4 hours in the *hlyU* mutant, the difference was not statistically significant (Figure 4.5A); However, at 4.5 hours the *hlyU* mutant demonstrated a statistically significant reduction in promoter activity (30%) compared to WT *V. parahaemolyticus* (Figure 4.5A). Since expression of the T3SS-1 is dual regulated by H-NS and HlyU and H-NS is a global transcriptional repressor, I considered whether H-NS plays a role in the regulation of *exeM.* Indeed, at 4.5 hours, there was a statistically significant 8-fold increase in promoter activity of the *hns* mutant compared to WT (Figure 4.5B). Finally, to determine if HlyU is required for derepression of the *exeM* promoter in the absence of H-NS or specifically implicated in relieving H-

NS from the promoter region, the same time course was performed in a double *hns* and *hlyU* mutant. The double mutant had an11-fold increase in promoter activity compared to WT (Figure 4.5B), indicating that in the absence of *hns,* HlyU is not required for the expression of *exeM*. This observation aligns with the current model of HlyU regulation.

Taken together, these results indicate that HlyU is a global virulence regulator in *V. parahaemolyticus,* implicated in both the regulation of the T3SS-1 and ExeM, a novel extracellular endonuclease (see discussion). Even more broadly, this data validates the ChIP-seq approach I have developed as an effective way to identify HlyU-regulated genetic loci in *V. parahaemolyticus.*

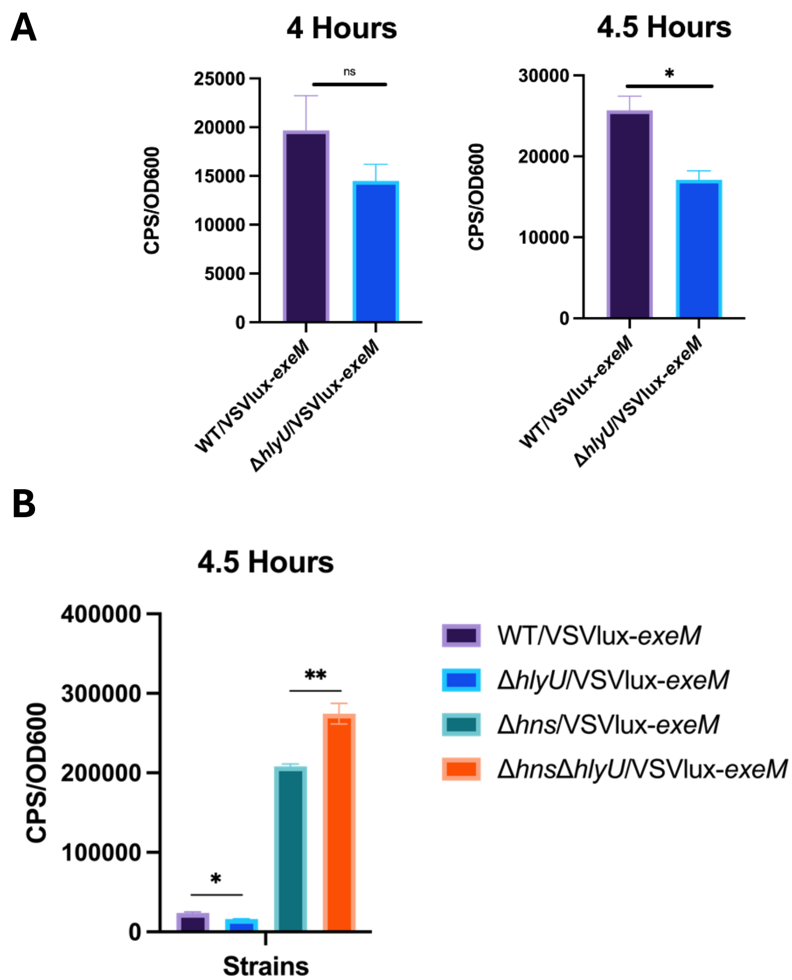

Figure 4.5 Characterization of HlyU regulatory activity at the *exeM* promoter locus in *V. parahaemolyticus*. (A) Lux reporter assays used to quantitively assess promoter activity in an hlyU-dependent manner. Strains were grown overnight and was inoculated into Inducing Media at a starting OD_{600nm} of 0.025 and grown at 30°C, 250rpm. CPS and OD_{600nm} measurements were recorded after 4 hours and 4.5 hours. Statistical significance was calculated using an unpaired t-test (n=3, *:p <0.05). (B) Conjugation of *ΔhnsΔhlyU V. parahaemolyticus* with VSVlux-*exeM* to assess whether HlyU is required for de-repression of the promoter proper or acts to relieve repressive H-NS activity. Statistical significance was calculated using an unpaired t-test (n=3, *: p<0.05, **:p<0.01).

Chapter 5 Discussion

5.1 Central Carbon Metabolism in the Aquatic Lifestyle of *V. parahaemolyticus*

In Chapter 3, I explored the transcriptional regulator HexR and the role of CCM in the aquatic lifestyle of *V. parahaemolyticus*. Multiple factors contribute to the survival of *V. parahaemolyticus* in the marine environment, but it is chitin – an abundant yet complex polymer of GlcNac – and its degradation that provides the necessary metabolic precursors for ATP generation and the biogenesis of amino acids and nucleotides via the PPP (125). Therefore, regulation of CCM is a critical fitness determinant for *V. parahaemolyticus* in the aquatic environment and dysregulation often results in global cellular impacts.

My investigation revealed the significant role HexR plays in metabolically reprogramming *V. parahaemolyticus* upon encountering a diverse array of nutrient sources. Despite the *hexR* mutant sharing a similar sigmoidal growth trend to WT upon introduction to LB, a nutrient rich growth media, the mutant strain developed a growth defect in late stationary phase (Figure 3.3A). It is well understood that when useable nutrients are depleted from the growth medium, cells enter a non-steady growth known as stationary phase. Entrance into stationary phase prompts significant changes in metabolism and carbon flux (152). Disruptions to bacterial CCM and associated regulators like HexR result in growth defects (including defects in stationary phase) under a diverse array of nutrient sources (107, 143). As seen in the Spent Media growth assays, the *hexR* mutant is unable to grow spent media, indicating the mutant strain is unable to metabolize the remaining macromolecules (Figure 3.3C-D). In contrast, overexpression of *hexR* in the WT strain promoted early growth in nutrient depleted conditions but was eventually outgrown by the WT strain by the endpoint of the experiment. The growth defect of the *hexR* mutants is worsened in defined marine minimal media with glycerol as a sole carbon source in comparison to LB, though entry into stationary phase is much closer in time to WT or complement strains. Here, the expression of HexR is providing a clear growth advantage in nutrient limited or deplete environments.

In the context of growth on chitin as a sole carbon source, loss of *hexR* results in significant fitness costs both in isolation and in head-to-head competition with WT *V. parahaemolyticus.* Colloidal chitin is a non-homogenous source of chitin due to the acid hydrolysis, meaning the MM9 media contains numerous chitin derivatives including chitohexose, GlcNac monomers, and other lengths of (GlcNac)n polymers (223). As such, chitin derivatives are entering the chitin catabolism pathways at various steps. Regardless, the endpoint for chitin degradation is CCM via fructose-6-P and the PPP. In MM9 supplemented with colloidal chitin, the *hexR* mutant had a statistically significant growth defect in the first 16 hours of growth. This may be attributed to a delayed shift to chitin-related pathways like the PPP which are required for synthesis of biomass. Unexpectedly, cells lacking functional *hexR* significantly outgrew the WT strain post-20 hours of growth, indicating that a broader dysregulation of carbon flux was occurring (Figure 3.4A).

While this initial observation contradicted the previous Tn-seq results, the context of these two experiments differs. Firstly, VP1236 was identified in a population of transposon mutants all competing for colloidal chitin while the *hexR* mutant was grown in isolation. And secondly, the MM9 colloidal chitin growth assays were performed over a 54-hour time course, much longer than the allotted time for growth for the Tn-seq experiment. Therefore, to further explore this preliminary observation, I developed a head-to-head competition assay for the WT and *hexR* mutant on colloidal chitin using a promoter-less GFP-transposon system. In accord with the Tn-seq result, the *hexR* mutant was competitively disadvantaged in comparison to the WT strain over the course of 48 hours (Figure 3.4B-C). I propose the following explanation: in isolation the *hexR* mutant can overcome the growth defect in the initial 16 hours of growth and is not at a disadvantage for taking longer to metabolize the colloidal chitin. But during competition, the *hexR* mutant is outcompeted by the WT strain and never recovers. Likely the *vp1236* transposon mutant had this same growth defect on chitin and could not compete with the rest of the transposon mutant population, resulting in its underrepresentation in the sequencing pool. These experiments reveal a critical regulatory role for HexR in chitin utilization and the overall fitness of *V. parahaemolyticus* in the aquatic environment (Figure 5.1).

The *hexR* mutant growth defect reflects an underlying dysregulation of CCM. Key regulon members *pgi* (gluconeogenesis and glycolysis) and *glgX* (glycogen catabolism) promoter activity is elevated in the *hexR* mutant, indicating that HexR acts repressively at these loci (Figure 3.7). The variable *glgX* promoter activity in WT *V. parahaemolyticus* could be attributed to the specific metabolism of glycogen. *E. coli* grown in nutrient rich media use glycogen only when preferential nutrient sources have been depleted (161). Utilization of glycogen allows for cells to overcome the nutrient deficiency and continue to metabolize effectively. This allows for bacteria to adapt to adverse conditions or specific ecological niches (161). The significant upregulation of *glgX* in WT *V. parahaemolyticus* at a later timepoint could reflect an adaptation to allow for growth in media being depleted of other preferred nutrient sources (236). In addition, the variable promoter activity of *glgX* may reflect the concomitant expression of glycogen biosynthetic and degradation enzymes. An interesting observation was that HexR appears to be a regulator of *zwf* expression in *V. parahaemolyticus*. Zwf is a member of the *P. putida* HexR regulon and is involved in the first step of the PPP and the ED pathways (140). Given how important the PPP is for growth on chitin as a sole carbon source, the deregulated flux of carbon through both the PPP and the ED pathway would have contributed to the *hexR* mutant phenotype.

The quantification of promoter activity at the *nagZ-murQP* and *murR-murQP* loci revealed another axis of HexR regulation. HexR did not regulate the *murR-murQP* locus, providing further evidence that VP1236 is not MurR. However, activity of the *nagZ-murQP* locus did differ in the *hexR* mutant. *nagZ* promoter activity was elevated in the *hexR* mutant indicating HexR-specific regulation (Figure 3.8). NagZ is implicated in cell wall recycling. During growth, *E. coli* releases CW-derived murein peptides into media culture which can be efficiently utilized for both CW recycling and metabolism (224, 225). These muropeptides accumulate in excess in rich media like LB, halting CW recycling pathways and the subsequent production of more muropeptides (226). However, the accumulated muropeptides can be used as a carbon source (139) and NagZ is a critical enzyme in this process, facilitating the cleavage of GlcNac from AnhMurNac. This could account for the increased activity of the *nagZ* promoter during later growth in LB subculture in *V. parahaemolyticus*. GlcNac can then be further metabolized into fructose-6P for CCM, providing an energy source in nutrient deficient or depleted medium. Overall, these quantitative reporter assays demonstrate the broad regulatory ability of HexR on both canonical pathways like the PPP, and non-canonical CCM pathways like NagZ-mediated catabolism of murein peptides.

Deregulated CCM impacts the aquatic fitness of *V. parahaemolyticus.* Notably, this dysregulation is reflected in *V. parahaemolyticus* ability to form biofilms. Biofilms are a key mechanism of aquatic survival for *V. parahaemolyticus* and contribute to the incidence of gastroenteritis by promoting cell adherence to both abiotic and biotic surfaces, including seafood (75). Biofilm formation is tightly linked to the cell's metabolic activity and reprogramming, as the formation of the extracellular matrix draws on cellular polysaccharides, nucleic acids, and proteins and in return provides adherence and increased persistence to the colonizing cells (227). Thus, disruptions in the production of the extracellular matrix have significant impacts on biofilm formation (228). As expected, WT *V. parahaemolyticus* formed robust biofilm in the marine minimal media, which represents the environmental conditions when biofilm formation would be favorable, and cells remained tightly adhered to the test tubes following multiple washes even under more limited nutrient conditions (e.g. MM9 supplemented only with glycerol). Despite normalizing cell number to remove any discrepancies due to growth defects, the *hexR* mutant exhibited a statistically significant reduction in biofilm formation upon growth in MM9 supplemented with glycerol and casamino acids and did not form adherent biofilms at all when media was supplemented with only glycerol (Figure 3.5A). Critically, remodeling of CCM (notably the TCA cycle and pentose phosphate pathway) provides the energy and reducing power to generate the components of the extracellular matrix during early biofilm development (229). Likely, the *hexR* mutant cannot produce as robust an exopolysaccharide matrix under the same nutrient conditions as WT, due to the high metabolic cost required and the dysregulation of CCM caused by the absence of HexR. Overall, this would limit the colonizing cells adherence to the test tube and delay the entry into early biofilm formation. As well, impacts on biofilm formation could partially explain the *hexR* mutant growth defect on colloidal chitin. To begin the chitin utilization cascade, cell adherence must be initiated and effects on cell adherence would have significant effects how efficiently the *hexR* mutant can metabolize chitin (Figure 5.1).

Additionally, deregulated CCM resulted in significant impacts on cell morphology. During its environmental lifecycle, *V. parahaemolyticus* uses two distinct cell types: the classical slightly curved rod-shaped cell and a highly elongated swarmer cell. Each cell type employs a uniquely specialized flagellar system that provides motility to the cells in the marine environment (88). Different modes of locomotion aid *V. parahaemolyticus* in colonizing a wide array of niches from the liquid marine water column to the formation of biofilms on the chitinous surfaces of various marine organism who play host including zooplankton, bivalves, and crustaceans (69, 106). Recent efforts have revealed that the different morphologies appear to contribute to the environmental dissemination of *V. parahaemolyticus* (73). Observations of cells cultured in nutrient rich LB media revealed no differences in rod cell shape. In contrast, WT bacteria cultured in MM9 supplemented with glycerol had dramatic cell morphology changes, resulting in stark cellular elongation and the development of a filamentous subpopulation that accounted for ~30% of total cell population. Strikingly, this subpopulation was missing in the *hexR* mutant background. The development of the swarmer cell subpopulation in liquid culture was likely attributed to the minimal but trace amounts of iron in the growth media which mimics the stimuli by nutrient starvation (78, 230). The underlying mechanisms that regulate *V. parahaemolyticus* cell differentiation remain unknown. Adjacent regulation by OpaR and the ScrABC operon during phase transition and cell swarming indicate some sort of sensing of environmental stimuli and assessment of nutrient availability is involved in cell morphology changes (82, 85). Perhaps HexR-facilitated shifting of carbon flux provides the necessary signal, in the form of cyclic-di-GMP precursors, for activation of swarming-specific genes. This is the first time to our knowledge that HexR has been implicated in the regulation of cell differentiation in *V. parahaemolyticus.*

The isolation and characterization of the *hexR* mutant is an important contribution to understanding the underlying molecular mechanisms that contribute to *V. parahaemolyticus* cell differentiation. Since Δ*hexR* appears to be unable to differentiate into swarmer cells, this provides an additional genetic tool that can be added to the experimental workflow for understanding the switch between these key morphological states of *V. parahaemolyticus*. In *Caulobacter crescentus,* experimental analyses of key mutations that locked cells in differentiated states provided the necessary molecular tools for dissecting the regulatory mechanisms that contributed to swarmer and stalked cells (244). Therefore, identification of these mutants lays the groundwork for broadening our understanding of the complex regulatory systems that govern bacterial physiology.

Swarmer cell formation is critical for *V. cholerae c*olonization of chitinous surfaces (231). Filamentation of cells results in marked increase in colonization of chitin particles under nutrient-limiting environments and outcompetes non-swarming, shorter, cell types. Filamentous colonization of particles is best suited for rapid turnaround, where long term biofilm formation would be excessive. This is ideal for environments like the marine biosphere where nutrients cycle and abiotic factors rapidly change (231). Likewise, impacts to *V. parahaemolyticus* swarmer cell formation may also significantly disadvantage the cell during chitin utilization, thus contributing to the *hexR* mutant phenotype during the competition experiment (Figure 5.1).

Furthermore, the differentiated cell morphologies contribute to the dissemination of *V. parahaemolyticus* in the aquatic environment, with cells of a body length of 5μm or shorter being highly motile. Longer cells have significantly reduced swim speed in comparison (73). Microscopy of the swimming plate growth confirms that the *hexR* mutant maintained swimmer or planktonic cells while both the WT and complement strains were made up of the heterogenous populations of swimming and swarming cells (data not shown). A reduction in total planktonic cells could account for the reduction in swimming of both WT and complement strains. Alternatively, given that the *hexR* mutant has reduced accessibility to carbon sources, the marked increase in motility could reflect how the cell has metabolized all useable nutrients in the local vicinity and must swim farther to find new energy sources.

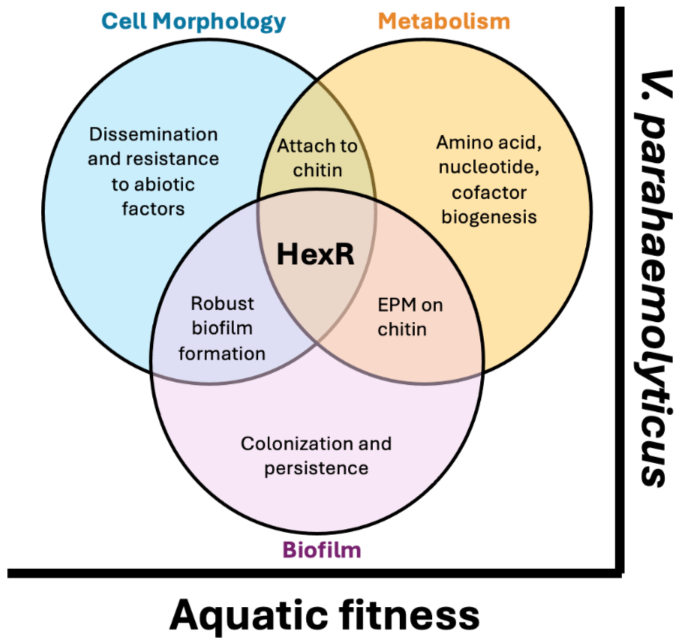

Figure 5.1 Interplay of HexR in *V. parahaemolyticus* chitin utilization and aquatic fitness. Disruptions to HexR results in significant loss of bacterial fitness. Reduced biofilm formation likely reduces bacterial colonization and utilization of chitin. In a similar manner, swarmer cell-mediated colonization of chitin and dispersal would be impacted in the *hexR* mutant background. Overall, these effects would result in significant fitness defects in nutrient poor environments like the marine water column where chitin is the dominant carbon source. EPM = Extracellular Polysaccharide Matrix

Ultimately, the data in chapter 3 demonstrates the contributions of HexR to *V. parahaemolyticus* fitness and demonstrates how *V. parahaemolyticus* is competitively advantaged during colonization of new niches against the endogenous microbiota. Specifically, coordinated regulation of CCM expression is the cornerstone to successful colonization by *V. parahaemolyticus,* and ultimately *Vibrio* spp., in niches with variable carbon sources and availability (143). The compounding effects caused by the loss of cell differentiation, which reduces colonization and dispersal, along with less biofilm formation reducing overall persistence, results in the significant fitness defect of the *hexR* mutant (Figure 5.1). Due to this fitness defect, it is extremely unlikely that a Δ*hexR* genotype would be maintained in the aquatic environment.

5.2 The Global Virulence Regulator HlyU

In Chapter 4, I investigated the global regulatory ability of the transcriptional regulator HlyU in the context of *V. parahaemolyticus* infection using a ChIP-seq approach and provided preliminary characterization of the novel extracellular endonuclease ExeM. ChIP-seq is the standard method for identifying interactions between DNA-binding proteins like transcriptional regulators (TR) and their DNA targets.

During optimization of the ChIP-seq protocol, effort needs to be made in the selection of controls carried through the experiment as generated datasets are often full of false-positive or spurious hits (232, 233). Intergenic regions, bound by the TR of interest, are often full of other TR binding sites. Recent reports have shown that this uneven binding of TRs can skew the enrichment step during immunoprecipitation, resulting in peaks of enrichment that do not represent true TR binding (233). Furthermore, regions of DNA that are highly expressed due to the high abundance of RNA polymerase and transcriptional machinery have also been found to be falsely over-represented in treatment samples. These peaks are reproducible between replicate ChIP-seq runs but do not represent any specific biological interactions between the TR and DNA targets (234). It is speculated that the clustered TRs and transcriptional machinery contain 'unstructured' protein regions that are highly charged or contain low sequence complexity (235, 236). These unstructured domains of other TRs or transcriptional machinery crosslinked to DNA may interact non-specifically with the antibody during immunoprecipitation, leading to the formation of false positive peaks of enrichment (236). Jain et al. (2015) observed that ChIP-seq performed in a specific TR knockout background detected >3000 binding sites, each falsely representative of an interaction (236). Therefore, selection of appropriate controls is important to distinguish these non-biologically relevant peaks of enrichment.

One proposed solution to overcome the abundance of spurious peak enrichment is to carry forward a deletion construct of the TR of interest as a control (236). For this reason, I used the *V. parahaemolyticus* strain Q55A as my control. This strain expresses a FLAG-tagged HlyU protein with a single point mutation at the 55th amino acid (glutamine to alanine) in the DNA-binding domain. This mutation abolishes HlyU-DNA binding and significantly reduces cytotoxicity against HeLa cells, acting like a deletion TR construct while still providing information on non-HlyU specific DNA binding and enrichment along with non-specific anti-FLAG antibody binding. Indeed, the Q55A and *hlyU* complement samples contained identical peaks of enrichment, indicative of spurious binding. Using the Q55A control, I removed those peaks from my analyses.

The genome wide screen of HlyU-binding regions identified three peaks that were unique to the *hlyU* complement strain. These three peaks corresponded to the intergenic regions of five potential targets. With minimal annotation in the *V. parahaemolyticus* RIMD 2210633 genome, I used a set of basic bioinformatic analyses, including NCBI Blast, InterProScan, SignalP-5.0, and TMHMM 2.0, to gain insight into the functional identities of the targets. The *in silico* analyses highlighted some interesting features discussed below.

A putative stress response protein was identified in the ChIP-seq screen. The DUF2892-domain containing protein (Locus tag: VP_RS19715) was predicted to contain a YgaP domain. YgaP is one of the numerous thiosulfate sulfurtransferases expressed by *E. coli* (237) but this class of enzymes are widespread across eukaryotic and prokaryotic organisms (217). These sulfurtransferases move sulfur between molecules via a catalytic cysteine located in the C-terminal active site (217) and participate in numerous functions including sulfur metabolism (238), cyanide detoxification (215), and maintenance of iron-sulfur clusters (216). It is this last function that may be significant to *V. parahaemolyticus* virulence. During infection, *V. parahaemolyticus* must cope with stressful environmental conditions. Nitric Oxide (NO), reactive nitrogen species (RNS), and reactive oxygen species (ROS) are generated in the host lumen via the innate immune system and exerts antimicrobial activity against enteric pathogens (239). The NO, RNS, and ROS target the reactive metal centers and iron-sulfur clusters of key enzymes, therefore disrupting metabolic, respiratory, and DNA-synthesizing processes (240, 241).

V. parahaemolyticus must then have some mechanism to detoxify the reactive species upon arrival into the host lumen to avoid terminal enzymatic damage, and this mechanism would maintain *V. parahaemolyticus* virulence. The enteric pathogen *Salmonella* Typhimurium highly expresses the sulfurtransferase PspE during infection (242) and Wallrodt et al. (2013) observed a significant loss in *Salmonella* Typhimurium virulence upon the deletion of both the sulfurtransferases *pspE* and *glpE* (243). Comparatively, *V. cholerae pspE* (Locus tag: VC_A0100) mutants are also deficient in colonization and infection of a zebrafish model, indicating a potential role for sulfurtransferases in *V. cholerae* pathogenesis (254). Interestingly, NO activates the master regulator OpaR, initiating biofilm formation in *V. parahaemolyticus* (255). Therefore, *V. parahaemolyticus* may be able to balance NO stimuli to promote colonization and establish an infection (e.g. biofilm formation) with the antibacterial activity of the reactive species via the putative sulfurtransferase activity of VP_RS19715.

Characterization of the target ExeM/NucH Extracellular Endonuclease validated my ChIP-seq approach to identify HlyU-regulated loci. *In vivo* quantitative analysis of *exeM* promoter activity in a WT and *hlyU* mutant background identified HlyU as a key regulator of *exeM* promoter activity during infection (Figure 4.5A). In pathogenic *Vibrio* spp., HlyU often coordinates gene expression alongside H-NS by relieving H-NS at the promoter (54, 201, 204, 205, 256). Congruently, HlyU was not required for *exeM* expression in the absence of H-NS, as demonstrated by the significant increase in *exeM* promoter activity in the *hns* and double *hns hlyU* mutant (Figure 4.5B). While the reporter assays were performed in the same growth conditions as those used for ExeM discovery via ChIP-seq, it remains to be seen what conditions promote maximal *exeM* expression. DNA supercoiling, and thus cruciform formation, responds to environmental conditions (261) including high temperature (262), low oxygen (263), and osmotic stress (264). These abiotic factors serve as signals for appropriate gene expression based on the bacterium's environment. The preliminary quantification of *exeM* promoter activity highlights how further investigation is required to identify the physiologically relevant conditions for *exeM* promoter activity.

In addition, the endonuclease ExeM may also play a role in *V. parahaemolyticus* virulence. *V. cholerae* utilizes two extracellular endonucleases during its lifecycle: Xds and Dns. These extracellular endonucleases are important contributors to *V. cholerae* biofilm formation by facilitating the formations of the three-dimensional architecture of the biofilm via alterations to extracellular DNA, while also permitting cellular detachment (227). Upon deletion of either endonuclease, the biofilm is dense, thick, and unstructured. Dns is the dominant nuclease in the maintenance of *V. cholerae* biofilm formation while Xds is most highly expressed during late biofilm development where it primarily degrades extracellular DNA down into nucleotides for further biogenesis (227). Dns expression is controlled via HapR, the functional homologue of quorum-sensing regulator LuxR (257), while Xds expression is partly facilitated via the PhoB/R two-component regulatory system (227, 258, 259). Moreover, Mg^{2+} and Ca^{2+} are critical for maximum Xds activity, while a crucial signal for *xds* induction is phosphate limitation (226, 227). My *in silico* analysis of protein domains identified significant similarity between ExeM and Xds, with the essential catalytic (EEP) and DNA-binding (OB-fold) domains present (Figure 4.3). Biofilm formation is a critical virulence factor for *V. parahaemolyticus* as it allows for cells to persist during infection of mammalian host and marine organisms (260). HlyU-mediated regulation of ExeM may promote biofilm formation during infection, allowing for *V. parahaemolyticus* persistence and access to nucleosides as a nutrient source under nutrient-limiting conditions.

Alternatively, ExeM may primarily function to aid in *V. parahaemolyticus* evasion of the innate immune system. Neutrophils are the most abundant leukocytes in circulation and are early responders during the innate immune response to contain and clear pathogens (261). During infection, neutrophils are recruited to the site of infection via the induction of pro-inflammatory cytokines (262). The antimicrobial activity of neutrophils is derived from the subsequent release of neutrophil extracellular traps (NETs), DNA-based extracellular structures containing decondensed chromatin, modified histones, and numerous primary and secondary granules, some of which include neutrophil elastases (263). Neutrophil elastases can degrade gram-negative virulence factors while the physical structure of the NET prevents pathogen spread and minimize damage to host tissue (264–266). To overcome this innate immune barrier, bacterial pathogens have evolved numerous evasion mechanisms. *V. cholerae* Xds and Dns contribute to the degradation of NETs during infection in a mammalian host (224). The endonucleases contribute greatly to *V. cholerae* virulence as the Δ*xds*Δ*dns* mutant resulted in a significant colonization defect in an immunocompetent mouse model (224). Another interesting mechanism of innate immune evasion is through the degradation of self-DNA. Group A *Streptococcus* utilize the nuclease Sda1 to degrade extracellular self-DNA, thus avoiding Toll-like receptor 9 (TLR9) recognition and TLR9-dependent cytokine release which promotes further innate immune cell recruitment (267). In a similar manner, ExeM may provide defense against NETs and TLR recognition during early *V. parahaemolyticus* infection.

Recent evidence has pointed towards *V. parahaemolyticus* using DNA cruciform to regulate gene expression. Preliminary *in silico* analysis of the promoter regions of *V. cholerae tlh-hlyA*, *V. vulnificus rtxA1,* and *V. anguillarum plp-vah,* which are all known to be bound and regulated by HlyU, identify a putative cruciform DNA structure that overlaps with the HlyU binding sites (99). This prompted my own investigation of the *exeM* intergenic region using *in silico* and *in vitro* methods. More than 20 DNA sequences capable of forming cruciform were identified in the *exeM* intergenic region, with two meeting the criteria for HlyU binding and regulation. Mapping of the cruciform with restriction enzymes supported the presence of two cruciform at the *exeM* intergenic region; however, based on the criteria for cruciform formation and HlyU binding, I hypothesize that the cruciform at 473rd base pair is likely the DNA superstructure regulating *exeM* expression. Firstly, HlyU has a propensity to bind A/T rich palindromes in the promoter regions of *Vibrio* spp. (99, 202, 205, 256, 268), and the cruciform at the 473rd base pair contains an imperfect A/T rich palindrome. Secondly, the predicted location of the cruciform is within 100bp of the start codon of ExeM which may encode the -10, and the -35 sequences of the promoter. Finally, the size of the spacer element and ΔG free energy value of the cruciform agrees with the known cruciform at the T3SS-1 in *V. parahaemolyticus* (99). Further investigation via electrophoretic mobility shift assays (EMSA) and DNase I footprinting assays to identify the HlyU binding site would provide clarity about which cruciform may be bound by HlyU.

Overall, my work in chapter 4 demonstrates the efficacy of using ChIP-seq as a genomic screen for targets of DNA-binding proteins and highlights the global virulence regulatory ability of HlyU. Preliminary *in silico* characterization of VP_RS19715 identified a stress-response protein which could be involved in resistance to host NO and RNS during luminal infection as a target for HlyU regulation. Additionally, characterization of ExeM reveals an interesting role of HlyU-regulated biofilm formation and NET evasion in *V. parahaemolyticus* infection. Finally, DNA sequences with cruciform forming potential are found at a variety of intergenic regions bound by HlyU, representing a conserved mechanism of gene regulation in pathogenic *Vibrio* spp.

5.3 Final Remarks

In this thesis, I have explored transcriptional regulation paradigms in *V. parahaemolyticus* through two studies. The first investigates how genes are regulated during the aquatic lifestyle to maintain bacterial fitness, while the second explores the contributions of genetic regulatory mechanisms to *V. parahaemolyticus* pathogenesis.

Vibrios are generalist species, making the cells adept at living in the marine water column, in brackish coastal waters, in the human gut, and on the chitinous surface of marine organisms (25, 63). In the case of *V. parahaemolyticus,* tightly coordinated gene regulation allows for the colonization of different niches, making the bacterium an extremely versatile colonist (63, 88). Despite climate change broadening *Vibrio* spp. geographic distribution in the ocean, *V. parahaemolyticus* remains an incredibly successful colonist due to the bacteria's ability to use diverse organic carbon and energy sources mediated through coordinated regulation of CCM pathways (63). As nutrient sources can be extremely variable in the marine environment, often separated by long periods of starvation, *Vibrio* spp. need to quickly react and take advantage of any nutrients encountered (269, 270). The open ocean is typically considered a nutrient-limited environment and is dominated by microorganisms capable of nutrient specialization (271). Alternatively, the coastal ocean zones, which are the sites for primary productivity and the release of terrestrial P, N, and Si, are frequently dominated by complex and rich nutrient sources (272). As *V. parahaemolyticus* move throughout the dual lifecycle from coastal to open ocean and back, having genetic regulatory mechanisms to cope with the significant fluxes in nutrient availability would be critical for maintaining cellular fitness.

The switch from a generalist to a specialist is tightly linked to coordinated CCM. Observations of *V. vulnificus* mutants in key stressosome proteins (273) demonstrated increased growth during late-log and early stationary phase in chemically defined media compared to wild type (274). Assessment of the activity of TCA cycle and glyoxylate shunt enzyme activity (*aceA* and *aceB*, both which are in the *V. parahaemolyticus* HexR regulon) revealed that dysregulated carbon flux and metabolism through those pathways contributed to the dysregulated but increased growth observed in the mutant strains (274). Shifting to alternative metabolism pathways (e.g. the glyoxylate shunt) in the WT strain allows for the cells to cope with metabolically demanding or stressful growth conditions but the payoff is a less efficient energy generation. Conversely, the mutants were unable to make that switch, instead becoming more specialized and able to use less efficient but more energetically favorable pathways like the TCA cycle (274). As a result, the mutant strains have an extended log phase and overall increased growth. In a similar manner, disruptions to HexR-regulated pathways may have shifted the *hexR* mutant from a generalist to a specialist-oriented lifestyle.

Furthermore, previous work has been aimed at assessing genes involved in bacterial fitness in the diverse array of environments that *Vibrio* spp. encounters during the bacteria's lifecycle (274, 275). There are significant shifts in local environmental conditions when pathogenic *Vibrio* are shed from the human gut to the aquatic environment. The bacteria must rapidly adapt to the significant drop in osmolarity, temperature, and nutrient availability (276). In *V. cholerae*, cells undergo rapid changes in gene expression, from a downregulation of genes involved in protein synthesis coupled with an upregulation of nitrogen and phosphate scavenging genes to cope with the more metabolically demanding conditions (276). This change in gene expression allows for host-passaged *V. cholerae* to persist and disseminate in the new environment, leading to an increase in the incidence of reinfection. In line with our observations on the importance of HexR in metabolically demanding conditions, Kamp et al. (2013) identified HexR as providing a significant fitness advantage to host-passaged *V. cholerae* survival in the aquatic environment (275). The data presented in this thesis supports the contribution of HexR, as the master regulator of CCM, to the generalist phenotype of *V. parahaemolyticus* thus promoting bacterial fitness in dual host-aquatic lifestyle (Figure 5.2).

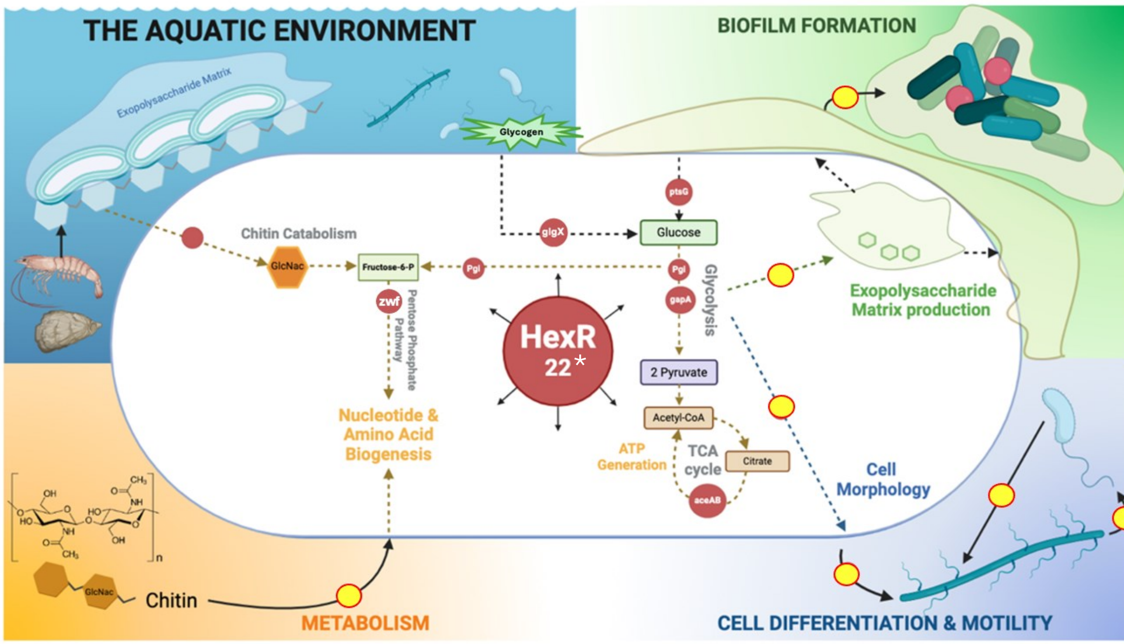

Figure 5.2 Model of HexR regulation and broad fitness impacts on the aquatic survival of *V. parahaemolyticus*. Master regulator HexR coordinates biofilm formation, cell differentiation, motility, and metabolism to promote bacterial fitness in the diverse aquatic environments occupied by *V. parahaemolyticus*, contributing to the ubiquitous distribution of the marine organism. HexR regulon was predicted to include 22 genes. The data presented in this thesis implicates *nagZ* and *zwf* in the *V. parahaemolyticus* HexR regulon (*). Known members of the HexR regulon are identified in white font on red circles while yellow circles represent the data implicating HexR in three broad domains of aquatic *V. parahaemolyticus* lifecycle. Note: listed regulon members are not exhaustive.

The role HexR plays in *V. parahaemolyticus* adaptation to nutrient-limited environments raises interesting considerations for bioremediation. In this thesis, I demonstrated that WT *V. parahaemolyticus* are adept at using diverse nutrient sources but could be modified via overexpression of *hexR* to have a significant growth increase in spent media (Figure 3.3C-D). Due to the insolubility and inertness of chitin, current methods of disposal include ocean dumping, incineration, and land filling. However, derivatives produced from chitin catabolism are beneficial for numerous industries including pharmaceuticals and ethanol production as well as preventing significant environmental pollution and biofouling (57, 277). Therefore, overexpression of *hexR* in chitinolytic bacteria may represent an interesting solution to the significant amount of chitinous shellfish waste that is produced by the seafood industry (278). The strain *Vibrio natriegens* has been proposed as a workhorse strain for biotechnology and molecular biology purposes due to its rapid growth and synthesis of cellular components, non-pathogenicity, and diverse metabolism (287–289). Using the developed molecular tools (288), *V. natriegens* could be engineered to overexpress *hexR* and in a batch system with continuous supply of nutrient-pour carbon sources, may be able to efficiently metabolize the waste products.

Much like how the adaptive ability of *V. parahaemolyticus* relies on tightly coordinated gene expression, *V. parahaemolyticus* must regulate the expression of genes during infection to adapt to the environment of a human host. Virulence factors play numerous roles in the lifestyle of pathogenic bacteria, from colonization to adherence to infiltration mechanisms (279, 280). Overall, these virulence factors contribute to the bacteria's fitness in the human host and influence the severity of disease. Understanding the underlying mechanisms of genetic regulation is critical for understanding bacterial pathogenesis.

In the case of pathogenic *Vibrio* spp., numerous virulence factors involved in the induction of cytotoxicity (204, 268) and the characteristic hemolytic activity (205, 207), are regulated by the transcriptional regulator HlyU. As a result, HlyU is often considered a global virulence regulator. In the case of *V. parahaemolyticus,* HlyU has been implicated in the regulation of the T3SS-1 (54) and the extracellular endonuclease ExeM. In addition, genomic screens of HlyU binding during infection using a ChIP-seq approach identified VP_RS19715, a putative sulfurtransferase. Comparison of ExeM and VP_RS19715 to similar proteins in other gram-negative pathogenic bacteria reveal another type of HlyU-regulated virulence factor. As opposed to directly promoting cytotoxicity, these virulence factors may play a more defensive role in *V. parahaemolyticus* infection by promoting bacterial persistence and host evasion. The expression of either a stress response protein or an extracellular endonuclease involved in biofilm formation and NET evasion alongside the expression of cytotoxic T3SS-1 and enterotoxic Tdh would enhance *V. parahaemolyticus* virulence and promote robust infection.

Xds homologues like ExeM are frequently found in pathogens that form biofilms (281, 282); However, broadly the homologues remain quite rare. Currently, no ExeM homologue is found within humans (226). As a result, ExeM represents an interesting therapeutic target for *V. parahaemolyticus* infection. Small molecule inhibitors (SMI) of bacterial virulence factors are a developing field for targeting pathogenic bacteria while avoiding selective pressure that drives resistance. These molecules represent an appealing alternative to antibiotic treatment given the rise in antibiotic resistance (283). Numerous SMI have been developed to target critical virulence determinants: T3SS (284), biofilm formation (285), fimbriae/pili (286), and cell division (287). Given the lack of human ExeM homologue, a highly specific inhibitor of ExeM could effectively target increasingly antibiotic-resistant *V. parahaemolyticus* (288) while preventing the gut dysbiosis caused by normal antibiotics.

Finally, HlyU binding during *V. parahaemolyticus* infection relieves a transcriptionally repressive DNA structure. The propensity of DNA cruciform to overlap with HlyU binding sites is multifactorial. Firstly, alternative DNA structures are preferentially located at intergenic regions (289). These intergenic regions are enriched in inverted repeats and are often A/T rich (176). Secondly, both H-NS and HlyU binding is facilitated by these A/T rich sequences, where H-NS binding maintains negative supercoiling, providing the energy required for cruciform formation. Substantial experimental evidence demonstrates HlyU-mediated relieving of H-NS at the promoter region in pathogenic *Vibrio* spp. (54, 201). The interplay of H-NS, cruciform formation, and HlyU binding represents an underexplored mechanism of virulence gene expression in pathogenic *Vibrio* spp.

Overall, HlyU is a global virulence regulator contributing to the fitness of *V. parahaemolyticus* in the host during infection by coordinating the expression of numerous virulence factors involved in colonization, dissemination, and persistence. This regulation is facilitated by HlyU-mediated attenuation of alternative DNA structures, a mechanism that appears to be conserved for other HlyU targets in pathogenic *Vibrio* spp.

Relieving these DNA cruciform via DNA-binding proteins like HlyU represents a novel mechanism to de-repress gene expression in bacteria.

The impacts of climate change on the global ocean are becoming increasingly apparent, affecting both the global food supply and human health. Warming sea surface temperatures (290) is driving significant redistribution of fish populations (291) and expansion of marine pathogens, bringing these organisms in closer contact with humans and their marine hosts (292). Improved climate suitability for pathogenic *Vibrio* spp. is resulting in outbreaks in areas where the disease is rare (293) and upregulation of genes affecting virulence (294). This leads to an overall greater incidence of infection and disease in both humans and marine hosts like shellfish (295, 296). Investigating the contributions of genetic regulatory mechanisms to the dual host-aquatic lifestyle is therefore critical in understanding the impacts of foodborne zoonosis as climate change continues. The data presented in this thesis identifies the roles of the transcriptional regulators HexR and HlyU in the dual host-aquatic lifestyle of *V. parahaemolyticus,* where HexR is a critical fitness determinant and promotes *V. parahaemolyticus* expansion into new aquatic niches while HlyU coordinates virulence gene expression within host infections, inducing cytotoxicity and promoting bacterial persistence.

5.4 Limitations

The data presented in this thesis is underscored by a few key limitations. Firstly, while the *hexR* mutant appears to be unable to efficiently utilize the remaining metabolites in late stationary phase growth in LB and completely in deplete LB, characterization of metabolites was not performed. High-performance liquid chromatography (HPLC) is an analytical method that can be used to identify and quantify molecules in growth media (274). It would be interesting to assess what metabolites are depleted from the growth media, representing accessible carbon sources for the *hexR* mutant, along with the remaining and accumulating metabolites. This would provide insight into how carbon is in flux in the context of the *hexR* mutant and support the *in vivo* quantitative assays of promoter activity which indicated dysregulated CCM. Secondly, quantification of biofilm by crystal violet (CV) staining assumes equal molecular composition between all biofilms and thus equal capture of CV stain. Biofilm compositions are not identical across bacterial species. Among *Vibrio* spp. alone, different polysaccharide loci are expressed leading to the production of distinct extracellular matrices (308). The *hexR* mutant could synthesize an extracellular matrix that is less able to capture CV, but the biofilm may still be quite robust. Therefore, the content of the *hexR* mutant and WT biofilm could not be quantified. The exact nature of the biofilms could be explored further with Mass Spectrometry.

Additionally, the GFP transposants generated for the colloidal chitin competition assays were not sequenced to identify the insertion location of Tn5::GFP. Care was made to phenotypically characterize both WT and *hexR* mutant Tn5::GFP transposants so that the selected strains for the competition assay had no observable changes in growth in comparison to parental strains that would result in false results. However, it is highly probable that the transposon insertion sites differ between WT and *hexR* mutant and subsequent impacts of this transposition event on the fitness of the strains during competitive growth in colloidal chitin cannot be ruled out. To resolve this, genetic marker retrieval can be performed as previously described (54), by taking advantage of the M13 forward priming site located in pEVS168 system.

Lastly, the ChIP-seq approach did not identify *exsA* as a target for HlyU expression. ExsA is an ideal positive control for the assay as it has been experimentally validated as a target for HlyU regulation (54). However, maximal *exsA* expression has been quantified at 2.5 to 3 hours post-induction of infection conditions, with near total HeLa cell killing by 4 hours (54). In contrast, the ChIP-seq assay was performed at 4 hours post-induction of infection conditions, when *exsA* expression is likely decreasing. Preliminary attempts to crosslink, fractionate, and immunoprecipitate samples collected at 2.5 to 3.5 hours post-induction were unsuccessful in collecting sufficient HlyU-FLAG protein and samples were not carried forward for library preparation. Scaling up the induction culture volumes could increase the concentration of HlyU-FLAG expressed at these earlier timepoints, allowing for the capture of *exsA* by the ChIP-seq screen. Nevertheless, the characterization of *exeM* promoter activity validates the developed ChIP-seq assay as capable of identifying HlyU-regulated targets.

Bibliography

1. Bar-On YM, Phillips R, Milo R. 2018. The biomass distribution on Earth. Proc Natl Acad Sci U S A 115.

2. Cavicchioli R, Ripple WJ, Timmis KN, Azam F, Bakken LR, Baylis M, Behrenfeld MJ, Boetius A, Boyd PW, Classen AT, Crowther TW, Danovaro R, Foreman CM, Huisman J, Hutchins DA, Jansson JK, Karl DM, Koskella B, Mark Welch DB, Martiny JBH, Moran MA, Orphan VJ, Reay DS, Remais J V., Rich VI, Singh BK, Stein LY, Stewart FJ, Sullivan MB, van Oppen MJH, Weaver SC, Webb EA, Webster NS. 2019. Scientists' warning to humanity: microorganisms and climate change. Nat Rev Microbiol https://doi.org/10.1038/s41579-019-0222-5.

3. Flemming HC, Wuertz S. 2019. Bacteria and archaea on Earth and their abundance in biofilms. Nat Rev Microbiol 17.

4. Worden AZ, Follows MJ, Giovannoni SJ, Wilken S, Zimmerman AE, Keeling PJ. 2015. Rethinking the marine carbon cycle: Factoring in the multifarious lifestyles of microbes. Science (1979) https://doi.org/10.1126/science.1257594.

5. York A. 2018. Marine biogeochemical cycles in a changing world. Nat Rev Microbiol 16.

6. Cabrerizo MJ, Medina-Sánchez JM, González-Olalla JM, Sánchez-Gómez D, Carrillo P. 2022. Microbial plankton responses to multiple environmental drivers in marine ecosystems with different phosphorus limitation degrees. Science of the Total Environment 816.

7. Feng Y, Hou S, Roleda MY, Fu FX. 2022. Editorial: Responses of marine microbes to multiple environmental drivers of global change: The interplay of abiotic and biotic factors. Front Microbiol https://doi.org/10.3389/fmicb.2022.975841.

8. Singh BK, Dawson LA, Macdonald CA, Buckland SM. 2009. Impact of biotic and abiotic interaction on soil microbial communities and functions: A field study. Applied Soil Ecology 41.

9. Harvell CD, Mitchell CE, Ward JR, Altizer S, Dobson AP, Ostfeld RS, Samuel MD. 2002. Climate warming and disease risks for terrestrial and marine biota. Science (1979) https://doi.org/10.1126/science.1063699.

10. Billaud M, Seneca F, Tambutté E, Czerucka D. 2022. An Increase of Seawater Temperature Upregulates the Expression of *Vibrio parahaemolyticus* Virulence Factors Implicated in Adhesion and Biofilm Formation. Front Microbiol 13.

11. Kimes NE, Grim CJ, Johnson WR, Hasan NA, Tall BD, Kothary MH, Kiss H, Munk AC, Tapia R, Green L, Detter C, Bruce DC, Brettin TS, Colwell RR, Morris PJ. 2012. Temperature regulation of virulence factors in the pathogen *Vibrio coralliilyticus*. ISME Journal 6.

12. Traylor-Knowles N, Connelly MT. 2017. What Is Currently Known About the Effects of Climate Change on the Coral Immune Response. Curr Clim Change Rep https://doi.org/10.1007/s40641-017-0077-7.

13. Mackenzie CL, Lynch SA, Culloty SC, Malham SK. 2014. Future oceanic warming and acidification alter immune response and disease status in a commercial shellfish species, Mytilus edulis L. PLoS One 9.

14. Bailey C, Segner H, Casanova-Nakayama A, Wahli T. 2017. Who needs the hotspot? The effect of temperature on the fish host immune response to *Tetracapsuloides bryosalmonae* the causative agent of proliferative kidney disease. Fish Shellfish Immunol 63.

15. Martinez-Urtaza J, Bowers JC, Trinanes J, DePaola A. 2010. Climate anomalies and the increasing risk of *Vibrio parahaemolyticus* and *Vibrio vulnificus* illnesses. Food Research International 43.

16. Belkin S, Colwell RR. 2005. Oceans and health: Pathogens in the marine environmentOceans and Health: Pathogens in the Marine Environment.

17. Pruzzo C, Huq A, Colwell RR, Donelli G. 2005. Pathogenic vibrio species in the marine and estuarine environment. Oceans and Health: Pathogens in the Marine Environment.

18. Caccamese SM, Rastegar DA. 1999. Chronic diarrhea associated with *Vibrio alginolyticus* in an immunocompromised patient. Clinical Infectious Diseases 29.

19. Liu Z, Miyashiro T, Tsou A, Hsiao A, Goulian M, Zhu J. 2008. Mucosal penetration primes *Vibrio cholerae* for host colonization by repressing quorum sensing. Proc Natl Acad Sci U S A 105.

20. Jahangir Alam M, Tomochika KI, Miyoshi SI, Shinoda S. 2002. Environmental investigation of potentially pathogenic *Vibrio parahaemolyticus* in the Seto-Inland Sea, Japan. FEMS Microbiol Lett 208.

21. Joh NJ, Shon HS. 1991. *Vibrio vulnificus* septicemia in Korea: Clinical and epidemiologic findings in seventy patients. J Am Acad Dermatol 24.

22. Travers MAS, Basuyaux O, Le Goïc N, Huchette S, Nicolas JL, Koken M, Paillard C. 2009. Influence of temperature and spawning effort on *Haliotis tuberculata* mortalities caused by *Vibrio harveyi:* An example of emerging vibriosis linked to global warming. Glob Chang Biol 15.

23. Myhr E, Larsen JL, Lillehaug A, Gudding R, Heum M, Hastein T. 1991. Characterization of *Vibrio anguillarum* and closely related species isolated from farmed fish in Norway. Appl Environ Microbiol 57.

24. Khimmakthong U, Sukkarun P. 2017. The spread of *Vibrio parahaemolyticus* in tissues of the Pacific white shrimp *Litopenaeus vannamei* analyzed by PCR and histopathology. Microb Pathog 113.

25. Huq A, Small EB, West PA, Huq MI, Rahman R, Colwell RR. 1983. Ecological relationships between *Vibrio cholerae* and planktonic crustacean copepods. Appl Environ Microbiol 45.

26. DePaola A, Hopkins LH, Peeler JT, Wentz B, McPhearson RM. 1990. Incidence of *Vibrio parahaemolyticus* in U.S. coastal waters and oysters. Appl Environ Microbiol 56.

27. Baker-Austin C, Trinanes JA, Salmenlinna S, Löfdahl M, Siitonen A, Taylor NGH, Martinez-Urtaza J. 2016. Heat wave-associated vibriosis, Sweden and Finland, 2014. Emerg Infect Dis 22.

28. Parveen S, Hettiarachchi KA, Bowers JC, Jones JL, Tamplin ML, McKay R, Beatty W, Brohawn K, DaSilva L V., DePaola A. 2008. Seasonal distribution of total and pathogenic *Vibrio parahaemolyticus* in Chesapeake Bay oysters and waters. Int J Food Microbiol 128.

29. Cholera – Global situation. https://www.who.int/emergencies/disease-outbreak-news/item/2023-DON437. Accessed May 12, 2024.

30. Trinanes J, Martinez-Urtaza J. 2021. Future scenarios of risk of *Vibrio* infections in a warming planet: a global mapping study. Lancet Planet Health 5.

31. Nair GB, Ramamurthy T, Bhattacharya SK, Dutta B, Takeda Y, Sack DA. 2007. Global dissemination of *Vibrio parahaemolyticus* serotype O3:K6 and its serovariants. Clin Microbiol Rev https://doi.org/10.1128/CMR.00025-06.

32. Davis BJK, Corrigan AE, Sun Z, Atherly E, DePaola A, Curriero FC. 2021. A case-control analysis of traceback investigations for *Vibrio parahaemolyticus* infections (vibriosis) and pre-harvest environmental conditions in Washington State, 2013–2018. Science of the Total Environment 752.

33. Diner RE, Kaul D, Rabines A, Zheng H, Steele JA, Griffith JF, Allen AE. 2021. Pathogenic *Vibrio* Species Are Associated with Distinct Environmental Niches and Planktonic Taxa in Southern California (USA) Aquatic Microbiomes. mSystems 6.

34. Frischkorn KR, Stojanovski A, Paranjpye R. 2013. *Vibrio parahaemolyticus* type IV pili mediate interactions with diatom-derived chitin and point to an unexplored mechanism of environmental persistence. Environ Microbiol 15.

35. Baker-Austin C, Oliver JD, Alam M, Ali A, Waldor MK, Qadri F, Martinez-Urtaza J. 2018. *Vibrio* spp. infections. Nat Rev Dis Primers 4.

36. Santoriello FJ, Kirchberger PC, Boucher Y, Pukatzki S. 2023. Pandemic *Vibrio cholerae* acquired competitive traits from an environmental Vibrio species. Life Sci Alliance 6.

37. Matz C, Nouri B, McCarter L, Martinez-Urtaza J. 2011. Acquired type III secretion system determines environmental fitness of epidemic *Vibrio parahaemolyticus* in the interaction with bacterivorous protists. PLoS One 6.

38. Makino K, Oshima K, Kurokawa K, Yokoyama K, Uda T, Tagomori K, Iijima Y, Najima M, Nakano M, Yamashita A, Kubota Y, Kimura S, Yasunaga T, Honda T, Shinagawa H, Hattori M, Iida T. 2003. Genome sequence of *Vibrio parahaemolyticus*: A pathogenic mechanism distinct from that of *V cholerae.* Lancet 361.

39. Morris JG, Black RE. 1985. Cholera and Other Vibrioses in the United States. New England Journal of Medicine 312.

40. Daniels NA, Mackinnon L, Bishop R, Altekruse S, Ray B, Hammond RM, Thompson S, Wilson S, Bean NH, Griffin PM, Slutsker L. 2000. *Vibrio parahaemolyticus* infections in the United States, 1973-1998. Journal of Infectious Diseases 181.

41. Tena D, Arias M, Álvarez BT, Mauleón C, Jiméneź MP, Bisquert J. 2010. Fulminant necrotizing fasciitis due to *Vibrio parahaemolyticus*. J Med Microbiol 59.

42. Bhadra RK, Roychoudhury S, Banerjee RK, Kar S, Majumdar R, Sengupta S, Chatterjee S, Khetawat G, Das J. 1995. Cholera toxin (CTX) genetic element in *Vibrio cholerae* O139. Microbiology (N Y) 141.

43. Lang PA, Kaiser S, Myssina S, Birka C, Weinstock C, Northoff H, Wieder T, Lang F, Huber SM. 2004. Effect of *Vibrio parahaemolyticus* haemolysin on human erythrocytes. Cell Microbiol 6.

44. Honda T, Ni Y, Miwatani T, Adachi T, Kim J. 1992. The thermostable direct hemolysin of *Vibrio parahaemolyticus* is a pore-forming toxin. Can J Microbiol 38.

45. Takahashi A, Sato Y, Shiomi Y, Cantarelli V V., Iida T, Lee M, Honda T. 2000. Mechanisms of chloride secretion induced by thermostable direct haemolysin of *Vibrio parahaemolyticus* in human colonic tissue and a human intestinal epithelial cell line. J Med Microbiol 49.

46. Raimondi F, Kao JPY, Fiorentini C, Fabbri A, Donelli G, Gasparini N, Rubino A, Fasano A. 2000. Enterotoxicity and cytotoxicity of *Vibrio parahaemolyticus* thermostable direct hemolysin in in vitro systems. Infect Immun 68.

47. Takahashi A, Iida T, Naim R, Naykaya Y, Honda T. 2001. Chloride secretion induced by thermostable direct haemolysin of *Vibrio parahaemolyticus* depends on colonic cell maturation. J Med Microbiol 50.

48. Matsuda S, Kodama T, Okada N, Okayama K, Honda T, Iida T. 2010. Association of *Vibrio parahaemolyticus* thermostable direct hemolysin with lipid rafts is essential for cytotoxicity but not hemolytic activity. Infect Immun 78.

49. Naim R, Yanagihara I, Iida T, Honda T. 2001. *Vibrio parahaemolyticus* thermostable direct hemolysin can induce an apoptotic cell death in Rat-1 cells from inside and ouside of the cells. FEMS Microbiol Lett 195.

50. Ham H, Orth K. 2012. The role of type III secretion System 2 in *Vibrio parahaemolyticus* pathogenicity. Journal of Microbiology https://doi.org/10.1007/s12275-012-2550-2.

51. Büttner D, Bonas U. 2002. Port of entry - The type III secretion translocon. Trends Microbiol https://doi.org/10.1016/S0966-842X(02)02331-4.

52. Matsuda S, Okada N, Kodama T, Honda T, Iida T. 2012. A cytotoxic type III secretion effector of *Vibrio parahaemolyticus* targets vacuolar H+-ATPase subunit C and ruptures host cell lysosomes. PLoS Pathog 8.

53. Broberg CA, Zhang L, Gonzalez H, Laskowski-Arce MA, Orth K. 2010. A *Vibrio* effector protein is an inositol phosphatase and disrupts host cell membrane integrity. Science (1979) 329.

54. Getz LJ, Thomas NA. 2018. The transcriptional regulator HlyU positively regulates expression of exsA, leading to type III secretion system 1 activation in *Vibrio parahaemolyticus.* J Bacteriol 200.

55. Park KS, Ono T, Rokuda M, Jang MH, Okada K, Iida T, Honda T. 2004. Functional characterization of two type III secretion systems of *Vibrio parahaemolyticus.* Infect Immun 72.

56. Sugiyama T, Iida T, Izutsu K, Park KS, Honda T. 2008. Precise region and the character of the pathogenicity island in clinical *Vibrio parahaemolyticus* strains. J Bacteriol 190.

57. Mathew GM, Mathew DC, Sukumaran RK, Sindhu R, Huang CC, Binod P, Sirohi R, Kim SH, Pandey A. 2020. Sustainable and eco-friendly strategies for shrimp shell valorization. Environmental Pollution https://doi.org/10.1016/j.envpol.2020.115656.

58. Reantaso MB. 2013. FAO Fisheries and Aquaculture Report No. 1053 FIRA/R1053 (En) FAO/MARD Technical Workshop on Early Mortality Syndrome (EMS) or Acute Hepatopancreatic Necrosis Syndrome (AHPNS) of Cultured Shrimp (under TCP/VIE/3304).

59. Yu LH, Teh CSJ, Yap KP, Ung EH, Thong KL. 2020. Comparative genomic provides insight into the virulence and genetic diversity of *Vibrio parahaemolyticus* associated with shrimp acute hepatopancreatic necrosis disease. Infection, Genetics and Evolution https://doi.org/10.1016/j.meegid.2020.104347.

60. Lee C Te, Chen IT, Yang YT, Ko TP, Huang YT, Huang JY, Huang MF, Lin SJ, Chen CY, Lin SS, Lightner D V., Wang HC, Wang AHJ, Wang HC, Hor LI, Lo CF. 2015. The opportunistic marine pathogen *Vibrio parahaemolyticus* becomes virulent by acquiring a plasmid that expresses a deadly toxin. Proc Natl Acad Sci U S A 112.

61. Castellanos A, Restrepo L, Bajaña L, Betancourt I, Bayot B, Reyes A. 2023. Genomic and Evolutionary Features of Nine AHPND Positive *Vibrio parahaemolyticus* Strains Isolated from South American Shrimp Farms. Microbiol Spectr 11.

62. Kaneko T, Colwell RR. 1973. Ecology of *Vibrio parahaemolyticus* in Chesapeake Bay. J Bacteriol 113.

63. Lovell CR. 2017. Ecological fitness and virulence features of *Vibrio parahaemolyticus* in estuarine environments. Appl Microbiol Biotechnol https://doi.org/10.1007/s00253-017-8096-9.

64. Flemming HC, Wingender J. 2010. The biofilm matrix. Nat Rev Microbiol https://doi.org/10.1038/nrmicro2415.

65. Jamal M, Ahmad W, Andleeb S, Jalil F, Imran M, Nawaz MA, Hussain T, Ali M, Rafiq M, Kamil MA. 2018. Bacterial biofilm and associated infections. Journal of the Chinese Medical Association https://doi.org/10.1016/j.jcma.2017.07.012.

66. Elexson N, Afsah-Hejri L, Rukayadi Y, Soopna P, Lee HY, Tuan Zainazor TC, Nor Ainy M, Nakaguchi Y, Mitsuaki N, Son R. 2014. Effect of detergents as antibacterial agents on biofilm of antibiotics-resistant *Vibrio parahaemolyticus* isolates. Food Control 35.

67. COLWELL RR, HUQ A. 1994. Environmental Reservoir of *Vibrio cholerae.* The Causative Agent of Cholera. Ann N Y Acad Sci 740.

68. de Magny GC, Mozumder PK, Grim CJ, Hasan NA, Naser MN, Alam M, Sack RB, Huq A, Colwell RR. 2011. Role of zooplankton diversity in *Vibrio cholerae* population dynamics and in the incidence of cholera in the Bangladesh sundarbans. Appl Environ Microbiol 77.

69. Kaneko T, Colwell RR. 1975. Adsorption of *Vibrio parahaemolyticus* onto Chitin and Copepods. Appl Microbiol 29.

70. Hall-Stoodley L, Costerton JW, Stoodley P. 2004. Bacterial biofilms: From the natural environment to infectious diseases. Nat Rev Microbiol https://doi.org/10.1038/nrmicro821.

71. Stoodley P, Sauer K, Davies DG, Costerton JW. 2002. Biofilms as complex differentiated communities. Annu Rev Microbiol https://doi.org/10.1146/annurev.micro.56.012302.160705.

72. Baty AM, Eastburn CC, Techkarnjanaruk S, Goodman AE, Geesey GG. 2000. Spatial and temporal variations in chitinolytic gene expression and bacterial biomass production during chitin degradation. Appl Environ Microbiol 66.

73. Freitas C, Glatter T, Ringgaard S. 2020. The release of a distinct cell type from swarm colonies facilitates dissemination of *Vibrio parahaemolyticus* in the environment. ISME Journal 14.

74. Gamble MD, Lovell CR. 2011. Infaunal burrows are enrichment zones for *Vibrio parahaemolyticus.* Appl Environ Microbiol 77.

75. Han N, Mizan MFR, Jahid IK, Ha S Do. 2016. Biofilm formation by *Vibrio parahaemolyticus* on food and food contact surfaces increases with rise in temperature. Food Control 70.

76. Song X, Ma Y, Fu J, Zhao A, Guo Z, Malakar PK, Pan Y, Zhao Y. 2017. Effect of temperature on pathogenic and non-pathogenic *Vibrio parahaemolyticus* biofilm formation. Food Control 73.

77. Shen X, Cai Y, Liu C, Liu W, Hui Y, Su YC. 2009. Effect of temperature on uptake and survival of *Vibrio parahaemolyticus* in oysters (*Crassostrea plicatula*). Int J Food Microbiol 136.

78. McCarter L, Silverman M. 1989. Iron regulation of swarmer cell differentiation of *Vibrio parahaemolyticus*. J Bacteriol 171.

79. Belas R, Simon M, Silverman M. 1986. Regulation of lateral flagella gene transcription in *Vibrio parahaemolyticus*. J Bacteriol 167.

80. Gode-Potratz CJ, Kustusch RJ, Breheny PJ, Weiss DS, McCarter LL. 2011. Surface sensing in *Vibrio parahaemolyticus* triggers a programme of gene expression that promotes colonization and virulence. Mol Microbiol 79.

81. McCarter L. 1999. The multiple identities of *Vibrio parahaemolyticus*. Journal of Molecular Microbiology and Biotechnology.

82. Chen SY, Jane WN, Chen YS, Wong H chung. 2009. Morphological changes of *Vibrio parahaemolyticus* under cold and starvation stresses. Int J Food Microbiol 129.

83. McCarter LL. 1998. OpaR, a homolog of *Vibrio harveyi* LuxR, controls opacity of *Vibrio parahaemolyticus.* J Bacteriol 180.

84. Kalburge SS, Carpenter MR, Rozovsky S, Fidelma Boyd E. 2017. Quorum sensing regulators are required for metabolic fitness in *Vibrio parahaemolyticus*. Infect Immun 85.

85. Enos-Berlage JL, McCarter LL. 2000. Relation of capsular polysaccharide production and colonial cell organization to colony morphology in *Vibrio parahaemolyticus*. J Bacteriol 182.

86. Boles BR, McCarter LL. 2002. *Vibrio parahaemolyticus* scrABC, a novel operon affecting swarming and capsular polysaccharide regulation. J Bacteriol 184.

87. Salomon D, Gonzalez H, Updegraff BL, Orth K. 2013. *Vibrio parahaemolyticus* Type VI Secretion System 1 Is Activated in Marine Conditions to Target Bacteria, and Is Differentially Regulated from System 2. PLoS One 8.

88. Kirn TJ, Jude BA, Taylor RK. 2005. A colonization factor links *Vibrio cholerae* environmental survival and human infection. Nature 438.

89. McCarter LL. 2004. Dual flagellar systems enable motility under different circumstances. J Mol Microbiol Biotechnol https://doi.org/10.1159/000077866.

90. Freitas C, Glatter T, Ringgaard S. 2020. Specific proteomic adaptation to distinct environments in *Vibrio parahaemolyticus* includes significant fluctuations in expression of essential proteins. Environ Microbiol 22.

91. Ellett AN, Rosales D, Jacobs JM, Paranjpye R, Parveen S. 2022. Growth Rates of *Vibrio parahaemolyticus* Sequence Type 36 Strains in Live Oysters and in Culture Medium. Microbiol Spectr 10.

92. Litvak Y, Bäumler AJ. 2019. The founder hypothesis: A basis for microbiota resistance, diversity in taxa carriage, and colonization resistance against pathogens. PLoS Pathog 15.

93. Freter R. 1981. Mechanisms of association of bacteria with mucosal surfaces. Ciba Found Symp https://doi.org/10.1002/9780470720639.ch4.

94. SEKI H. 1966. Seasonal Fluctuation of Heterotrophic Bacteria in the Sea of Aburatsubo Inlet. Journal of the Oceanographical Society of Japan 22.

95. Raimundo I, Silva R, Meunier L, Valente SM, Lago-Lestón A, Keller-Costa T, Costa R. 2021. Functional metagenomics reveals differential chitin degradation and utilization features across free-living and host-associated marine microbiomes. Microbiome 9.

96. Kadokura K, Rokutani A, Yamamoto M, Ikegami T, Sugita H, Itoi S, Hakamata W, Oku T, Nishio T. 2007. Purification and characterization of *Vibrio parahaemolyticus* extracellular chitinase and chitin oligosaccharide deacetylase involved in the production of heterodisaccharide from chitin. Appl Microbiol Biotechnol 75.

97. Lin H, Yu M, Wang X, Zhang XH. 2018. Comparative genomic analysis reveals the evolution and environmental adaptation strategies of *vibrios*. BMC Genomics 19.

98. Mansergh S, Zehr JP. 2014. *Vibrio* diversity and dynamics in the Monterey Bay upwelling region. Front Microbiol 5.

99. Regmi A, Boyd EF. 2019. Carbohydrate metabolic systems present on genomic islands are lost and gained in *Vibrio parahaemolyticus*. BMC Microbiol 19.

100. Getz LJ. 2022. GENOME-WIDE INVESTIGATION OF *VIBRIO PARAHAEMOLYTICUS* TYPE III SECRETION SYSTEM-1 REGULATION AND CHITIN METABOLISM.

101. Getz LJ, Brown JM, Sobot L, Chow A, Mahendrarajah J, Thomas NA. 2023. Attenuation of a DNA cruciform by a conserved regulator directs T3SS1 mediated virulence in *Vibrio parahaemolyticus.* Nucleic Acids Res 51.

102. Kim BS. 2020. Spatiotemporal Regulation of *Vibrio* Exotoxins by HlyU and Other Transcriptional Regulators. Toxins (Basel) https://doi.org/10.3390/toxins12090544.

103. Dunn AK, Millikan DS, Adin DM, Bose JL, Stabb E V. 2006. New rfp- and pES213-derived tools for analyzing symbiotic *Vibrio fischeri* reveal patterns of infection and lux expression in situ. Appl Environ Microbiol 72.

104. Stabb E V., Ruby EG. 2002. RP4-based plasmids for conjugation between *Escherichia coli* and members of the *vibrionaceae*. Methods Enzymol 358.

105. Lyell NL, Dunn AK, Bose JL, Vescovi SL, Stabb E V. 2008. Effective mutagenesis of *Vibrio fischeri* by using hyperactive mini-Tn5 derivatives. Appl Environ Microbiol 74.

106. Edwards RA, Keller LH, Schifferli DM. 1998. Improved allelic exchange vectors and their use to analyze 987P fimbria gene expression. Gene 207.

107. O'Toole GA, Kolter R. 1998. Initiation of biofilm formation in *Pseudomonas fluorescens* WCS365 proceeds via multiple, convergent signalling pathways: A genetic analysis. Mol Microbiol 28.

108. Enos-Berlage JL, Guvener ZT, Keenan CE, McCarter LL. 2005. Genetic determinants of biofilm development of opaque and translucent *Vibrio parahaemolyticus.* Mol Microbiol 55.

109. Keller M, Han X, Dörr T. 2023. Disrupting Central Carbon Metabolism Increases β-Lactam Antibiotic Susceptibility in *Vibrio cholerae.* J Bacteriol 205.

110. Lemos Rocha LF, Peters K, Biboy J, Depelteau JS, Briegel A, Vollmer W, Blokesch M. 2022. The VarA-CsrA regulatory pathway influences cell shape in *Vibrio cholerae.* PLoS Genet 18.

111. Zhang H, Li L, Zhao Z, Peng D, Zhou X. 2016. Polar flagella rotation in *Vibrio parahaemolyticus* confers resistance to bacteriophage infection. Sci Rep 6.

112. Taylor RK, Miller VL, Furlong DB, Mekalanos JJ. 1987. Use of phoA gene fusions to identify a pilus colonization factor coordinately regulated with cholera toxin. Proc Natl Acad Sci U S A 84.

113. Grainger DC, Overton TW, Reppas N, Wade JT, Tamai E, Hobman JL, Constantinidou C, Struhl K, Church G, Busby SJW. 2004. Genomic studies with *Escherichia coli* MelR protein: Applications of chromatin immunoprecipitation and microarrays. J Bacteriol 186.

114. Gu D, Liu H, Yang Z, Zhang Y, Wang Q. 2016. Chromatin immunoprecipitation sequencing technology reveals global regulatory roles of low-cell-density quorum-sensing regulator AphA in the pathogen *Vibrio alginolyticus.* J Bacteriol 198.

115. Jaskolska M, Stutzmann S, Stoudmann C, Blokesch M. 2018. QstR-dependent regulation of natural competence and type VI secretion in *Vibrio cholerae.* Nucleic Acids Res 46.

116. Li H, Durbin R. 2010. Fast and accurate long-read alignment with Burrows-Wheeler transform. Bioinformatics 26.

117. Ramírez F, Ryan DP, Grüning B, Bhardwaj V, Kilpert F, Richter AS, Heyne S, Dündar F, Manke T. 2016. deepTools2: a next generation web server for deep-sequencing data analysis. Nucleic Acids Res 44.

118. Freese NH, Norris DC, Loraine AE. 2016. Integrated genome browser: Visual analytics platform for genomics. Bioinformatics 32.

119. Guan C, Kumar S. 2005. A single catalytic domain of the junction-resolving enzyme T7 endonuclease I is a non-specific nicking endonuclease. Nucleic Acids Res 33.

120. Mahmoudi N, Enke TN, Beaupré SR, Teske AP, Cordero OX, Pearson A. 2020. Illuminating microbial species-specific effects on organic matter remineralization in marine sediments. Environ Microbiol 22.

121. Arnosti C. 2011. Microbial extracellular enzymes and the marine carbon cycle. Ann Rev Mar Sci 3.

122. Li X, Wang LX, Wang X, Roseman S. 2007. The chitin catabolic cascade in the marine bacterium *Vibrio cholerae*: Characterization of a unique chitin oligosaccharide deacetylase. Glycobiology 17.

123. Poulicek M, Jeuniaux C. 1991. Chitin biodegradation in marine environments: An experimental approach. Biochem Syst Ecol 19.

124. Li X, Roseman S. 2004. The chitinolytic cascade in *Vibrios* is regulated by chitin oligosaccharides and a two-component chitin catabolic sensor/kinase. Proc Natl Acad Sci U S A 101.

125. Hunt DE, Gevers D, Vahora NM, Polz MF. 2008. Conservation of the chitin utilization pathway in the *Vibrionaceae*. Appl Environ Microbiol 74.

126. Keyhani NO, Roseman S. 1999. Physiological aspects of chitin catabolism in marine bacteria. Biochim Biophys Acta Gen Subj https://doi.org/10.1016/S0304-4165(99)00172-5.

127. Keyhani NO, Li XB, Roseman S. 2000. Chitin catabolism in the marine bacterium *Vibrio furnissii.* Identification and molecular cloning of a chitoporin. Journal of Biological Chemistry 275.

128. Bouma CL, Roseman S. 1996. Sugar transport by the marine chitinolytic bacterium *Vibrio furnissii*: Molecular cloning and analysis of the glucose and N-acetylglucosamine permeases. Journal of Biological Chemistry 271.

129. Keyhani NO, Roseman S. 1996. The chitin catabolic cascade in the marine bacterium *Vibrio furnissii:* Molecular cloning, isolation, and characterization of a periplasmic β-N-acetylglucosaminidase. Journal of Biological Chemistry 271.

130. Keyhani NO, Roseman S. 1996. The chitin catabolic cascade in the marine bacterium *Vibrio furnissii:* Molecular cloning, isolation, and characterization of a periplasmic chitodextrinase. Journal of Biological Chemistry 271.

131. Blokesch M. 2012. Chitin colonization, chitin degradation and chitin-induced natural competence of *Vibrio cholerae* are subject to catabolite repression. Environ Microbiol 14.

132. Debnath A, Mizuno T, Miyoshi SI. 2020. Regulation of chitin-dependent growth and natural competence in *Vibrio parahaemolyticus*. Microorganisms 8.

133. Udden SMN, Zahid MSH, Biswas K, Ahmad QS, Cravioto A, Nair GB, Mekalanos JJ, Faruque SM. 2008. Acquisition of classical CTX prophage from *Vibrio cholerae* O141 by El Tor strains aided by lytic phages and chitin-induced competence. Proc Natl Acad Sci U S A 105.

134. Sinha-Ray S, Alam MT, Bag S, Morris JG, Ali A. 2019. Conversion of a recA-Mediated Non-toxigenic *Vibrio cholerae* O1 Strain to a Toxigenic Strain Using Chitin-Induced Transformation. Front Microbiol 10.

135. Blokesch M, Schoolnik GK. 2007. Serogroup conversion of *Vibrio cholerae* in aquatic reservoirs. PLoS Pathog 3.

136. Sun S, Tay QXM, Kjelleberg S, Rice SA, McDougald D. 2015. Quorum sensing-regulated chitin metabolism provides grazing resistance to *Vibrio cholerae* biofilms. ISME Journal 9.

137. Thompson FL, Neto AA, Santos E de O, Izutsu K, Iida T. 2011. Effect of N-acetyl-D-glucosamine on gene expression in *Vibrio parahaemolyticus.* Microbes Environ 26.

138. Meiborn KL, Li XB, Nielsen AT, Wu CY, Roseman S, Schoolnik GK. 2004. The *Vibrio cholerae* chitin utilization program. Proc Natl Acad Sci U S A 101.

139. Martinez-Urtaza J, Blanco-Abad V, Rodriguez-Castro A, Ansede-Bermejo J, Miranda A, Rodriguez-Alvarez MX. 2012. Ecological determinants of the occurrence and dynamics of *Vibrio parahaemolyticus* in offshore areas. ISME Journal 6.

140. Bateman A. 1999. The SIS domain: a phosphosugar-binding domain.

141. Jaeger T, Mayer C. 2008. The transcriptional factors MurR and catabolite activator protein regulate N-acetylmuramic acid catabolism in *Escherichia coli*. J Bacteriol 190.

142. Daddaoua A, Krell T, Ramos JL. 2009. Regulation of glucose metabolism in *Pseudomonas*. The phosphorylative branch and Entner-Doudoroff enzymes are regulated by a repressor containing a sugar isomerase domain. Journal of Biological Chemistry 284.

143. Goodell EW. 1985. Recycling of murein by *Escherichia coli.* J Bacteriol 163.

144. Zhang Y, Chen W, Wu D, Liu Y, Wu Z, Li J, Zhang SY, Ji Q. 2022. Molecular basis for cell-wall recycling regulation by transcriptional repressor MurR in *Escherichia coli*. Nucleic Acids Res 50:5948–5960.

145. Leyn SA, Li X, Zheng Q, Novichkov PS, Reed S, Romine MF, Fredrickson JK, Yang C, Osterman AL, Rodionov DA. 2011. Control of proteobacterial central carbon metabolism by the HexR transcriptional regulator: A case study in *Shewanella oneidensis*. Journal of Biological Chemistry 286.

146. Yamamoto H, Serizawa M, Thompson J, Sekiguchi J. 2001. Regulation of the glv operon in *Bacillus subtilis*: YfiA (GlvR) is a positive regulator of the operon that is repressed through CcpA and cre. J Bacteriol 183.

147. Sørensen KI, Hove-Jensen B. 1996. Ribose catabolism of *Escherichia coli*: Characterization of the rpiB gene encoding ribose phosphate isomerase B and of the rpiR gene, which is involved in regulation of rpiB expression. J Bacteriol 178.

148. Novichkov PS, Kazakov AE, Ravcheev DA, Leyn SA, Kovaleva GY, Sutormin RA, Kazanov MD, Riehl W, Arkin AP, Dubchak I, Rodionov DA. 2013. RegPrecise 3.0 - A resource for genome-scale exploration of transcriptional regulation in bacteria. BMC Genomics 14.

149. Mayer C, Kluj RM, Mühleck M, Walter A, Unsleber S, Hottmann I, Borisova M. 2019. Bacteria’s different ways to recycle their own cell wall. International Journal of Medical Microbiology https://doi.org/10.1016/j.ijmm.2019.06.006.

150. Li W, Li Y, Shi W, Zhang W. 2024. GlpD involved in the virulence and persistence of a marine pathogen *Vibrio splendidus*. Aquaculture 585.

151. Nikel PI, Romero-Campero FJ, Zeidman JA, Goñi-Moreno Á, de Lorenzo V. 2015. The glycerol-dependent metabolic persistence of *Pseudomonas putida* KT2440 reflects the regulatory logic of the GlpR repressor. mBio 6.

152. Navarro Llorens JM, Tormo A, Martínez-García E. 2010. Stationary phase in gram-negative bacteria. FEMS Microbiol Rev https://doi.org/10.1111/j.1574-6976.2010.00213.x.

153. Ishihama A. 1997. Adaptation of gene expression in stationary phase bacteria. Curr Opin Genet Dev 7.

154. Jaishankar J, Srivastava P. 2017. Molecular basis of stationary phase survival and applications. Front Microbiol https://doi.org/10.3389/fmicb.2017.02000.

155. Subramanian K, Sadaiappan B, Aruni W, Kumarappan A, Thirunavukarasu R, Srinivasan GP, Bharathi S, Nainangu P, Renuga PS, Elamaran A, Balaraman D, Subramanian M. 2020. Bioconversion of chitin and concomitant production of chitinase and N-acetylglucosamine by novel *Achromobacter xylosoxidans* isolated from shrimp waste disposal area. Sci Rep 10.

156. 2012. Simplified Method of Preparing Colloidal Chitin Used For Screening of Chitinase- Producing Microorganisms. Internet J Microbiol 10.

157. Hirano T, Okubo M, Tsuda H, Yokoyama M, Hakamata W, Nishio T. 2019. Chitin heterodisaccharide, released from chitin by chitinase and chitin oligosaccharide deacetylase, enhances the chitin-metabolizing ability of *Vibrio parahaemolyticus*. J Bacteriol 201.

158. Irnov I, Wang Z, Jannetty ND, Bustamante JA, Rhee KY, Jacobs-Wagner C. 2017. Crosstalk between the tricarboxylic acid cycle and peptidoglycan synthesis in *Caulobacter crescentus* through the homeostatic control of α-ketoglutarate. PLoS Genet 13.

159. Westfall CS, Levin PA. 2018. Comprehensive analysis of central carbon metabolism illuminates connections between nutrient availability, growth rate, and cell morphology in *Escherichia coli.* PLoS Genet 14.

160. Roller BRK, Hellerschmied C, Wu Y, Miettinen TP, Gomez AL, Manalis SR, Polz MF. 2023. Single-cell mass distributions reveal simple rules for achieving steady-state growth. mBio 14.

161. Zhao J, Baba T, Mori H, Shimizu K. 2004. Global metabolic response of *Escherichia coli* to gnd or zwf gene-knockout, based on 13C-labeling experiments and the measurement of enzyme activities. Appl Microbiol Biotechnol 64.

162. Rashida Z, Laxman S. 2021. The pentose phosphate pathway and organization of metabolic networks enabling growth programs. Curr Opin Syst Biol https://doi.org/10.1016/j.coisb.2021.100390.

163. Dauvillée D, Kinderf IS, Li Z, Kosar-Hashemi B, Samuel MS, Rampling L, Ball S, Morell MK. 2005. Role of the *Escherichia coli* glgX gene in glycogen metabolism. J Bacteriol 187.

164. Hua Q, Yang C, Baba T, Mori H, Shimizu K. 2003. Responses of the Central Metabolism in *Escherichia coli* to Phosphoglucose Isomerase and Glucose-6-Phosphate Dehydrogenase Knockouts. J Bacteriol 185.

165. Cheng Q, Li H, Merdek K, Park JT. 2000. Molecular characterization of the β-N-acetylglucosaminidase of *Escherichia coli* and its role in cell wall recycling. J Bacteriol 182.

166. Thompson JR, Randa MA, Marcelino LA, Tomita-Mitchell A, Lim E, Polz MF. 2004. Diversity and dynamics of a North Atlantic coastal *Vibrio* community. Appl Environ Microbiol 70.

167. Meparambu Prabhakaran D, Ramamurthy T, Thomas S. 2020. Genetic and virulence characterisation of *Vibrio parahaemolyticus* isolated from Indian coast. BMC Microbiol 20.

168. Watson JD, Crick FHC. 1953. Molecular structure of nucleic acids: A structure for deoxyribose nucleic acid. Nature 171.

169. Bettotti P, Visone V, Lunelli L, Perugino G, Ciaramella M, Valenti A. 2018. Structure and Properties of DNA Molecules over the Full Range of Biologically Relevant Supercoiling States. Sci Rep 8.

170. Krasilnikov AS, Podtelezhnikov A, Vologodskii A, Mirkin SM. 1999. Large-scale effects of transcriptional DNA supercoiling in vivo. J Mol Biol 292.

171. Dai X, Greizerstein MB, Nadas-Chinni K, Rothman-Denes LB. 1997. Supercoil-induced extrusion of a regulatory DNA hairpin. Proc Natl Acad Sci U S A 94.

172. Wang AHJ, Quigley GJ, Kolpak FJ, Crawford JL, Van Boom JH, Van Der Marel G, Rich A. 1979. Molecular structure of a left-Handed double helical DNA fragment at atomic resolution. Nature 282.

173. Murat P, Balasubramanian S. 2014. Existence and consequences of G-quadruplex structures in DNA. Curr Opin Genet Dev https://doi.org/10.1016/j.gde.2013.10.012.

174. Matek C, Ouldridge TE, Levy A, Doye JPK, Louis AA. 2012. DNA cruciform arms nucleate through a correlated but asynchronous cooperative mechanism. Journal of Physical Chemistry B 116.

175. Mikheikin AL, Lushnikov AY, Lyubchenko YL. 2006. Effect of DNA supercoiling on the geometry of holliday junctions. Biochemistry 45.

176. Brázda V, Laister RC, Jagelská EB, Arrowsmith C. 2011. Cruciform structures are a common DNA feature important for regulating biological processes. BMC Mol Biol https://doi.org/10.1186/1471-2199-12-33.

177. Brazda V, Fojta M, Bowater RP. 2020. Structures and stability of simple DNA repeats from bacteria. Biochemical Journal https://doi.org/10.1042/BCJ20190703.

178. Lavi B, Karin EL, Pupko T, Hazkani-Covo E. 2018. The prevalence and evolutionary conservation of inverted repeats in proteobacteria. Genome Biol Evol 10.

179. Mizuuchi K, Mizuuchi M, Gellert M. 1982. Cruciform structures in palindromic DNA are favored by DNA supercoiling. J Mol Biol 156.

180. Tsao YP, Wu HY, Liu LF. 1989. Transcription-driven supercoiling of DNA: Direct biochemical evidence from in vitro studies. Cell 56.

181. Tupper AE, Owen-Hughes TA, Ussery DW, Santos DS, Ferguson DJ, Sidebotham JM, Hinton JC, Higgins CF. 1994. The chromatin-associated protein H-NS alters DNA topology in vitro. EMBO J 13.

182. Lang B, Blot N, Bouffartigues E, Buckle M, Geertz M, Gualerzi CO, Mavathur R, Muskhelishvili G, Pon CL, Rimsky S, Stella S, Babu MM, Travers A. 2007. High-affinity DNA binding sites for H-NS provide a molecular basis for selective silencing within proteobacterial genomes. Nucleic Acids Res 35.

183. Gomes ALC, Johns NI, Yang A, Velez-Cortes F, Smillie CS, Smith MB, Alm EJ, Wang HH. 2020. Genome and sequence determinants governing the expression of horizontally acquired DNA in bacteria. ISME Journal 14.

184. Yang J, Tauschek M, Strugnell R, Robins-Browne RM. 2005. The H-NS protein represses transcription of the eltAB operon, which encodes heat-labile enterotoxin in enterotoxigenic *Escherichia coli,* by binding to regions downstream of the promoter. Microbiology (N Y) 151.

185. Figueroa-Bossi N, Sanchez-Romero MA, Kerboriou P, Naquin D, Mendes C, Bouloc P, Casadesus J, Bossi L. 2022. Pervasive transcription enhances the accessibility of H-NS-silenced promoters and generates bistability in *Salmonella* virulence gene expression. Proc Natl Acad Sci U S A 119.

186. Barth M, Marschall C, Muffler A, Fischer D, Hengge-Aronis R. 1995. Role for the histone-like protein H-NS in growth phase-dependent and osmotic regulation of σ(S) and many σ(S)-dependent genes in *Escherichia coli*. J Bacteriol 177.

187. Atlung T, Ingmer H. 1997. H-NS: A modulator of environmentally regulated gene expression. Mol Microbiol https://doi.org/10.1046/j.1365-2958.1997.3151679.x.

188. Hommais F, Krin E, Laurent-Winter C, Soutourina O, Malpertuy A, Le Caer JP, Danchin A, Bertin P. 2001. Large-scale monitoring of pleiotropic regulation of gene expression by the prokaryotic nucleoid-associated protein, H-NS. Mol Microbiol 40.

189. Falconi M, Colonna B, Prosseda G, Micheli G, Gualerzi CO. 1998. Thermoregulation of *Shigella* and *Escherichia coli* EIEC pathogenicity. A temperature-dependent structural transition of DNA modulates accessibility of virF promoter to transcriptional repressor H-NS. EMBO Journal 17.

190. Kohno K, Yasuzawa K, Hirose M, Rano Y, Goshima N, Tanaka H, Imamoto F. 1994. Autoregulation of Transcription of the hup A Gene in *Escherichia coli:* Evidence for Steric Hindrance of the Functional Promoter Domains Induced by HUJ Biochem.

191. Fang M, Wu HY. 1998. A promoter relay mechanism for sequential gene activation. J Bacteriol 180.

192. Stefanovsky VY, Moss T. 2009. The cruciform DNA mobility shift assay: A tool to study proteins that recognize bent DNA. Methods in Molecular Biology 543.

193. Chasovskikh S, Dimtchev A, Smulson M, Dritschilo A. 2005. DNA transitions induced by binding of PARP-1 to cruciform structures in supercoiled plasmids. Cytometry Part A 68.

194. Wu C, Zhao Z, Liu Y, Zhu X, Liu M, Luo P, Shi Y. 2020. Type III Secretion 1 Effector Gene Diversity Among *Vibrio* Isolates From Coastal Areas in China. Front Cell Infect Microbiol 10.

195. Zhou X, Konkel ME, Call DR. 2009. Type III secretion system 1 of *Vibrio parahaemolyticus* induces oncosis in both epithelial and monocytic cell lines. Microbiology (N Y) 155.

196. Zhou X, Shah DH, Konkel ME, Call DR. 2008. Type III secretion system 1 genes in *Vibrio parahaemolyticus* are positively regulated by ExsA and negatively regulated by ExsD. Mol Microbiol 69.

197. Liu AC, Thomas NA. 2015. Transcriptional profiling of *Vibrio parahaemolyticus* exsA reveals a complex activation network for type III secretion. Front Microbiol 6.

198. Mukherjee D, Datta AB, Chakrabarti P. 2014. Crystal structure of HlyU, the hemolysin gene transcription activator, from *Vibrio cholerae* N16961 and functional implications. Biochim Biophys Acta Proteins Proteom 1844.

199. Brennan RG. 1993. The winged-helix DNA-binding motif: Another helix-turn-helix takeoff. Cell https://doi.org/10.1016/0092-8674(93)90456-Z.

200. Kim YR, Lee SE, Kim CM, Kim SY, Shin EK, Shin DH, Chung SS, Choy HE, Progulske-Fox A, Hillman JD, Handfield M, Rhee JH. 2003. Characterization and pathogenic significance of *Vibrio vulnificus* antigens preferentially expressed in septicemic patients. Infect Immun 71.

201. Williams SG, Attridge SR, Manning PA. 1993. The transcriptional activator HIyU of *Vibrio cholerae*: nucleotide sequence and role in virulence gene expression. Mol Microbiol 9.

202. Xiangyu Mou, Spinard EJ, Driscoll M V., Zhao W, Nelson DR. 2013. H-NS is a negative regulator of the two hemolysin/cytotoxin gene clusters in *Vibrio anguillarum*. Infect Immun 81.

203. Liu M, Naka H, Crosa JH. 2009. HlyU acts as an H-NS antirepressor in the regulation of the RTX toxin gene essential for the virulence of the human pathogen *Vibrio vulnificus* CMCP6. Mol Microbiol 72.

204. Gao H, Xu J, Lu X, Li J, Lou J, Zhao H, Diao B, Shi Q, Zhang Y, Kan B. 2018. Expression of hemolysin is regulated under the collective actions of HapR, Fur, and HlyU in *Vibrio cholerae* El Tor serogroup O1. Front Microbiol 9.

205. Williams SG, Varcoe LT, Attridge SR, Manning PA. 1996. *Vibrio cholerae* Hcp, a secreted protein coregulated with HlyA. Infect Immun 64.

206. Liu M, Crosa JH. 2012. The regulator HlyU, the repeat-in-toxin gene rtxA1, and their roles in the pathogenesis of *Vibrio vulnificus* infections. Microbiologyopen 1.

207. Li L, Mou X, Nelson DR. 2011. HlyU is a positive regulator of hemolysin expression in *Vibrio anguillarum.* J Bacteriol 193.

208. Jang KK, Lee ZW, Kim B, Jung YH, Han HJ, Kim MH, Kim BS, Choi SH. 2017. Identification and characterization of *Vibrio vulnificus* plpA encoding a phospholipase A2 essential for pathogenesis. Journal of Biological Chemistry 292.

209. Mukherjee D, Pal A, Chakravarty D, Chakrabarti P. 2015. Identification of the target DNA sequence and characterization of DNA binding features of HlyU, and suggestion of a redox switch for hlyA expression in the human pathogen *Vibrio* cholerae from in silico studies. Nucleic Acids Res 43.

210. Solomon MJ, Larsen PL, Varshavsky A. 1988. Mapping protein-DNA interactions in vivo with formaldehyde: Evidence that histone H4 is retained on a highly transcribed gene. Cell 53.

211. Kidder BL, Hu G, Zhao K. 2011. ChIP-Seq: Technical considerations for obtaining high-quality data. Nat Immunol https://doi.org/10.1038/ni.2117.

212. Hoffman EA, Frey BL, Smith LM, Auble DT. 2015. Formaldehyde crosslinking: A tool for the study of chromatin complexes. Journal of Biological Chemistry https://doi.org/10.1074/jbc.R115.651679.

213. Park PJ. 2009. ChIP-seq: Advantages and challenges of a maturing technology. Nat Rev Genet https://doi.org/10.1038/nrg2641.

214. Shin JH, Lanz M, Smolka MB, Dörr T. 2020. Characterization of an anti-FLAG antibody binding protein in *V. cholerae.* Biochem Biophys Res Commun 528.

215. Maqueda JJ, Giovanazzi A, Rocha AM, Rocha S, Silva I, Saraiva N, Bonito N, Carvalho J, Maia L, Wauben MHM, Oliveira C. 2023. Adapter dimer contamination in sRNA-sequencing datasets predicts sequencing failure and batch effects and hampers extracellular vesicle-sRNA analysis. Journal of Extracellular Biology 2.

216. Eichmann C, Tzitzilonis C, Bordignon E, Maslennikov I, Choe S, Riek R. 2014. Solution NMR structure and functional analysis of the integral membrane protein YgaP from *Escherichia coli*. Journal of Biological Chemistry 289.

217. Cipollone R, Ascenzi P, Tomao P, Imperi F, Visca P. 2008. Enzymatic detoxification of cyanide: Clues from *Pseudomonas aeruginosa* rhodanese. J Mol Microbiol Biotechnol https://doi.org/10.1159/000121331.

218. BONOMI F, PAGANI S, KURTZ DM. 1985. Enzymic synthesis of the 4Fe–4S clusters of *Clostridium pasteurianum* ferredoxin. Eur J Biochem 148.

219. Bordo D, Bork P. 2002. The rhodanese/Cdc25 phosphatase superfamily. Sequence-structure-function relations. EMBO Rep https://doi.org/10.1093/embo-reports/kvf150.

220. Heidelberg JF, Elsen JA, Nelson WC, Clayton RA, Gwinn ML, Dodson RJ, Haft DH, Hickey EK, Peterson JD, Umayam L, Gill SR, Nelson KE, Read TD, Tettelin H, Richardson D, Ermolaeva MD, Vamathevan J, Bass S, Halving Q, Dragol I, Sellers P, McDonald L, Utterback T, Fleishmann RD, Nierman WC, White O, Saizberg SL, Smith HO, Colwell RR, Mekalanos JJ, Venter CJ, Fraser CM. 2000. DNA sequence of both chromosomes of the cholera pathogen *Vibrio cholerae*. Nature 406.

221. Bobay BG, Andreeva A, Mueller GA, Cavanagh J, Murzin AG. 2005. Revised structure of the AbrB N-terminal domain unifies a diverse superfamily of putative DNA-binding proteins. FEBS Lett 579.

222. Kamada K, Hanaoka F, Burley SK. 2003. Crystal structure of the MazE/MazF complex: Molecular bases of antidote-toxin recognition. Mol Cell 11.

223. Hamon MA, Stanley NR, Britton RA, Grossman AD, Lazazzera BA. 2004. Identification of AbrB-regulated genes involved in biofilm formation by *Bacillus subtilis.* Mol Microbiol 52.

224. Chen Y, Stine OC, Badger JH, Gil AI, Nair GB, Nishibuchi M, Fouts DE. 2011. Comparative genomic analysis of *Vibrio parahaemolyticus*: Serotype conversion and virulence. BMC Genomics 12.

225. Song X, Lin Z, Yuan W. 2022. Toxin–antitoxin systems in pathogenic *Vibrio* species: a mini review from a structure perspective. 3 Biotech https://doi.org/10.1007/s13205-022-03178-3.

226. Seper A, Hosseinzadeh A, Gorkiewicz G, Lichtenegger S, Roier S, Leitner DR, Röhm M, Grutsch A, Reidl J, Urban CF, Schild S. 2013. *Vibrio cholerae* Evades Neutrophil Extracellular Traps by the Activity of Two Extracellular Nucleases. PLoS Pathog 9.

227. Bridges AA, Fei C, Bassler BL. 2020. Identification of signaling pathways, matrix-digestion enzymes, and motility components controlling *Vibrio cholerae* biofilm dispersal. Proc Natl Acad Sci U S A 117.

228. Pressler K, Mitterer F, Vorkapic D, Reidl J, Oberer M, Schild S. 2019. Characterization of *Vibrio cholerae*'s Extracellular Nuclease Xds. Front Microbiol 10.

229. Seper A, Fengler VHI, Roier S, Wolinski H, Kohlwein SD, Bishop AL, Camilli A, Reidl J, Schild S. 2011. Extracellular nucleases and extracellular DNA play important roles in *Vibrio cholerae* biofilm formation. Mol Microbiol 82.

230. Jones P, Binns D, Chang HY, Fraser M, Li W, McAnulla C, McWilliam H, Maslen J, Mitchell A, Nuka G, Pesseat S, Quinn AF, Sangrador-Vegas A, Scheremetjew M, Yong SY, Lopez R, Hunter S. 2014. InterProScan 5: Genome-scale protein function classification. Bioinformatics 30.

231. Mans BJ, Anantharaman V, Aravind L, Koonin E V. 2004. Comparative genomics, evolution and origins of the nuclear envelope and nuclear pore complex. Cell Cycle 3.

232. Flynn RL, Zou L. 2010. Oligonucleotide/oligosaccharide-binding fold proteins: A growing family of genome guardians. Crit Rev Biochem Mol Biol https://doi.org/10.3109/10409238.2010.488216.

233. Murzin AG. 1993. OB(oligonucleotide/oligosaccharide binding)-fold: common structural and functional solution for non-homologous sequences. EMBO J 12.

234. Brázda V, Kolomazník J, Lýsek J, Hároníková L, Coufal J, Šťastný J. 2016. Palindrome analyser – A new web-based server for predicting and evaluating inverted repeats in nucleotide sequences. Biochem Biophys Res Commun 478.

235. Ahmad E, Pant KK. 2018. Lignin conversion: A key to the concept of lignocellulosic biomass-based integrated biorefineryWaste Biorefinery: Potential and Perspectives.

236. Bourassa L, Camilli A. 2009. Glycogen contributes to the environmental persistence and transmission of *Vibrio cholerae.* Mol Microbiol 72.

237. Goodell EW, Schwarz U. 1985. Release of cell wall peptides into culture medium by exponentially growing *Escherichia coli.* J Bacteriol 162.

238. Chaloupka J, Strnadová M. 1972. Turnover of murein in a diaminopimelic acid dependent mutant of *Escherichia coli.* Folia Microbiol (Praha) 17.

239. Simpson BW, Gilmore MC, McLean AB, Cava F, Stephen Trent M. 2023. *Escherichia coli* utilizes multiple peptidoglycan recycling permeases with distinct strategies of recycling. Proc Natl Acad Sci U S A 120.

240. Malviya J, Alameri AA, Al-Janabi SS, Fawzi OF, Azzawi AL, Obaid RF, Alsudani AA, Alkhayyat AS, Gupta J, Mustafa YF, Karampoor S, Mirzaei R. 2023. Metabolomic profiling of bacterial biofilm: trends, challenges, and an emerging antibiofilm target. World J Microbiol Biotechnol https://doi.org/10.1007/s11274-023-03651-y.

241. Hall-Stoodley L, Stoodley P. 2002. Developmental regulation of microbial biofilms. Curr Opin Biotechnol https://doi.org/10.1016/S0958-1669(02)00318-X.

242. Pisithkul T, Schroeder JW, Trujillo EA, Yeesin P, Stevenson DM, Chaiamarit T, Coon JJ, Wang JD, Amador-Noguez D. 2019. Metabolic remodeling during biofilm development of *Bacillus subtilis*. mBio 10.

243. Muraleedharan S, Freitas C, Mann P, Glatter T, Ringgaard S. 2018. A cell length-dependent transition in MinD-dynamics promotes a switch in division-site placement and preservation of proliferating elongated *Vibrio parahaemolyticus* swarmer cells. Mol Microbiol 109.

244. Gober JW, Marques M V. 1995. Regulation of cellular differentiation in *Caulobacter crescentus*. Microbiol Rev https://doi.org/10.1128/mmbr.59.1.31-47.1995.

245. Wucher BR, Bartlett TM, Hoyos M, Papenfort K, Persat A, Nadell CD. 2019. *Vibrio cholerae* filamentation promotes chitin surface attachment at the expense of competition in biofilms. Proc Natl Acad Sci U S A 116.

246. Xu J, Kudron MM, Victorsen A, Gao J, Ammouri HN, Navarro FCP, Gevirtzman L, Waterston RH, White KP, Reinke V, Gerstein M. 2021. To mock or not: A comprehensive comparison of mock IP and DNA input for ChIP-seq. Nucleic Acids Res 49.

247. Xu J, Gao J, Ni P, Gerstein M. 2024. Less-is-more: selecting transcription factor binding regions informative for motif inference. Nucleic Acids Res 52.

248. Teytelman L, Thurtle DM, Rine J, Van Oudenaarden A. 2013. Highly expressed loci are vulnerable to misleading ChIP localization of multiple unrelated proteins. Proc Natl Acad Sci U S A 110.

249. Uversky VN. 2002. Natively unfolded proteins: A point where biology waits for physics. Protein Science 11.

250. Jain D, Baldi S, Zabel A, Straub T, Becker PB. 2015. Active promoters give rise to false positive “Phantom Peaks” in ChIP-seq experiments. Nucleic Acids Res 43.

251. Cheng H, Donahue JL, Battle SE, Ray WK, Larson TJ. 2008. Biochemical and Genetic Characterization of PspE and GlpE, Two Singledomain Sulfurtransferases of *Escherichia coli.* Open Microbiol J 2.

252. Donadio S, Shafiee A, Hutchinson CR. 1990. Disruption of a rhodaneselike gene results in cysteine auxotrophy in *Saccharopolyspora erythraea*. J Bacteriol 172.

253. Fang FC, Vázquez-Torres A. 2019. Reactive nitrogen species in host–bacterial interactions. Curr Opin Immunol https://doi.org/10.1016/j.coi.2019.05.008.

254. Fang FC. 1997. Perspectives series: host/pathogen interactions. Mechanisms of nitric oxide-related antimicrobial activity. Journal of Clinical Investigation 99.

255. Hyduke DR, Jarboe LR, Tran LM, Chou KJY, Liao JC. 2007. Integrated network analysis identifies nitric oxide response networks and dihydroxyacid dehydratase as a crucial target in *Escherichia coli.* Proc Natl Acad Sci U S A 104.

256. Eriksson S, Lucchini S, Thompson A, Rhen M, Hinton JCD. 2003. Unravelling the biology of macrophage infection by gene expression profiling of intracellular *Salmonella enterica*. Mol Microbiol 47.

257. Wallrodt I, Jelsbak L, Thorndahl L, Thomsen LE, Lemire S, Olsen JE. 2013. The Putative Thiosulfate Sulfurtransferases PspE and GlpE Contribute to Virulence of *Salmonella Typhimurium* in the Mouse Model of Systemic Disease. PLoS One 8.

258. DeAngelis CM, Nag D, Withey JH, Matson JS. 2019. Characterization of the *Vibrio cholerae* Phage Shock Protein ResponseJournal of Bacteriology.

259. Ueno T, Fischer JT, Boon EM. 2019. Nitric Oxide Enters Quorum Sensing via the H-NOX Signaling Pathway in *Vibrio parahaemolyticus*. Front Microbiol 10.

260. Liu M, Alice AF, Naka H, Crosa JH. 2007. The HlyU protein is a positive regulator of rtxA1, a gene responsible for cytotoxicity and virulence in the human pathogen *Vibrio vulnificus*. Infect Immun 75.

261. Dorman CJ. 1991. DNA supercoiling and environmental regulation of gene expression in pathogenic bacteria. Infect Immun https://doi.org/10.1128/iai.59.3.745-749.1991.

262. Goldstein E, Drlica K. 1984. Regulation of bacterial DNA supercoiling: Plasmid linking numbers vary with growth temperature. Proc Natl Acad Sci U S A 81.

263. Yamamoto N, Droffner ML. 1985. Mechanisms determining aerobic or anaerobic growth in the facultative anaerobe *Salmonella typhimurium*. Proc Natl Acad Sci U S A 82.

264. Higgins CF, Dorman CJ, Stirling DA, Waddell L, Booth IR, May G, Bremer E. 1988. A physiological role for DNA supercoiling in the osmotic regulation of gene expression in *S. typhimurium* and *E. coli*. Cell 52.

265. Jobling MG, Holmes RK. 1997. Characterization of hapR, a positive regulator of the *Vibrio cholerae* HA/protease gene hap, and its identification as a functional homologue of the *Vibrio harveyi* luxR gene. Mol Microbiol 26.

266. Blokesch M, Schoolnik GK. 2008. The extracellular nuclease Dns and its role in natural transformation of *Vibrio cholerae*. J Bacteriol 190.

267. Mcdonough E, Lazinski DW, Camilli A. 2014. Identification of in vivo regulators of the *Vibrio cholerae* xds gene using a high-throughput genetic selection. Mol Microbiol 92.

268. Jiang F, Lei T, Wang Z, He M, Zhang J, Wang J, Zeng H, Chen M, Xue L, Ye Q, Pang R, Wu S, Gu Q, Ding Y, Wu Q. 2021. A Novel Gene vp0610 Negatively Regulates Biofilm Formation in *Vibrio parahaemolyticus*. Front Microbiol 12.

269. Fine N, Tasevski N, McCulloch CA, Tenenbaum HC, Glogauer M. 2020. The Neutrophil: Constant Defender and First Responder. Front Immunol https://doi.org/10.3389/fimmu.2020.571085.

270. Bandyopadhaya A, Sarkar M, Chaudhuri K. 2007. Transcriptional upregulation of inflammatory cytokines in human intestinal epithelial cells following *Vibrio cholerae infection*. FEBS Journal 274.

271. Brinkmann V, Reichard U, Goosmann C, Fauler B, Uhlemann Y, Weiss DS, Weinrauch Y, Zychlinsky A. 2004. Neutrophil Extracellular Traps Kill Bacteria. Science (1979) 303.

272. Averhoff P, Kolbe M, Zychlinsky A, Weinrauch Y. 2008. Single Residue Determines the Specificity of Neutrophil Elastase for *Shigella* Virulence Factors. J Mol Biol 377.

273. Weinrauch Y, Drujan D, Shapiro SD, Weiss J, Zychlinsky A. 2002. Neutrophil elastase targets virulence factors of enterobacteria. Nature 417.

274. Papayannopoulos V, Zychlinsky A. 2009. NETs: a new strategy for using old weapons. Trends Immunol https://doi.org/10.1016/j.it.2009.07.011.

275. Uchiyama S, Andreoni F, Schuepbach RA, Nizet V, Zinkernagel AS. 2012. Dnase Sda1 allows invasive M1T1 group a *streptococcus* to prevent TLR9-dependent recognition. PLoS Pathog 8.

276. Shao CP, Lo HR, Lin JH, Hor LI. 2011. Regulation of cytotoxicity by quorum-sensing signaling in *Vibrio vulnificus* is mediated by SmcR, a repressor of hlyU. J Bacteriol 193.

277. Fisher TR, Gustafson AB, Sellner K, Lacouture R, Haas LW, Wetzel RL, Magnien R, Everitt D, Michaels B, Karrh R. 1999. Spatial and temporal variation of resource limitation in Chesapeake Bay. Mar Biol 133.

278. Pearman JK, Ellis J, Irigoien X, Sarma YVB, Jones BH, Carvalho S. 2017. Microbial planktonic communities in the Red Sea: high levels of spatial and temporal variability shaped by nutrient availability and turbulence. Sci Rep 7.

279. Dupont CL, Rusch DB, Yooseph S, Lombardo MJ, Alexander Richter R, Valas R, Novotny M, Yee-Greenbaum J, Selengut JD, Haft DH, Halpern AL, Lasken RS, Nealson K, Friedman R, Craig Venter J. 2012. Genomic insights to SAR86, an abundant and uncultivated marine bacterial lineage. ISME Journal 6.

280. Giraud X, Le Quéré C, da Cunha LC. 2008. Importance of coastal nutrient supply for global ocean biogeochemistry. Global Biogeochem Cycles 22.

281. Heinz V, Jäckel W, Kaltwasser S, Cutugno L, Bedrunka P, Graf A, Reder A, Michalik S, Dhople VM, Madej MG, Conway M, Lechner M, Riedel K, Bange G, Boyd A, Völker U, Lewis RJ, Marles-Wright J, Ziegler C, Pané-Farré J. 2022. The *Vibrio vulnificus* stressosome is an oxygen-sensor involved in regulating iron metabolism. Commun Biol 5.

282. Cutugno L, Tamayo BKS, Lens PNL, O'Byrne C, Pané-Farré J, Boyd A. 2023. In vivo characterisation of the *Vibrio vulnificus* stressosome: A complex involved in reshaping glucose metabolism and motility regulation, in nutrient- and iron-limited growth conditions. Curr Res Microb Sci 4.

283. Kamp HD, Patimalla-Dipali B, Lazinski DW, Wallace-Gadsden F, Camilli A. 2013. Gene Fitness Landscapes of *Vibrio cholerae* at Important Stages of Its Life Cycle. PLoS Pathog 9.

284. Nelson EJ, Chowdhury A, Flynn J, Schild S, Bourassa L, Shao Y, Larocque RC, Calderwood SB, Qadri F, Camilli A. 2008. Transmission of *Vibrio cholerae* is antagonized by lytic phage and entry into the aquatic environment. PLoS Pathog 4.

285. Inokuma K, Takano M, Hoshino K. 2013. Direct ethanol production from N-acetylglucosamine and chitin substrates by Mucor species. Biochem Eng J 72.

286. Kumar A, Kumar D, George N, Sharma P, Gupta N. 2018. A process for complete biodegradation of shrimp waste by a novel marine isolate *Paenibacillus* sp. AD with simultaneous production of chitinase and chitin oligosaccharides. Int J Biol Macromol 109.

287. Fernández-Llamosas H, Castro L, Blázquez ML, Díaz E, Carmona M. 2017. Speeding up bioproduction of selenium nanoparticles by using *Vibrio natriegens* as microbial factory. Sci Rep 7.

288. Tschirhart T, Shukla V, Kelly EE, Schultzhaus Z, Newringeisen E, Erickson JS, Wang Z, Garcia W, Curl E, Egbert RG, Yeung E, Vora GJ. 2019. Synthetic Biology Tools for the Fast-Growing Marine Bacterium *Vibrio natriegens*. ACS Synth Biol 8.

289. Weinstock MT, Hesek ED, Wilson CM, Gibson DG. 2016. *Vibrio natriegens* as a fast-growing host for molecular biology. Nat Methods 13.

290. Hiyoshi H, Kodama T, Iida T, Honda T. 2010. Contribution of *Vibrio parahaemolyticus* virulence factors to cytotoxicity, enterotoxicity, and lethality in mice. Infect Immun 78.

291. Sarowska J, Futoma-Koloch B, Jama-Kmiecik A, Frej-Madrzak M, Ksiazczyk M, Bugla-Ploskonska G, Choroszy-Krol I. 2019. Virulence factors, prevalence and potential transmission of extraintestinal pathogenic *Escherichia coli* isolated from different sources: Recent reports. Gut Pathog https://doi.org/10.1186/s13099-019-0290-0.

292. Allesen-Holm M, Barken KB, Yang L, Klausen M, Webb JS, Kjelleberg S, Molin S, Givskov M, Tolker-Nielsen T. 2006. A characterization of DNA release in *Pseudomonas aeruginosa* cultures and biofilms. Mol Microbiol 59.

293. Sahu PK, Iyer PS, Oak AM, Pardesi KR, Chopade BA. 2012. Characterization of eDNA from the clinical strain *Acinetobacter baumannii* AIIMS 7 and its role in biofilm formation. The Scientific World Journal 2012.

294. Lv C, Li Y, Wei Y, Wang J, Yu H, Gao F, Zhu C, Jia X, Tong M, Dong P, Gao Q, Geng L. 2022. Research Progress on Small Molecular Inhibitors of the Type 3 Secretion System. Molecules https://doi.org/10.3390/molecules27238348.

295. Nordfelth R, Kauppi AM, Norberg HA, Wolf-Watz H, Elofsson M. 2005. Small-molecule inhibitors specifically targeting type III secretion. Infect Immun 73.

296. Liu C, Zhang H, Peng X, Blackledge MS, Furlani RE, Li H, Su Z, Melander RJ, Melander C, Michalek S, Wu H. 2023. Small Molecule Attenuates Bacterial Virulence by Targeting Conserved Response Regulator. mBio 14.

297. Cegelski L, Pinkner JS, Hammer ND, Cusumano CK, Hung CS, Chorell E, Åberg V, Walker JN, Seed PC, Almqvist F, Chapman MR, Hultgren SJ. 2009. Small-molecule inhibitors target *Escherichia coli* amyloid biogenesis and biofilm formation. Nat Chem Biol 5.

298. Wang J, Galgoci A, Kodali S, Herath KB, Jayasuriya H, Dorso K, Vicente F, González A, Cully D, Bramhill D, Singh S. 2003. Discovery of a Small Molecule that Inhibits Cell Division by Blocking FtsZ, a Novel Therapeutic Target of Antibiotics. Journal of Biological Chemistry 278.

299. Obaidat MM, Salman AEB, Roess AA. 2017. Virulence and antibiotic resistance of *Vibrio parahaemolyticus* isolates from seafood from three developing countries and of worldwide environmental, seafood, and clinical isolates from 2000 to 2017. J Food Prot 80.

300. Du X, Wojtowicz D, Bowers AA, Levens D, Benham CJ, Przytycka TM. 2013. The genome-wide distribution of non-B DNA motifs is shaped by operon structure and suggests the transcriptional importance of non-B DNA structures in *Escherichia coli.* Nucleic Acids Res 41.

301. Johnson GC, Lyman JM. 2020. Warming trends increasingly dominate global ocean. Nat Clim Chang 10.

302. Cheung WWL, Lam VWY, Sarmiento JL, Kearney K, Watson R, Zeller D, Pauly D. 2010. Large-scale redistribution of maximum fisheries catch potential in the global ocean under climate change. Glob Chang Biol 16.

303. Mora C, McKenzie T, Gaw IM, Dean JM, von Hammerstein H, Knudson TA, Setter RO, Smith CZ, Webster KM, Patz JA, Franklin EC. 2022. Over half of known human pathogenic diseases can be aggravated by climate change. Nat Clim Chang https://doi.org/10.1038/s41558-022-01426-1.

304. Burge CA, Mark Eakin C, Friedman CS, Froelich B, Hershberger PK, Hofmann EE, Petes LE, Prager KC, Weil E, Willis BL, Ford SE, Harvell CD. 2014. Climate change influences on marine infectious diseases: Implications for management and society. Ann Rev Mar Sci 6.

305. Oh MH, Lee SM, Lee DH, Choi SH. 2009. Regulation of the *Vibrio vulnificus* hupA gene by temperature alteration and cyclic AMP receptor protein and evaluation of its role in virulence. Infect Immun 77.

306. Harrison J, Nelson K, Morcrette H, Morcrette C, Preston J, Helmer L, Titball RW, Butler CS, Wagley S. 2022. The increased prevalence of *Vibrio* species and the first reporting of *Vibrio jasicida* and *Vibrio rotiferianus* at UK shellfish sites. Water Res 211.

307. Archer EJ, Baker-Austin C, Osborn TJ, Jones NR, Martínez-Urtaza J, Trinanes J, Oliver JD, González FJC, Lake IR. 2023. Climate warming and increasing *Vibrio vulnificus* infections in North America. Sci Rep 13.

308. Yildiz FH, Visick KL. 2009. *Vibrio* biofilms: so much the same yet so different. Trends Microbiol 17.